

**PHOTOLUMINESCENT RESPONSES OF  
POLYPROPYLENETHIOPHENOIMINE-CO-PEDOT/  
POLYSTYRENESULFONIC ACID AND ZINC SELENIDE  
QUANTUM DOT COMPOSITE MATERIALS**



**UNIVERSITY of the  
WESTERN CAPE**

**SIYABONGA BEIZEL MDLULI**  
**BSc Honours Chemistry (*Cum Laude*)**

**A mini-thesis submitted in partial fulfilment of the requirement  
for the degree of**

**Magister Scientiae in Nanoscience**

**In the**

**Faculty of Science, University of the Western Cape,  
Bellville, Cape Town, South Africa**

**Supervisor: Prof Emmanuel I. Iwuoha**

**Co-supervisor: Dr Kwena D. Modibane**

**January 2018**

# ABSTRACT

---

Research in renewable energy has gained momentum and become a centre of attention as a possible alternative solution to the energy catastrophe. This is attained by the use of solar energy as an alternative clean energy source. The creation of solar energy arises as a consequence of direct conversion of light photons from the sun into electrical energy by the use of solar cells made up of semiconducting materials incorporated into the system. In the context of solar energy, hybrid photovoltaics comprising of organic molecules and nanomaterials have emerged to be one of the most promising candidates to lower the cost of construction of solar cells as well as improving the power conversion efficiency (PCE). This is mainly due to the ease of processability of the active layer and the unique properties brought by the use of nanomaterials. In the exponentially increasing wide field of nanotechnology, focus has shifted to novel hybrid dendritic star copolymers as the organic donor materials and quantum dots as the inorganic acceptor materials. In this work, we present the synthesis, characterisation, and photoluminescent responses of the newly developed active layer based on the blend of a second generation Poly(propylenethiophinoimine)-co-PEDOT/poly(styrene sulfonic acid) (G2PPT-co-PEDOT-PSSA) as a donor material with zinc selenide quantum dot (ZnSe QD) as the acceptor material. Both the donor and acceptor were synthesized chemically. The preparation of the star copolymer involved a Schiff base condensation chemical reaction between the primary amine group of a G2PPI dendrimer and 2-thiophene carboxaldehyde, to afford the thiophene functionalized PPI dendrimer (G2PPT) which was followed by the copolymerization of G2PPT with ethylenedioxythiophene (EDOT) monomer in the presence of iron chloride ( $\text{FeCl}_3$ ) as an oxidant. The structure and properties of the as-prepared materials were studied by the employment of Fourier transform infrared spectroscopy (FTIR), proton

nuclear magnetic resonance spectroscopy ( $^1\text{H}$  NMR), Ultraviolet-Visible spectroscopy (UV-Vis), X-ray diffraction (XRD), thermogravimetric analysis (TGA), high resolution transmission electron microscopy (HRTEM), scanning electron microscopy (SEM), photoluminescence (PL), square wave voltammetry (SWV), and cyclic voltammetry (CV). There was a clear growth of EDOT on the surface of G2PPT through  $\alpha - \alpha$  coupling in the thiophene ring as evident by both  $^1\text{H}$  NMR and FTIR. UV-Vis of the star copolymer showed redshift compared to the parent polymers, PEDOT and G2PPT, which was attributed to the increase in conjugation as a result of the growth of the PEDOT on the surface of G2PPT. With the help of UV-Vis, the band gap ( $E_g$ ) of the polymers was determined and was found to be 2.96, 2.92, and 2.85 eV for PEDOT, G2PPT-co-PEDOT, and G2PPT-co-PEDOT-PSSA respectively. UV-Vis of ZnSe QD gave an absorption peak at 416 nm with a band gap of 2.95 eV. G2PPT-co-PEDOT-PSSA exhibited improved thermal stability due to enhancement in crystallinity and conjugation as confirmed by TGA. SEM images of G2PPT-co-PEDOT-PSSA exhibited tubular-like structures with many tentacles which are separated from each other while HRTEM revealed cloudy-like morphology with some microporous structures. HRTEM of ZnSe QD revealed well-dispersed small spherical particles. XRD revealed broad peaks indicating amorphousness in all polymers. The photoluminescence of the dendritic star copolymer was observed to be an average of its starting materials or components indicating a hybrid material. Both CV and SWV revealed a low oxidation potential of less than 0.2 V. The electrochemical band gap of the polymers was determined and found to be 0.202, 0.201, 0.199 eV for PEDOT, G2PPT-co-PEDOT, and G2PPT-co-PEDOT-PSSA respectively.

# DECLARATION

---

I declare that “*Photoluminescent responses of polypropylenethiophenimine-co-PEDOT/polystyrenesulfonic acid and zinc selenide quantum dot composite materials*” is my own work, that it has not been submitted before for any degree or examination in any other university and that all sources used or quoted have been indicated or acknowledged as complete references.



Full names : Siyabonga Beizel

Surname : Mdluli



Signature : ...

.....

Date : January 2018

# DEDICATION

---

I dedicate this thesis to my parents: Hlatshwayo Hlabase Elizabeth and Mdluli Sikelele Johannes. To my brothers: Mdluli Desmomd Mike and Mdluli Mpho Emmanuel. Last but not least to my wonderful and beautiful daughter: Mdluli Olwethu Hazel.



# ACKNOWLEDGEMENTS

---

I would firstly like to thank the creator of all living and non-living organisms, the one above us all, origin of all being, GOD the ALMIGHT, for blessing and shining light onto me and for giving me strength to face all the challenges I went through when conducting this research project.

I would like to express my sincere gratitude to an extra-ordinary man, my father far away from home, my supervisor, Prof Emmanuel Iwuoha for his valuable encouragement, effortless work, inspiration, love, care, good advice both socially and academically, and teaching me so many things related to this field of study.

I would also like to thank my mentor, Dr Milua Masikini for playing a significant role in this research work, for showing me all the necessary steps, for believing in me and always sharing critical ideas with me, and lastly your patience and humbleness.

Gratitude also goes to my laboratory group mates (SensorImmuno Lab), Ramoroka Emmanuel, Januarie Kaylin, Sass Danielle, Qakala Sinazo, and Wilson Lindsay for making the lab a powerful and fascinating environment to work on because I enjoyed every single moment of it. Let me not forget to thank all other SensorLab researchers belonging to the other different labs for welcoming me with warm hands and always there to show me where to find what when I needed assistance. I quickly settled to life in the SensorLab family because of all your warmth, love, caring, and happiness. With that I say thank you.

A very fat giant thank goes to the MDLULI family for bringing me thus far. A special thanks to my MOM for being there my entire life, giving me love, showing me the right path to follow, installing education within me and giving me all the support I needed for this journey. LOVE YOU VERY MUCH.

To the University of Limpopo Nanotechnology group: Dr Kwena Modibane, Prof Joseph Hato, Mr Ramohlola Edmond, and Mr Monama Release for supporting and believing in me. Leaving the group was not easy but I never felt abandoned because you kept your support both academically and socially close to me. All the published work so far that I was included in gave me the enthusiasm to continue working hard, the strength, and passion for research. Without you none of this would have become possible so thank you.

I would also like to thank the following people for offering help in some of the characterization instruments:

- Ms Natasha Peterson and Mr Earl McDonald from the Physics Department at the University of the Western Cape for HRTEM and SEM analysis.
- Mr Yunus Kippie from the Pharmacy School at the University of the Western Cape for helping with TGA analysis.
- Dr Edith Beukes from Chemistry Department for helping with NMR analysis.
- Dr Remy Bucher from the iTemba Labs for helping with XRD measurements.
- Mr Timothy Letch from Chemistry Department for helping with FTIR measurements.

I would also like to thank my friends, Maapola Praise, Matlala Moses, Shumbula Ndivhuwo, Tshindane Pfano, Masha Karabo, Ngoasheng Joel, and Ramoroka Emmanuel whom I share with the “Honourable group” for all the encouragement and positive criticism that we always share amongst each other. May God also bless you guys in finishing your Masters degrees in your different respective Universities. You are all truly my brothers.

Lastly, I would also like to acknowledge the Department of Science and Technology (DST) for funding this project and the National Nanotechnology Postgraduate Teaching and Training Platform (NNPTTP), especially Valencia Jamalie and Chyril Abrahams for all the administrative help they provided me.


# RESEARCH OUTPUT

---

## BOOK CHAPTER

1. Kabelo E. Ramohloa, Milua Masikini, **Siyabonga B. Mdluli**, Gobeng R. Monama, Mpitloane J. Hato, Kerileng M. Molapo, Emmanuel I. Iwuoha, Kwena D. Modibane. *Electrocatalytic Hydrogen Production Properties of Polyaniline Doped With Metal-Organic Frameworks*. In: Kaneko S. et al. (eds) Carbon-related Materials in Recognition of Nobel Lectures by Prof. Akira Suzuki in ICCE. Springer, Cham (2017) 373-389.

## PUBLICATIONS

- 
1. Kabelo E. Ramohlola, Milua Masikini, **Siyabonga B. Mdluli**, Gobeng R. Monama, Mpitloane J. Hato, Kerileng M. Molapo, Emmanuel I. Iwuoha, Kwena D. Modibane. *Electrocatalytic Hydrogen Production Properties of Metal Organic Frameworks decorated with poly (3-aminobenzoic acid)*. *Electrochimica Acta* 246 (2017) 1174–1182.
  2. Kabelo E. Ramohlola, Milua Masikini, **Siyabonga B. Mdluli**, Gobeng R. Monama, Mpitloane J. Hato, Kerileng M. Molapo, Emmanuel I. Iwuoha, Kwena D. Modibane. *Electrocatalytic Hydrogen Production Properties of Poly(3-aminobenzoic acid) doped with Metal Organic Frameworks*. *International Journal of Electrochemical Science* 12 (2017) 4392-4405.
  3. Kabelo Edmond Ramohlola, Gobeng Release Monama, Kwena Desmond Modibane, Milua Masikini, Kerileng Mildred Molapo, **Siyabonga Beizel Mdluli**, Emmanuel Iwuoha, Mpitloane Joseph Hato. *Polyaniline-metal organic framework nanocomposite*



*as an efficient electrocatalyst for hydrogen evolution reaction. Composites Part B* 137 (2018) 129–139.

4. Gobeng R. Monama, **Siyabonga B. Mdluli**, Gloria Mashao, Mogwasha D. Makhafola, Kabelo E. Ramohlola, Kerileng M. Molapo, Mpitloana J. Hato, Katlego Makgopa, Emmanuel I. Iwuoha, Kwena D. Modibane. *Palladium deposition on copper(II) phthalocyanine/metal organic framework composite and electrocatalytic activity of the modified electrode towards the hydrogen evolution reaction. Renewable Energy* 119 (2018) 62-72.

## PRESENTATIONS

1. **Mdluli S. B**, Masikini M, Ramoroka M. E, Iwuoha E. I. *Photophysics of novel electroresponsive 3-dimensional Poly(propylene thiophenoimine)-co-poly(3, 4-ethylenedioxythiophene) dendritic copolymer.* 9<sup>th</sup> International Conference of the African Materials Research Society (AMRS) (11-14<sup>th</sup> December 2017) GICC, Gaborone, Botswana. Poster presentation.

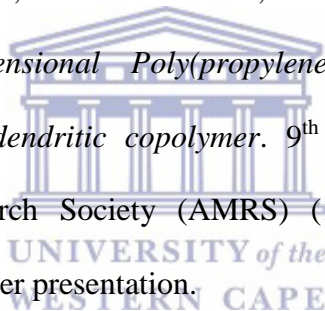


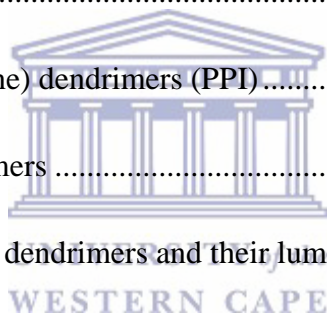
# TABLE OF CONTENT

---

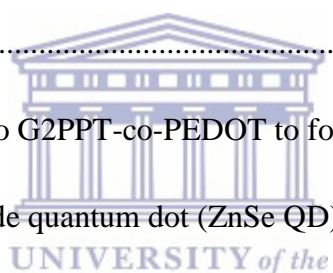
ABSTRACT.....	i
DECLARATION.....	iii
DEDICATION.....	iv
ACKNOWLEDGEMENTS.....	v
RESEARCH OUTPUT.....	vii
BOOK CHAPTER.....	vii
PUBLICATIONS.....	vii
PRESENTATIONS.....	viii
TABLE OF CONTENT.....	ix
LIST OF FIGURES.....	xiii
LIST OF SCHEMES.....	xvi
LIST OF TABLES.....	xvii
LIST OF ABBREVIATIONS.....	xviii
CHAPTER ONE.....	1
1. Introduction.....	1
1.1. Background.....	1
1.2. Problem statement.....	3
1.3. Rationale or Motivation.....	4
1.4. Aims and Objectives.....	5



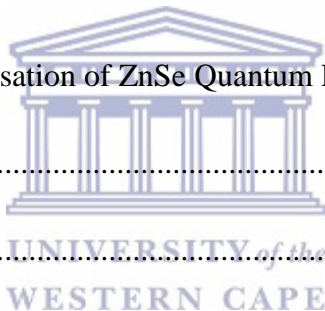
1.4.1. Aim .....	5
1.4.2. Objectives .....	6
1.5. Thesis outline/structure .....	7
1.6. References .....	8
CHAPTER TWO .....	11
2. Literature Review.....	11
Luminescence efficiency of functionalised Poly(propylene imine) dendritic compounds.....	11
2.1. Background .....	11
2.1.1. Dendrimers.....	11
2.1.2. Poly(propylene imine) dendrimers (PPI).....	14
2.2. Synthesis of PPI dendrimers .....	15
2.3. Functionalization of PPI dendrimers and their luminiscence.....	18
2.3.1. Organic/polymer-functionalized PPI dendrimers .....	18
2.3.2. Metal-functionalized PPI dendrimers (metallo-dendrimers).....	22
2.3.3. Nanoparticle-functionalized PPI dendrimers .....	25
2.4. Factors that affect the luminescence properties of functionalised PPI dendrimers...	26
2.4.1. Influence of pH on the fluorescence properties .....	26
2.4.2. Influence of temperature on the fluorescence properties .....	27
2.4.3. Influence of solvent on the fluorescence properties .....	28
2.4.4. Influence of concentration on the fluorescence properties .....	29
2.5. References .....	30



CHAPTER THREE .....	37
3. Experimental .....	37
3.1. Materials and Reagents .....	37
3.2. Chemical synthesis of Poly(3, 4-ethylenedioxythiophene) (PEDOT) .....	38
3.3. Chemical synthesis of Poly(3, 4-ethylenedioxythiophene)-poly(4-styrene sulfonic acid) (PEDOT-PSSA) .....	39
3.4. Synthesis of thiophene-functionalized generation 2 poly(propylene imine) dendrimer (G2PPT) .....	40
3.5. Chemical oxidative polymerization of EDOT from functionalized G2PPT to form star copolymer G2PPT-co-PEDOT.....	40
3.6. Incorporation of PSSA to G2PPT-co-PEDOT to form G2PPT-co-PEDOT-PSSA ..	41
3.7. Synthesis of Zinc selenide quantum dot (ZnSe QD).....	42
3.8. Preparation of the active layer: G2PPT-co-PEDOT-PSSA: ZnSe QD .....	42
3.9. Analytical Techniques.....	43
3.9.1. Proton Nuclear Magnetic Resonance spectroscopy ( <sup>1</sup> H NMR).....	43
3.9.2. Fourier Transform Infrared Spectroscopy (FTIR) .....	45
3.9.3. Ultraviolet-Visible Spectroscopy (UV-Vis) .....	46
3.9.4. Fluorescence/ Photoluminescence Spectroscopy (PL) .....	47
3.9.5. X-Ray Diffraction (XRD).....	49
3.9.6. Thermogravimetric Analysis (TGA).....	50
3.9.7. Scanning Electron Microscopy (SEM) .....	51
3.9.8. High-Resolution Transmission Electron Microscopy (HRTEM) .....	51



3.9.9. Cyclic Voltammetry (CV).....	52
3.9.10. Square Wave Voltammetry (SWV) .....	54
3.10. References .....	55
CHAPTER FOUR.....	57
4. Results and Discussion .....	57
4.1. Synthesis and Characterisation of polymers .....	57
4.1.1. Synthesis .....	57
4.1.2. Structural Characterisation.....	65
4.1.3. Electrochemical Characterisation .....	81
4.2. Synthesis and Characterisation of ZnSe Quantum Dot (QD) .....	90
4.2.1. Synthesis .....	90
4.2.2. Characterisation .....	91
4.3. Optical properties of G2PPT-co-PEDOT-PSSA: ZnSe QD blends .....	95
4.3.1. Ultraviolet -Visible Spectroscopy (UV-Vis) .....	95
4.3.2. Photoluminescence (PL) Spectroscopy.....	96
4.4. References .....	98
CHAPTER FIVE .....	103
5. Conclusion and Recommendations.....	103
5.1. Conclusion.....	103
5.2. Recommendations .....	106



# LIST OF FIGURES

---

Figure 2. 1: Excitation and emission spectra of (a) PPI-co-PPY (b) PPI dendrimer and (c) polypyrrole [22].	21
Figure 2. 2: Fluorescence spectra of PPI dendrimer in acetonitrile at various concentrations of $Pb^{2+}$ [34].	24
Figure 2. 3: Fluorescence spectra of PPI in acetonitrile at different concentrations of (A) $Pb^{2+}$ (B) $Cu^{2+}$ [44].	25
Figure 2. 4: pH dependence of normalised fluorescence intensity for PPI dendrimers [34, 44]	27
Figure 2. 5: Fluorescence intensity as a function of concentration [55].	29
Figure 3. 1: Typical cyclic voltammogram showing the peak cathodic and anodic current respectively for a reversible reaction [14].	53
Figure 4. 1: $^1H$ NMR of (A) 2Th, (B) pristine G2PPI, and (C) G2PPT.	65
Figure 4. 2: $^1H$ NMR of (A) EDOT, (B) PEDOT, and (C) PEDOT-PSSA.	66
Figure 4. 3: $^1H$ NMR of (A) G2PPT-co-PEDOT and (B) G2PPT-co-PEDOT-PSSA.	68
Figure 4. 4: FTIR of (A) EDOT and PEDOT, (B) G2PPT and G2PPT-co-PEDOT, and (C) PEDOT and PEDOT-PSSA.	69
Figure 4. 5: (A) Absorption spectra of G2PPI and G2PPT, (B) Absorption spectra of PEDOT, GEPPT-co-PEDOT, and G2PPT-co-PEDOT-PSSA.	71
Figure 4. 6: Tauc plot of (A) PEDOT, (B) G2PPT-co-PEDOT, (C) G2PPT-co-PEDOT-PSSA.	72
Figure 4. 7: Emission spectra of (A) PEDOT, (B) G2PPT, (C) G2PPT-co-PEDOT, and (D) G2PPT-co-PEDOT-PSSA.	74

Figure 4. 9: Thermogravimetric plot of PEDOT, PEDOT-PSSA, G2PPT-co-PEDOT, and G2PPT-co-PEDOT-PSSA.....	76
Figure 4. 10: SEM images of (A) PEDOT, (B) PEDOT-PSSA, (C) G2PPT-co-PEDOT, and (D) G2PPT-co-PEDOT-PSSA.....	78
Figure 4. 11: HRTEM images of (A) PEDOT (C) PEDOT-PSSA (E) G2PPT-co-PEDOT (G) G2PPT-co-PEDOT-PSSA, and EDX of (B) PEDOT (D) PEDOT-PSSA (F) G2PPT-co-PEDOT (H) G2PPT-co-PEDOT-PSSA. Inset: SAED of all the samples.....	80
Figure 4. 12: Cyclic voltammograms of PEDOT, PEDOT-PSSA, G2PPT-co-PEDOT, and G2PPT-co-PEDOT-PSSA in 0.1 M TBAP/DMSO electrolyte at 100 mV/s.....	82
Figure 4. 13: Multi-scan rate cyclic voltammograms of (A) PEDOT, (B) PEDOT-PSSA, (C) G2PPT-co-PEDOT, and (D) G2PPT-co-PEDOT-PSSA at 10-100 mV/s scan rates in 0.1M TBAP/DMSO.....	84
Figure 4. 14: Randels-Sevcik plots for GCE in 0.1M TBAP/DMSO electrolytic system at scan rates range of 10-100 mV/s.....	86
Figure 4. 15: Logarithm plot of peak current vs scan rate for $\alpha$ determination.....	87
Figure 4. 16: SWV representing (A) Oxidation (B) Reduction of the polymers in 0.1M TBAP/DMSO at 100 mV/s.....	89
Figure 4. 17: SWV oxidation of (A) PEDOT (B) PEDOT-PSSA (C) G2PPT-co-PEDOT (D) G2PPT-co-PEDOT-PSSA in 0.1M TBAP/DMSO at scan rate range of 10-100 mV/s.....	90
Figure 4. 18: SWV reduction of (A) PEDOT (B) PEDOT-PSSA (C) G2PPT-co-PEDOT (D) G2PPT-co-PEDOT-PSSA in 0.1M TBAP/DMSO at scan rate range of 10-100 mV/s.....	90
Figure 4. 20: Tauc plot of ZnSe QD for band gap determination.....	92
Figure 4. 21: Photoluminescence spectra of ZnSe.....	93
Figure 4. 22: (A) HRTEM image of ZnSe and (B) EDX results. Inset: SAED of ZnSe.....	94

Figure 4. 23: UV-Vis absorption spectra of G2PPT-co-PEDOT-PSSA: ZnSe QD blends in different ratios in terms of volume.....95

Figure 4. 24: Photoluminescence of G2PPT-co-PEDOT-PSSA: ZnSe QD (1:3) blends in a mixture of DMSO/toluene. ....97





# LIST OF SCHEMES

---

Scheme 2. 1: Typical representation of a dendrimer ranging from generation zero (G0) to generation four (G4) [1].....	12
Scheme 2. 2: G2 PPI dendrimer.....	14
Scheme 2. 3: Synthesis of PPI dendrimers using the divergent approach [25]. ....	17
Scheme 2. 5: Cupper-poly(propylene imine) metallodendrimer (CuPPI) [36].....	22
Scheme 3. 1: (a) No applied external magnetic field, (b) external magnetic field is applied. .....	43
Scheme 3. 2: Typical 1-deminsional proton spectrum.....	44
Scheme 3. 3: Simplified schematic illustration of a dispersive IR spectrometer [9].....	45
Scheme 3. 4: Possible electronic transitions of $\pi$ , $\sigma$ , and n electrons [10].....	46
Scheme 3. 5: Jablonski diagram showing the electronic transition levels [6]. ....	48
Scheme 4. 1: Synthetic pathway to PEDOT via oxidative polymerization of EDOT monomer. .....	57
Scheme 4. 2: Polymerization mechanism of the formation of PEDOT via step (1-5) [2].....	59
Scheme 4. 3: Functionalization of G2PPI to G2PPT through a condensation reaction.....	61
Scheme 4. 4: G2PPT formation mechanism between the primary imine of the dendrimer and the carbonyl group of the aldehyde via step (1-5). ....	63
Scheme 4. 5: Synthetic pathway to G2PPT-co-PEDOT via oxidative polymerization of EDOT monomer on the surface of G2PPT.....	64

# LIST OF TABLES

---

Table 2. 1: Photophysical properties of PPI in different organic solvents [34, 44].....	28
Table 4. 1: Summary of HUMO, LUMO, and the band gap.....	83
Table 4. 2: Electrochemical parameters of all the polymers.....	88



# LIST OF ABBREVIATIONS

---

CNTs	: Carbon Nanotubes
CuPPI	: Copper-Poly(propylene imine)
CV	: Cyclic Voltammetry
DAB	: Diamminobutane
DCM	: Dichloromethane
DMF	: Dimethyl Formamide
DMSO	: Dimethyl Sulfoxide
EDA	: Ethylene Diamine
EDOT	: 3, 4-Ethylenedioxythiophene
EDX or EDS	: Energy Dispersive X-ray Spectroscopy
FTIR	: Fourier Transform Infrared Spectroscopy
G1-G5	: First to Fifth Generation
HNMR	: Proton Nuclear Magnetic Resonance
HOMO	: Highest Occupied Molecular Orbital
HRTEM	: High Resolution Transmission Electron Microscopy
ICPs	: Intrinsic Conducting Polymers
LUMO	: Lowest Unoccupied Molecular Orbital
MWCNTs	: Multiwalled Carbon Nanotubes
OA	: Oleic Acid
PA	: Polyacetylene
PAMAM	: Poly(amido amine)
PANI	: Polyaniline
PCE	: Power Conversion Efficiency
PEDOT	: Poly(3, 4-ethylenedioxythiophene)
PEDOT-PSSA	: Poly(ethylenedioxythiophene)-Poly(styrene sulfonic acid)
PL	: Photoluminescence
POPAM	: Poly(propylene amine)

PPI	: Poly(propylene imine)
PPI-co-PPY	: Poly(propylene imine)-co-Polypyrrole
PPT	: Poly(propylene thiophenoimine)
PPT-co-PEDOT	: Poly(propylene thiophenoimine)-co-Poly(ethylenedioxythiophene)
PPY	: Polypyrrole
PSSA	: Poly(styrene sulfonic acid)
PTh	: Polythiophene
PV	: Photovoltaic
QD	: Quantum Dot
SAED	: Selected Area Electron Diffraction
SEM	: Scanning Electron Microscopy
SWV	: Square Wave Voltammetry
TBAP	: Tetrabutylammonium Perchlorate
TGA	: Thermogravimetric Analysis
2Th	: 2-Thiophene carbaxalydehyde
TOP	: Trioctylphosphine
UV-Vis	: Ultraviolet-Visible Spectroscopy
XRD	: X-ray Diffraction

# CHAPTER ONE

## 1. Introduction

---

### 1.1. Background

Life without energy is not imaginable, it is like imagining to yield fruits on a tree that does not have roots and a stem. This means that the life of both living and non-living organisms depend solely on the availability of energy. In basic terms, energy is the ability to do work. In other terms, energy is the power extracted from the employment or usage of chemical or physical asserts, with the intension of providing heat and light or to work machines. With the above mentioned, it is quite obvious that energy is the fundamental needs of man as it is utilized daily in all sectors of life. We use energy in everything we do: (1) we need energy to walk to school, (2) to play, (3) to run a computer, (4) to cook our daily food, (5) etc. However, in the current state of the world, the demand of energy have managed to exceed its supply. One of the major contributions to this is the rapid growth of global population, which in turn affects the quality of life by affecting the economic growth both nationally and internationally. Therefore, there is a need for the rapid increase in global population to be accompanied by a rapid increase in energy supply in order to consistently maintain human needs without compromising the quality of the world that we live in. For this to happen, it is of utmost significance to conserve, protect, and sustain the already available energy resources.

Over the past centuries, the world energy consumption has been majorly based on fossil fuels. Fossil fuels are knowns as primary energy sources. They consist of petroleum, coal, natural

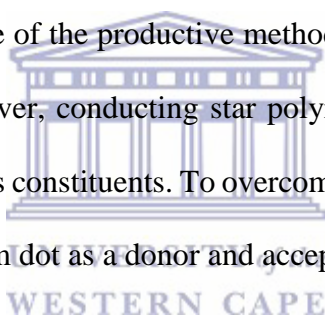
gas, propane, and uranium. They are all classified as non-renewable energy sources. Fossil fuels contribute 80% of the energy produced or utilized globally [1]. The major challenge encountered by fossil fuels is the unfriendly circumstances that comes along with the production of energy such as: (1) water pollution, (2) operational safety, (3) radioactive waste disposal, (4) emission of substances like SO<sub>2</sub>, NO<sub>2</sub>, and CO<sub>2</sub> contributing to acid deposition and global climate change. One other major challenge is their non-reusability, which implies that the world will reach a point at which fossil fuel reserves are completely extracted or depleted. Therefore, because of this, there is an undisputable need for new technologically clean and environmentally friendly methods that needs to be employed to address the challenge of depletion of fossil fuels without compromising the depletion of the ozone layer (O<sub>3</sub>). One of the alternative methods to harness energy is by the employment of renewable energy sources even though they account for a little percentage in global energy supply [2-3]. The major advantage in utilising renewable energy sources is that they are environmentally friendly, so they have minimal negative impact on the environment [4]. Their major drawbacks lies with the less quantity of energy being generated and the large capital cost accompanied by this technological way of harnessing energy [2]. The renewable energy sources consists of Biomass, geothermal, hydrothermal, solar, and wind. Therefore, because of the large capital cost problem encountered by renewable energy sources, solar energy, amongst all renewable energy sources, has attracted most attention; not only due to the fact that it is renewable, but mostly due to the continuous availability of sunlight throughout the year and almost all the surface on earth. It is estimated that solar energy collected by planet earth annually is several thousand times more than the energy used by humans and the earth's energy reserve put together. Therefore, the main advantage of solar energy is that it is an endless producer of photons with a wide range of wavelength. Thus conversion of energy via photovoltaic (PV) processes is considered to be the ideal process that satisfies the requirements for the demand

of clean energy and large energy supply that can reach or accommodate the overpopulation growth.

## **1.2. Problem statement**

The shortage of energy and pollution of the environment are the two primary challenges faced by the society nowadays. As previously mentioned, sunlight has turned out to be the most reliable and sustainable supply of green (clean) energy and this makes the exploration of solar energy an ideal approach in addressing both energy and environmental problems, in comparison to the traditional fossil fuel energy method. A photovoltaic device is a device that converts solar irradiation directly into electricity by exploiting the photovoltaic effect exhibited by metals and inorganic semi-conductors. The main component in a photovoltaic device is the semi-conductor material, since it is the one that absorbs and ultimately determines how much energy is taken up by the photovoltaic device. The currently most used semi-conductor is crystalline silicon because of its power conversion efficiency (PCE) of up to 25% [6]. However, researchers have also come up with alternative methods such as CdTe solar cells with PCE of 19.6% [7] and GIGS solar cells with PCE of 20.3% [8]. The key challenge that restricts or hinder the development or application of these type of solar cells is the cost of the semi-conducting material, cost of fabrication of the device, and the toxicity of some elements. The price of the fabrication process depends on the semi-conducting material that is utilised, therefore it is of utmost significance to find cheaper and non-toxic semi-conducting materials, without compromising the requirements of the semi-conductor. Suitable semi-conductors must possess the following requirements: (1) good processability, (2) good conductivity, (3) good mechanical and thermochemical stability. With this requirements, intrinsic conducting polymers (ICPs) such as polyaniline (PANI), polyparaphenylene, polypyrrole (PPY), polythiophene (PTh), poly(3,4-ethylenedioxythiophene) (PEDOT), and polyacetylene (PA), have all been studied and have shown good conductivity, optoelectrical, and luminescence

properties as potential good materials for photovoltaic devices [9-10]. Amongst all ICPs, PEDOT has emerged an indispensable material due to its extensive range of technological applicability, in diverse areas, such as light-emitting diodes, electrochromic display devices, and capacitors. The wide range of its applicability is due to its ease of synthesis, elevated air stability, superior electrical conductivity, and possesses optical properties similar to those of semi-conductors and metals [11]. However, the key challenge with PEDOT and other ICPs or purely organic materials based photovoltaic devices is: (1) the recombination of excited molecules upon absorption which limits the amount of energy that can be generated, (2) poor processability which is due to their insolubility in many organic solvents [9, 12], (3) poor mechanical and physical properties [13]. Therefore, research has shown that, synthesis of conducting star copolymers is one of the productive methods to upgrade the processability of conducting polymers [14]. However, conducting star polymers are known to have emission properties that are an average of its constituents. To overcome this, a hybrid material consisting of the star copolymer and quantum dot as a donor and acceptor respectively can be utilised.



### **1.3. Rationale or Motivation**

A possible solution for the use of PEDOT as a semi-conductor is to counter act the previously mentioned limitations. Synthesis of conducting star copolymers are some of the effective ways of improving the processability of conducting polymers [14]. It is reported that, synthesis of star copolymers allows direct chemical connection between the enclosing matrix (peripheral groups) and the conjugated polymer, thus strengthening the physico-chemical stability of the material [15]. Star copolymers are classified as branched giant molecules that have an intermedial core to which numerous linear polymer chains are joined. The resultant three-dimensional structure with enlarged conjugated linear polymer chains render star copolymers properties that are non-identical from the two-dimensional linear polymers. According to research, the fusion of star copolymer and conducting polymer structures offer an advance



towards preparing materials that have advantageous properties of both enhanced processability and electrical conductivity. The improved processability is as a consequence of the spheroidal structure of hyperbranched, dendrimeric and starburst polymers. Therefore, a conducting star copolymer may be formed by which two or more non-identical conjugated arms diverge from the central core [16]. The formation of the star copolymer involves a condensation reaction followed by copolymerization of the conducting linear polymer using oxidising agents such as ferric chloride, ferric tosylate, etc. The most used central core is poly(propylene imine) dendrimer (PPI). This is due to its amino groups at the periphery, thus can be used as hydrogen donor because of the high density of amino groups. It is known that the properties of dendrimers are strongly affected or governed by the terminal groups [17-18]. Therefore, in this project, a dendritic conducting star copolymer made from G2PPI as a central core and PEDOT as a conducting extending polymer shell is proposed. To counter act the insolubility challenge of PEDOT, poly(styrenesulfonic acid) (PSSA) is incorporated into the star copolymer. It is incorporated because functional groups such as carboxylic and sulfonic acids have been reported to be able to enhance the solubility challenge of the polymer without compromising the conductivity of the material. To address the challenge of recombination of excited molecules upon absorption of light and the physical properties, ZnSe QD are incorporated to make a hybrid system made of a donor and acceptor material.

## **1.4. Aims and Objectives**

### **1.4.1. Aim**

The aim of the project is to synthesise and study the luminescent responses of second generation Polypropylenethiophenoimine-co-PEDOT/poly(styrenesulfonic acid) dendritic star copolymer and zinc selenide quantum dot composite materials as donor and acceptor respectively, for photovoltaics application

## 1.4.2. Objectives

The objectives of the work are:

- To synthesise 2<sup>nd</sup> generation Poly(propylenethiophenoimine) (G2PPT) by functionalizing poly(propylene imine) (G2PPI) with 2-thiophene aldehyde through a Schiff base condensation reaction.
- To synthesize the parent polymer, PEDOT through chemical oxidative polymerization of ethylenedioxythiophene (EDOT) monomer with and without the presence of PSSA.
- To synthesise the star copolymers, G2PPT-co-PEDOT and G2PPT-co-PEDOT-PSSA, through chemical oxidative copolymerisation of EDOT monomer on the surface of G2PPT with and without the presence of PSSA.
- To study the optical, structural, morphological, and electrochemical properties of the synthesised materials using Ultraviolet-Visible spectroscopy (UV-Vis), Photoluminescence (PL), Fourier transform infrared spectroscopy (FTIR), Proton nuclear magnetic resonance (<sup>1</sup>H NMR), X-ray diffraction (XRD), Thermogravimetric analysis (TGA), High resolution transmission electron microscopy (HRTEM), Scanning electron microscopy (SEM), Selected area electron diffraction (SAED), Energy dispersive x-ray spectroscopy (EDS or EDX), Cyclic voltammetry (CV), and Square wave voltammetry (SWV)
- To synthesise zinc selenide quantum dot (ZnSe QD) and characterise them using UV-Vis and PL.
- To blend G2PPT-co-PEDOT-PSSA with ZnSe QD and study the luminescent responses of the blend using PL.

## 1.5. Thesis outline/structure

The thesis comprises of 5 chapters and are summarised as follows:

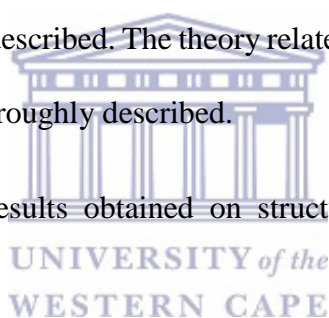
**Chapter One:** Presents the general introduction, problem statement which is what led to the study, motivation of the study, aim and objectives.

**Chapter Two:** Presents a critical review of functionalised Poly(propylene imine) dendritic compounds, their synthetic procedures, luminescent properties, and factors affecting their luminescent properties.

**Chapter Three:** Presents the materials or reagents and methods used for synthesis and characterization. Experimental methodologies for the chemical synthesis of the star copolymers and quantum dot are described. The theory related to analytical technique that were used throughout the project is thoroughly described.

**Chapter Four:** Discusses the results obtained on structural, optical, morphological, and electrochemical characterisation.

**Chapter Five:** Summary of the conclusion and recommendation of the work



## 1.6. References

- [1]- K. E. Ramohlola. *Polyaniline based metal-organic framework composite for hydrogen fuel cell*. MSc Thesis, Department of Chemistry, University of Limpopo, (2017).
- [2]- N. L. Panwar, S. C. Kaushik, S. Kothari. *Role of renewable energy sources in environmental protection-A review*. Renewable and Sustainable Energy Reviews 15 (2011) 1513-1524.
- [3]- A. Demirbas. *Potential applications of renewable energy sources, biomass combustion problems in boiler power systems and combustions related environmental issues*. Progress in Energy and Combustion Science 31 (2005) 171-192.
- [4]- A. A. Bazmi, G. Zahedi. *Sustainable energy systems: Role of optimization modelling techniques in power generation-A review*. Renewable and Sustainable Energy Reviews 15 (2011) 3480-3500.
- [5]- S. Kazim, M. K. Nazeeruddin, M. Gratzel, S. Ahmad. *Perovskite as light harvester: a game changer in photovoltaics*. Angewandte Chemie International Edition 53 (2014) 2812–2824.
- [6]- M. A. Green. *The path to 25% silicon solar cell efficiency: History of silicon cell evolution*. Progress in Photovoltaics 17 (2009) 183 – 189.
- [7]- M. A. Green. *Solar cell efficiency tables (version 42)*. Progress in photovoltaics: Research and Applications 21 (2013) 827 – 837.
- [8]- P. Jackson and D. Hariskos, E. Lotter, S. Paetel, R. Wuerz, R. Menner, W. Wischmann, M. Powalla. *New world record efficiency for Cu(In, Ga)Se<sub>2</sub> thin-film solar cells beyond 20%*. Progress in Photovoltaics 19 (2011) 894 – 897.

- [9]- S. Bhadra, D. Khastgir, N. K. Singha, J. H. Lee. *Progress in preparation, processing and applications of polyaniline*. Progress in Polymer Science 34 (2009) 783-810.
- [10]- J. Pecher, S. Mecking. *Nanoparticles of conjugated polymers*. Chemical Reviews 110 (2010) 6260-6279.
- [11]- A. J. Heeger. *Semiconducting and metallic polymers: the fourth generation of polymeric materials*. Synthetic Metals 125 (2001) 23-42.
- [12]- M. Jaymand. *Recent progress in chemical modification of polyaniline*. Progress in Polymer Science 38 (2013) 1287-1306.
- [13]- R. Qian, J. Qiu, D. Shen. *Conducting polypyrrole electrochemically prepared from aqueous solutions*. Synthetic Metals 18 (1987) 13-18.
- [14]- M. Ak, L. Toppare. *Synthesis of star-shaped pyrrole and thiophene functionalized monomers and optoelectrochemical properties of corresponding copolymers*. Materials Chemistry and physics 114 (2009) 789-794.
- [15]- S. Brahim, A. Guiseppi-Elie. *Electroconductive hydrogels: electrical and electrochemical properties of polypyrrole-poly(HEMA) composites*. Electroanalysis 17 (2005) 556-570.
- [16]- G. A. Sotzing, J. R. Reynolds, P. J. Steel P. *Electrochromic conducting polymers via electrochemical polymerization of bis(2-(3,4-ethylenedioxy)thienyl) monomers*. Chemistry of Materials 8 (1996) 882-889.
- [17]- A. P. H. J. Schenning, P. Jonkheijm, J. Hofkens, S. D. Feyter, T. Asavei, M. Cotlet, F. C. D. Schryver, E. W. Meijer. *Formation and manipulation of supramolecular structures of oligo(p-phenylenevinylene) terminated poly(propylene imine) dendrimers*. Chemical Communications 12 (2002).

[18]- A. P. H. J. Schenning, E. Peeters, E. W. Meijer. *Energy transfer in supramolecular assemblies of oligo(p-phenylene vinylene)s terminated poly(propylene imine) dendrimers.* Journal of the American Chemical Society 122 (2000) 4489-4495.



# CHAPTER TWO

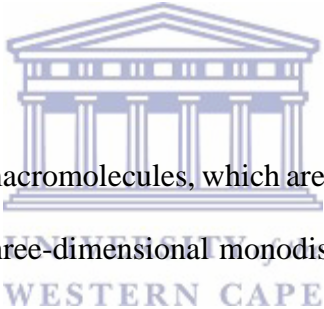
## 2. Literature Review

### Luminescence efficiency of functionalised Poly(propylene imine) dendritic compounds

---

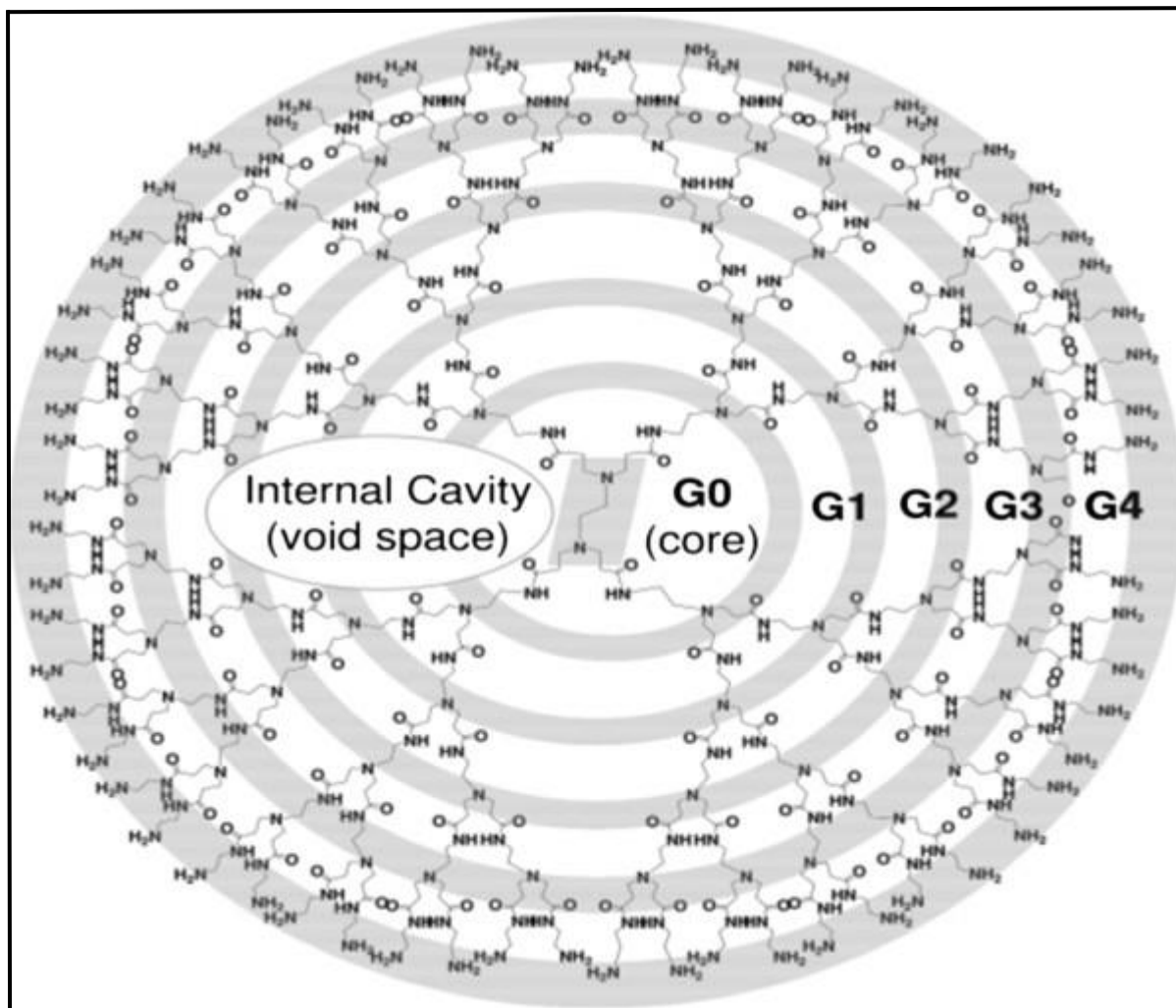
#### 2.1. Background

##### 2.1.1. Dendrimers



Dendrimers are a unique class of macromolecules, which are characterised by being symmetric, homogenous, well-defined, and three-dimensional monodisperse structure with branches [1]. The word ‘dendrimer’ refers to its characteristic or physical appearance. This term is extracted from two Greek words: ‘dendron’, which symbolises a tree, and ‘meros’ which symbolises a part [2-3]. The first person who came across these giant macromolecules is Fritz Vogtle in 1978 [4], then followed by Tomalia Donald and his co-workers in the early years of 1980s [5], and simultaneously but working individually by George R. Newkome [6]. They called them ‘arborols’ meaning ‘trees’ in Latin. However, they are also known as the ‘cascade molecules’ but this terminology is not as much preferred as ‘dendrimers’ because of their ability of being polyvalent and monodisperse character [6]. A typical dendrimer structure is mainly composed of 3 components, the core, the end-groups, and branching units that link the two components together, thus keeping them intact. The surface of the dendrimer is characterised by a carefully customized architecture, the insulating matrix (i.e the peripheral groups) which can be utilized

as a backbone for multiple attachments, thus altering their biological or physicochemical properties [7-8]. These dendritic compounds are known to increase their diameter linearly while adopting a more pronounced globular shape with increase in dendrimer generation (G0-Gn) (See scheme 2.1).



Scheme 2. 1: Typical representation of a dendrimer ranging from generation zero (G0) to generation four (G4) [1].

The increase in dendrimer generation results in an increase in branch density. This is believed to have a pivotal influence on the enhancement of the properties of the dendrimers. The presence of internal cavities together with the fact that they are globular in shape make



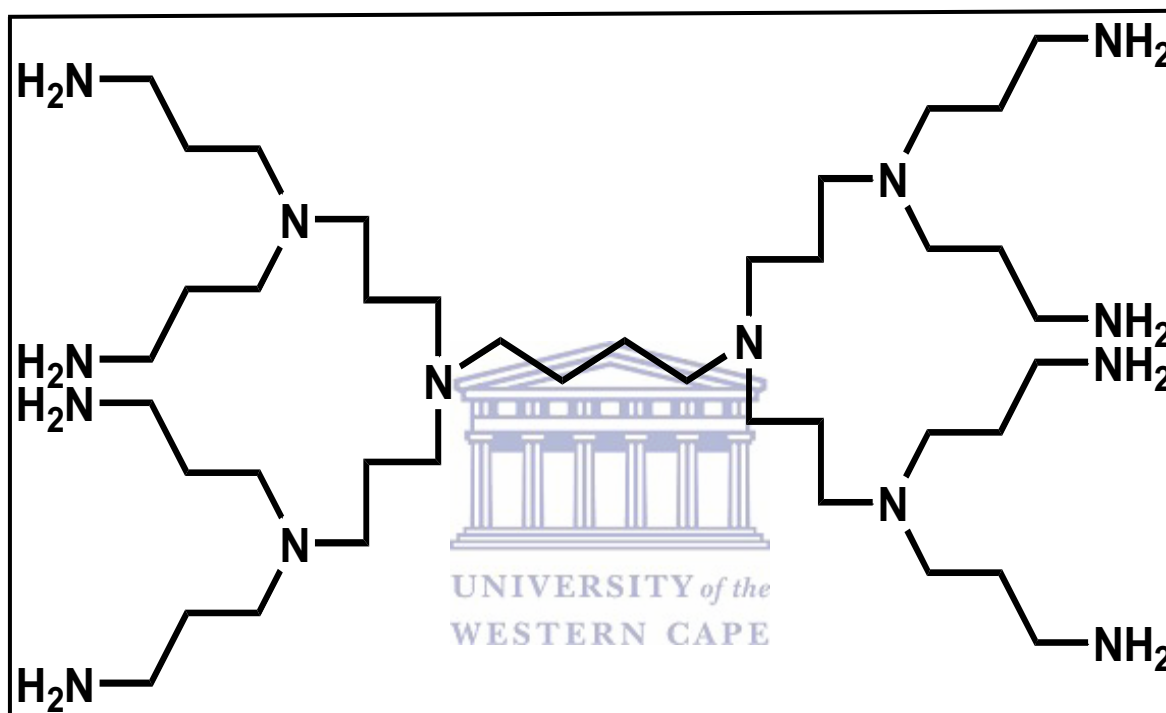
dendrimers to possess unique properties. The most important of those properties is the ability to encapsulate guest molecules in the interior of the macromolecular structure.

The chemistry of dendrimers is one of the most eye catching and rapidly growing areas of new chemistry [9-10]. They are just in the middle of polymer chemistry and molecular chemistry. They are related to the world of molecular chemistry because of their step-by-step controlled synthesis, and they are related to the world of polymer chemistry because of their structure made of repeated units of monomers [11-12]. They are produced in iterative steps, in which each additional step results in a higher generation dendrimer (see scheme 2.1 above), either prepared using the divergent or convergent method [1, 13]. In the different methods which are discussed below, the dendrimer grows outward from a multi-functional core molecule. The core or central molecule reacts with monomer units having atleast one dormant and reactive groups, giving rise to the first-generation dendrimer. Then, the new insulating matrix of the molecule is triggered for reactions with more monomers. This unique architecture and functionality makes dendrimers excellent materials to be used as light-harvesting agents [14], chemical sensors [15], catalyst [16], cross-linking agents [17], drug delivery [18], gene therapy [19], and imaging contrast agents [20].

In this study, G2PPI dendrimer having a diamminobutane (DAB) core, also denoted as DAB-Amy or PPI<sub>y</sub> where y refers to the number of terminal (periphery) amine groups (i.e y= 8 In this case) was used as a light harvesting material for solar cell application. It was chosen because of its commercial availability, its well defined internal cavities, and it's very reactive (functionalizable) amine end-groups. The background of PPI dendrimers is discussed in section 2.1.2 below.

### 2.1.2. Poly(propylene imine) dendrimers (PPI)

Poly(propylene imine) dendrimers, like all other dendrimers, are highly branched macromolecules that resembles a tree-like symmetrically well-defined structure. The difference is that, these dendrimers are terminated with amino groups in their periphery with a number of interesting characteristics [21-22] (See scheme 2.2)



Scheme 2. 2: G2 PPI dendrimer.

Because of the long chains of amine groups, in general they are known as poly-alkylamines consisting of primary amines as the end groups in their periphery, while the interior of the dendrimer consists of a number of tertiary tris-poly(propylene amines). The availability or presence of the nitrogen atoms at the periphery makes the dendrimer easily functionalizable. The functionalizability is enabled by the presence of the lone pair of electrons on the nitrogen atoms, thus acting as reactive and branching or attachment sites. PPI dendrimers are sometimes referred to as “DAB-dendrimers” referring to diamino butane which acts as a core for the synthesis of different generations of PPI dendrimers [23]. It is known that the number of

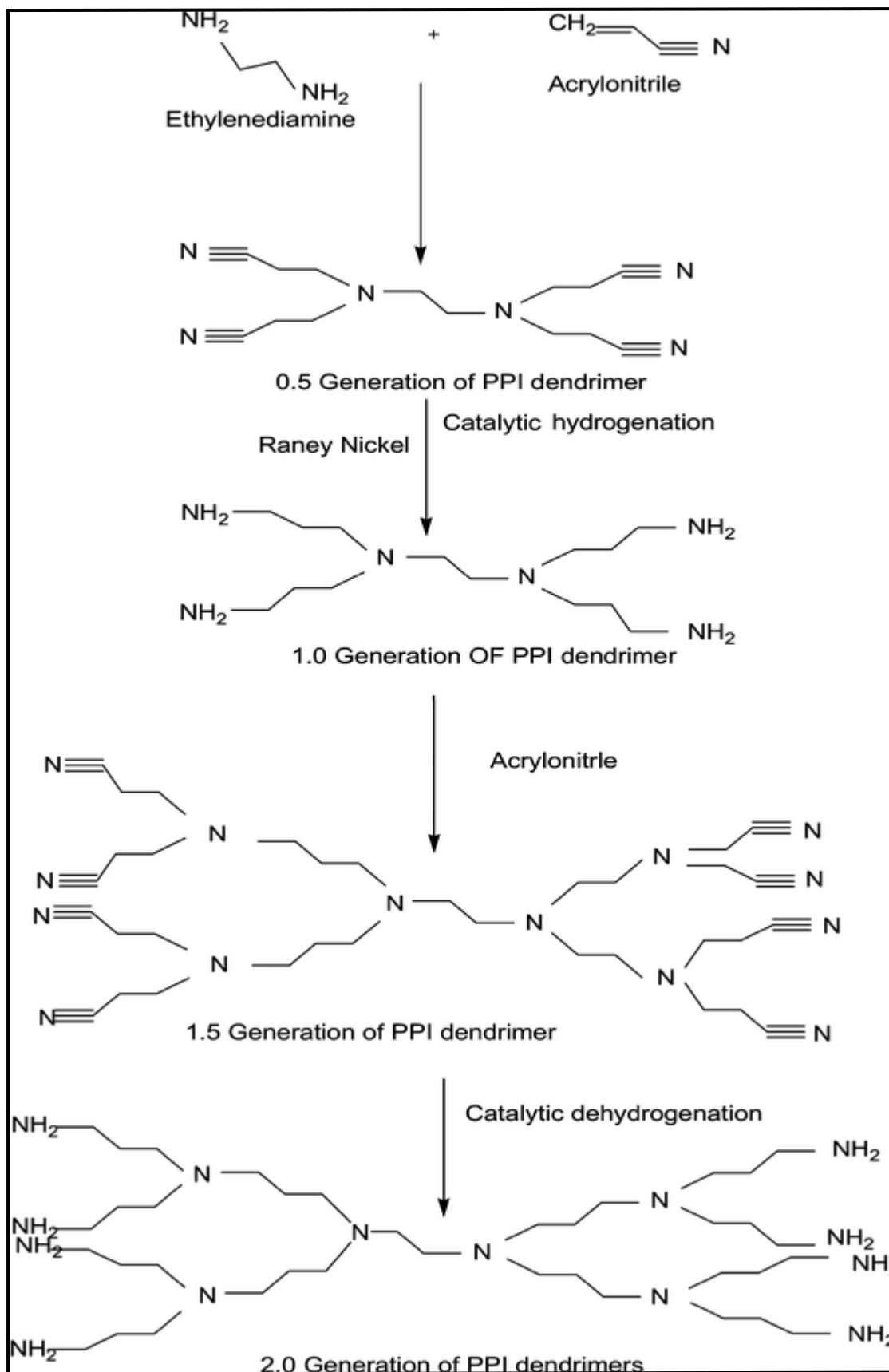
generations of PPI dendrimers are directly proportional to cationic groups present on the surface of the dendrimer [24]. These increment of dendrimer generations which increases the number of surface groups, also increases the toxicological behaviour of the PPI dendrimers [25]. With these being said, it is well documented that 5G dendrimers are more toxic than 4G PPI dendrimers [26-27]. Due to the toxicological problems encountered with increase in dendrimer surface groups, PPI dendrimers are available in the market up to G5. An alternative name to describe this class of PPI dendrimers is POPAM [25]. POPAM in full is known as poly(propylene amine) which is nearly the same as the PPI abbreviation. There is always a comparative study or similar properties between PPI and poly(amido amine) (PAMAM) dendrimers. However, research has increasingly shifted attention towards PPI dendrimers in comparison to PAMAM dendrimers because of the extra-ordinary properties exhibited by PPI dendrimers such as: (1) size is comparatively smaller than PAMAM dendrimers [25], (2) 3G of PPI dendrimers contain 32 amino groups while 4G of PAMAM dendrimers also contain the same number of amino groups [28], (3) toxicity depends on the number of amino groups on PPI [29] while PAMAM shows dose-dependent toxicity [30], and (4) PPI has good biocompatibility while on PAMAM, polyethylene glycol is used as conjugating agent [31]. These dendrimers are synthesised using the divergent approach described below.

## **2.2. Synthesis of PPI dendrimers**

Dendrimers are usually prepared using either the convergent or divergent method. However, amongst the two methods, PPI dendrimers are prepared by the divergent method. This method was the first to be used to prepare dendrimer macromolecules. In the divergent method, the building up of the dendrimer takes place in a step wise manner starting from the core DAB [32], branching outwards until the number of branches wanted is obtained. Therefore, the term generation, results from the addition of branches which then doubles the number of end groups. The major drawback of the divergent method is that it leads to dendrimers with more defects

especially at higher generations (G4-G5) [33], hence making their synthesis more difficult. Therefore, this method is most suitable for the preparation of lower generation dendrimers (G1-G3). To be brief about the preparation of this class of dendrimers, the synthesis involves Michael addition of acrylonitrile to the core DAB or ethylene diamine (EDA) leading to the production of half-generation dendrimer [23] (**see scheme 2.3**).





Scheme 2. 3: Synthesis of PPI dendrimers using the divergent approach [25].

Half-generation formation is followed by the conversion of  $-CN$  groups into  $-NH_2$  groups leading to the formation of full-generation dendrimer by heterogeneous hydrogenation which is catalysed by Raney Nickel. It is quite important to note that the conversion of half- to full-generation is done with the help of hydrogenation. In this reaction, solution of half-generation dendrimers in methanol is mixed with pre-activated Raney Nickel which is then filled in the hydrogenation vessel.

### **2.3. Functionalization of PPI dendrimers and their luminiscence**

Several strategies can be used to improve the properties or performance of PPI dendrimers. One possible approach is to modify the dendrimer backbone structure by functionalizing it with different molecules of interest at their periphery (end-groups) depending on the application of interest, thus increasing its affinity towards that application through formation of PPI composites/derivatives or functionalized PPI. Functionalized PPI dendrimer can be regarded as a material consisting of PPI as a core and one or more components incorporated in the PPI periphery as a shell such as metals, organic compounds (e.g, polymers), and nanoparticles in order to improve properties or extend its functionalities. Therefore, in this review, we focus on the functionalization of PPI with polymers, metals, and nanoparticles.

#### **2.3.1. Organic/polymer-functionalized PPI dendrimers**

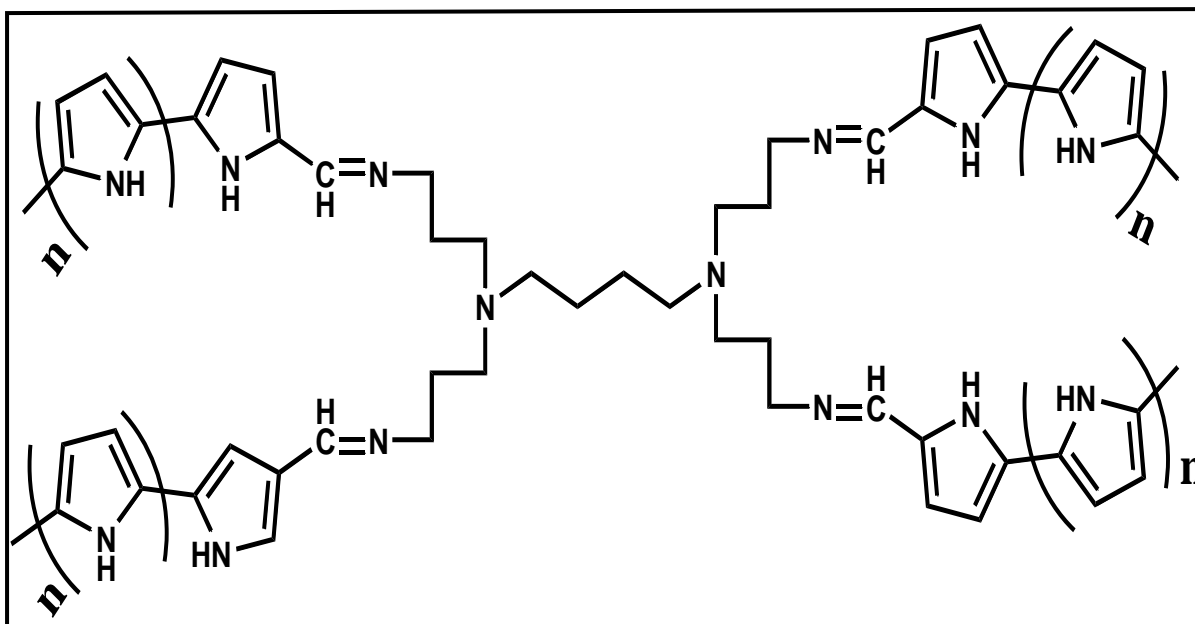
Blending of the spherical structures of PPI dendrimers with linear conducting polymers and other organic compounds is one of the most focal points of the current growing research on dendritic compounds. This interest is motivated by the recognition that the controlled branching of dendritic structures may provide a three-dimensional architecture that allows organic compounds to be incorporated in a geometrically well-defined fashion without losing their attractive properties. However, not only the architecture is important for understanding the

properties of dendrimers, but also the interaction between the polymer functional groups at the exterior of the dendritic surface.

Research has shown that incorporation of different functional units could be used in order to prepare multi-functional materials, for specific applications, in this work being photovoltaics. Thus the incorporation of conductive and photoactive polymer units, such as poly(ethylenedioxythiophene) (PEDOT), poly(pyrrole) (PPY), and poly(aniline) (PANI), may offer advantages over the conventional polymers. It is important to note that polymers are one of the most electron donors and have been widely used in the design of fluorescent and hole-transporting materials. Therefore, the combination of PPI with PEDOT to form the copolymer PPI-co-PEDOT makes this study very interesting.

Functionalization of PPI with polymers is achieved by a Schiff-base condensation reaction of the commercially available PPI's, reacting it with an aldehyde. Briefly, the reaction is between the primary amine of the dendrimer and the carbonyl carbon of the aldehyde. The mechanism proceeds via five steps, which involves the nucleophilic attack (step 1) of the lone pair of  $\text{NH}_2$  attacking the electron deficient carbonyl carbon of the aldehyde, followed by a proton transfer (step 2) resulting in the rearrangement of the position of the proton. Once this is done, protonation of OH (step 3) occurs with the help of the solvent thus enabling the removal of water (step 4) leaving behind a cationic primary imine. The cationic primary imine is then neutralised by deprotonation to form the resultant new imine bond ( $\text{C}=\text{N}$ ).

Recently, Baleg *et al* (2011, 2014) reported on the chemical synthesis of PPI-co-PPY by first functionalizing PPI with 2-pyrrole aldehyde (2-py) which then enabled him to grow the pyrrole polymer on the surface of the dendrimer by coupling via the alpha position of the pyrrole using pyrrole as a monomer [21-22] (see scheme 2.4).



Scheme 2. 4: Example of polymer functionalized PPI: Structure of PPI-co-PPY copolymer functionalized with 2-py [22].

In his photoluminescence studies, the dendritic star copolymer PPI-co-PPY exhibited fluorescence studies with excitation and emission bands at 385 and 422 nm while the parent materials, PPY and PPI, showed excitation and emission bands at 351 and 384 nm, 448 and 391 nm respectively. Looking closely at the results, the bands of the PPI-co-PPY copolymer is observed to be an average of its components indicating the production of a hybrid material. The results are presented in **figure 2.1 below**. Grabchev *et al* (2008) [34] reported on the detection of protons and metal cations by functionalizing PPI with 1, 8-naphthalimide units as fluorescence sensors. When the dendrimer was functionalized with a nitro group as a substituent in a DMF solvent, it was found not to emit any fluorescence. The lack of colour and fluorescence are due to the electron acceptor nature of the nitro group at C4 position. Grabchev further explained that another reason is that the nitro group fails to get into donor-acceptor interaction with the electron acceptor carbonyl groups in the 1, 8-naphthalimide fluorophores. However, upon substitution with an electron donating amino group, the naphthalimide fluorophores are polarised and emit fluorescence in all solvents [34].



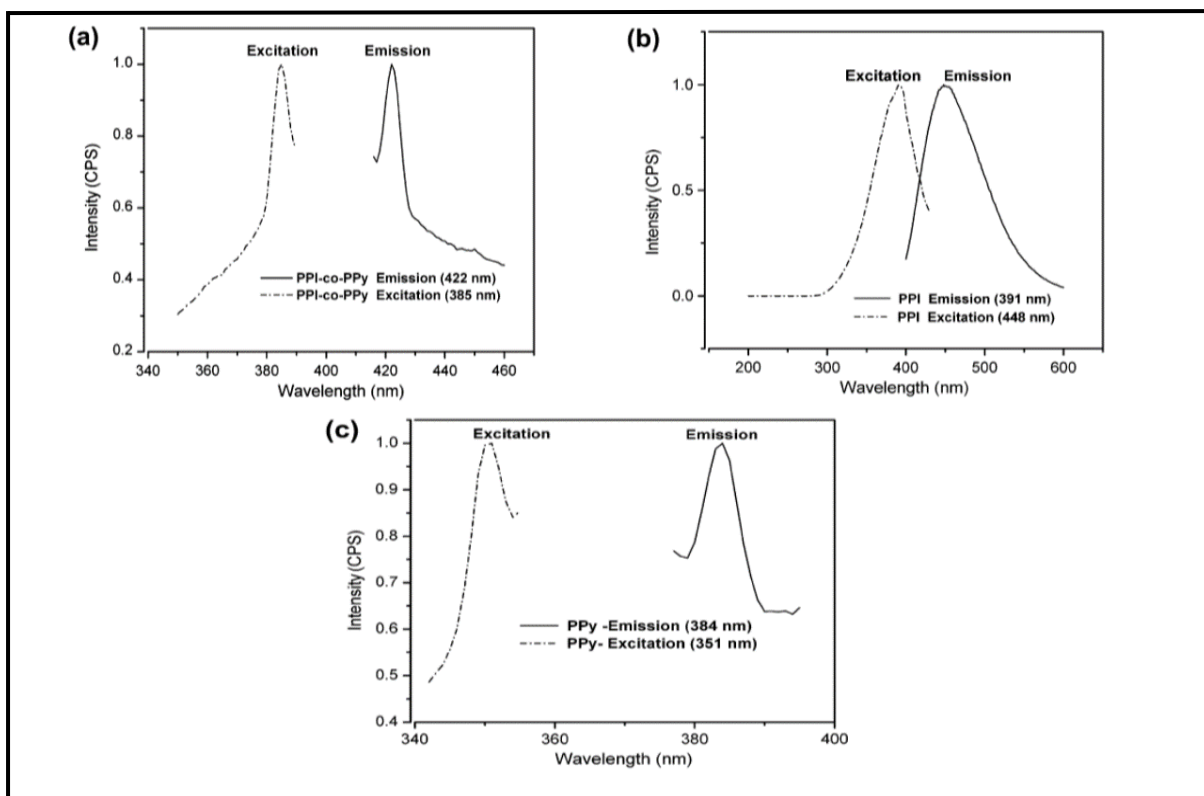
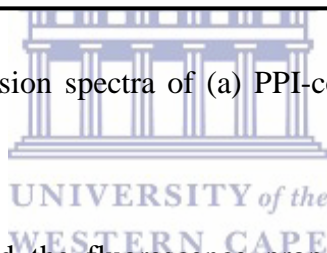


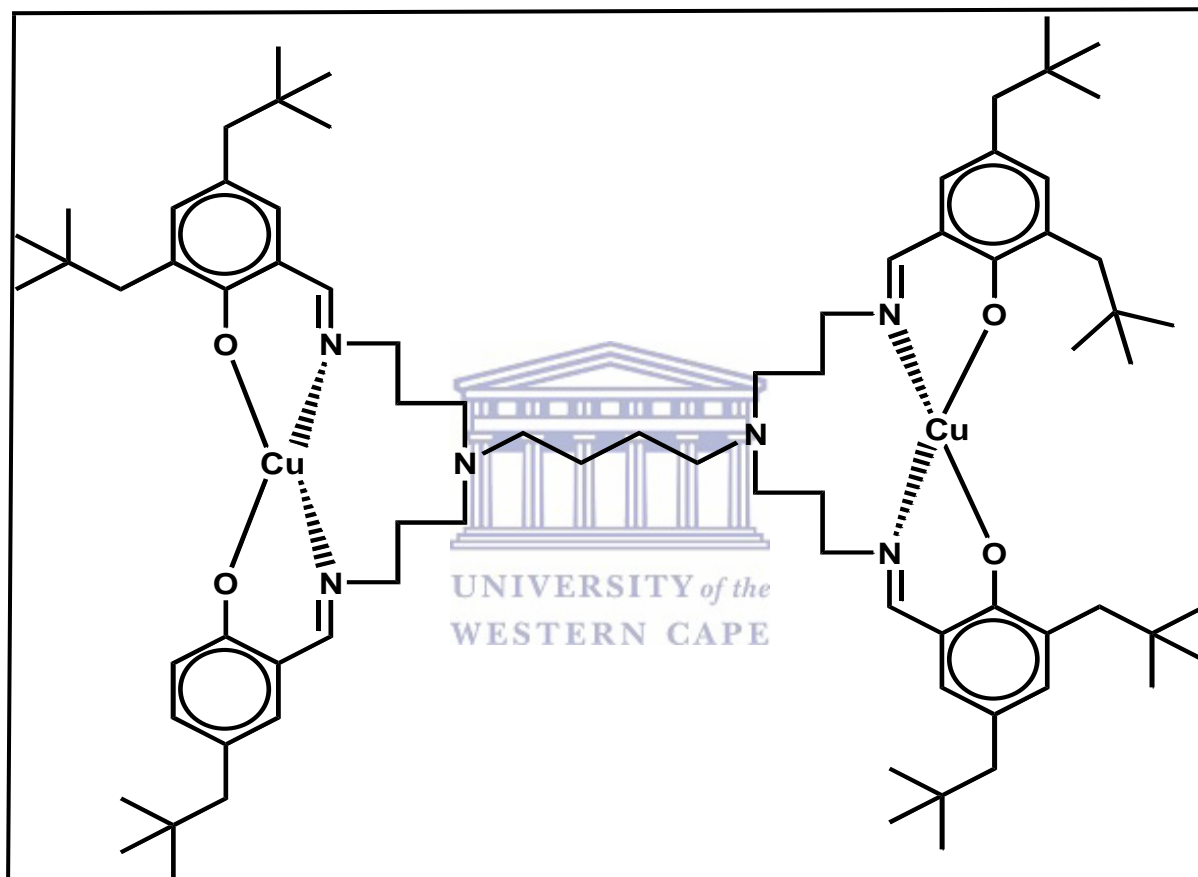
Figure 2. 1: Excitation and emission spectra of (a) PPI-co-PPY (b) PPI dendrimer and (c) polypyrrole [22].



Olowu *et al* (2011) [35] studied the fluorescence properties of PPI functionalised with polythiophene. He observed that the functionalised dendrimer exhibits fluorescence properties with a shift in excitation and emission wavelength to 381 and 480 nm respectively compared to 385 and 455 nm exhibited by pristine PPI. His results are similar to the results obtained by Baleb *et al* (2011) [22]. Therefore this implies that the red shift in emission wavelength is brought by the unique properties of the organic molecules used to functionalize the dendrimer, hence confirming the reason why there is a rapidly growing research interest in functionalised PPI dendrimers for photovoltaic applications.

### 2.3.2. Metal-functionalized PPI dendrimers (metallo-dendrimers)

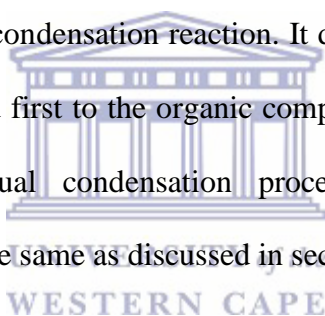
The study of metals coordinated to dendrimer structures dates back to the year 1992. The incorporation of metals to dendrimer moieties creates a new class of compounds called “metallo-dendrimer”. In a simple definition, a metallo-dendrimer is a type of dendrimer functionalised or containing metal atoms in its periphery (see scheme 2.5).



Scheme 2. 5: Copper-poly(propylene imine) metallo-dendrimer (CuPPI) [36].

From an architectural point of view, the coordination of metal-dendrimer can be splitted into three groups: (1) Metal being located at the core to assemble the different wages [37] or to add functionality [38], (2) Metal used as an assembly point in the dendrimer branches. Examples of metals that have been used as connectors are Ru (II), Pt (II), and Pd (II) [39], (3) Dendrimers have been functionalised at the periphery with a manifold of metals [40]. This incorporation of metals onto PPI dendrimers has resulted in materials with enhanced and potential useful

properties. As such, metallodendrimers are now the well-described and well-constructed term of global research due to endeavours of both fields of innovative inorganic and dendrimer chemistry. Owing to their unique properties such as solubility in water, well-defined molecular architecture, and spherical shape, metallodendrimers have found numerous applications in chemical, physical, and biological processes [41]. Recent research has shown that metallodendrimers are suitable materials to overcome the drawbacks faced by linear-chain polymers and metal-less dendritic compounds such that they are capable to act as light harvesting antennas [42], and to be appropriate compounds for optoelectronics applications [42]. Similarly to dendrimers, metallodendrimers can be synthesized by either the divergent or convergent method [43]. With this being said, functionalization of dendrimers with metals can also be achieved via Schiff base condensation reaction. It differs to organic functionalization with that the metal is coordinated first to the organic compound that is used to functionalize the dendrimer before the actual condensation process begins. The reactivity and functionalization mechanism is the same as discussed in section 2.3.1 above.



Grabchev *et al* (2008) [34] investigated the influence of metal cations on the functionalization of first generation PPI dendrimers with 1, 8-naphthalimide units. The focus was specifically on  $Zn^{2+}$ ,  $Cu^{2+}$ ,  $Pb^{2+}$ ,  $Co^{2+}$ ,  $Ni^{2+}$ ,  $Fe^{3+}$ ,  $Mn^{2+}$ , and  $Ag^+$  metal cations. The dendrimers showed substantial increase in fluorescence intensity in the presence of the above mentioned metal cations. **Figure 2.2 below** represents as exemplary case of the changes on the fluorescence intensity as a function of the concentration of  $Pb^{2+}$  cations. The dendrimers free of metal cations showed a very weak fluorescence emission. The addition of  $Pb^{2+}$  cations to the dendrimer led to a considerable increase in the fluorescence emission.

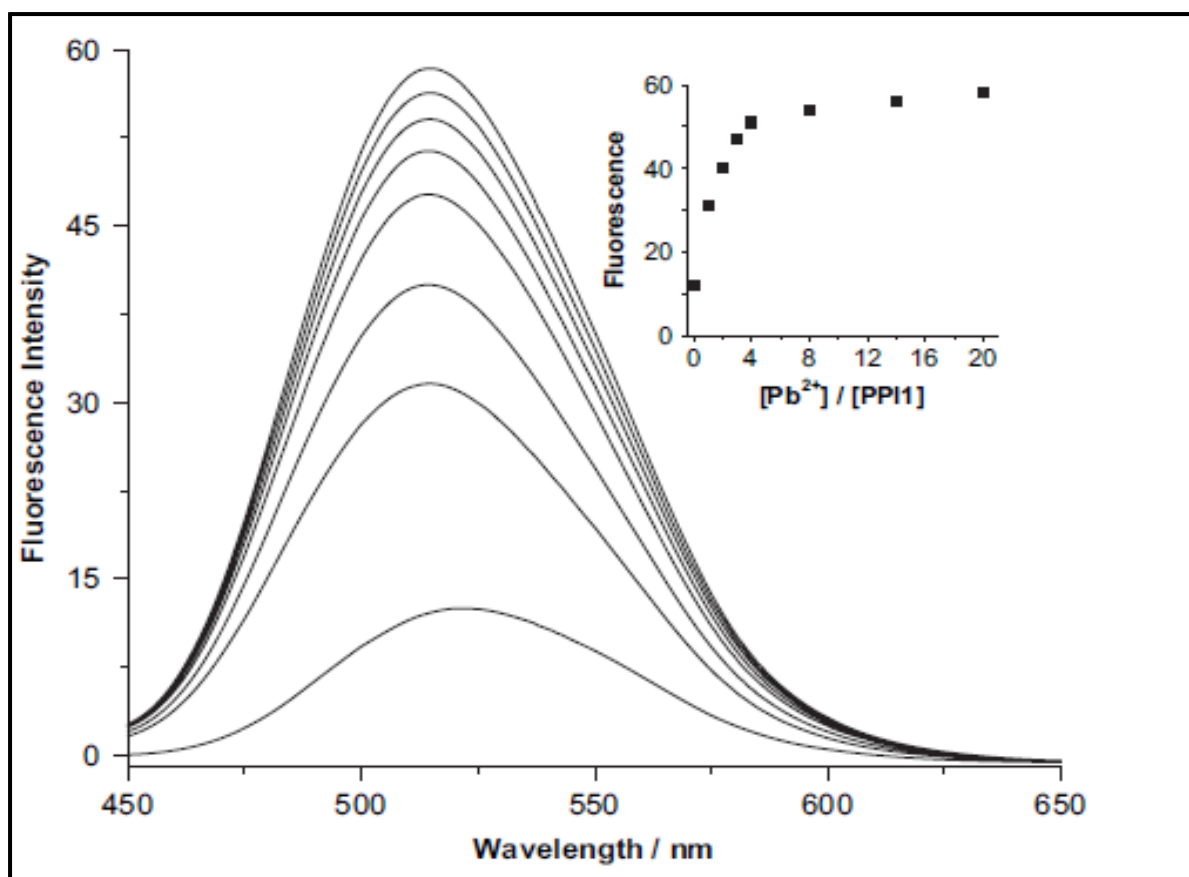
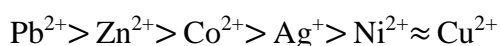


Figure 2. 2: Fluorescence spectra of PPI dendrimer in acetonitrile at various concentrations of  $Pb^{2+}$  [34].

From the figure, it is observed that the position of the fluorescence maxima progressively shifted from 523 to 513 nm with the addition of  $Pb^{2+}$ . The fluorescence of PPI was found to be influenced in the same way with the addition of the other metal cations investigated.

However, another study by Grabchev *et al* (2007) [44] indicated that the influence of the metal cations on the fluorescence intensity is ranked as follows:



This is due to the individual ability of the metal cations to form stable complexes with the PPI dendrimer either at the core or at the periphery. Then the total observed intensity results from the competitive effects of both complexes formation. With the above mentioned, significant

quenching of the fluorescence was observed when  $\text{Cu}^{2+}$  was added to the PPI solution. The quenching was attributed to the formation of a stable complex between the  $\text{Cu}^{2+}$  ions and the tertiary dendrimer core nitrogen atoms. The results comparing the influence of  $\text{Pb}^{2+}$  and  $\text{Cu}^{2+}$  on the fluorescence intensity of the PPI dendrimers are presented in **figure 2.3** below.

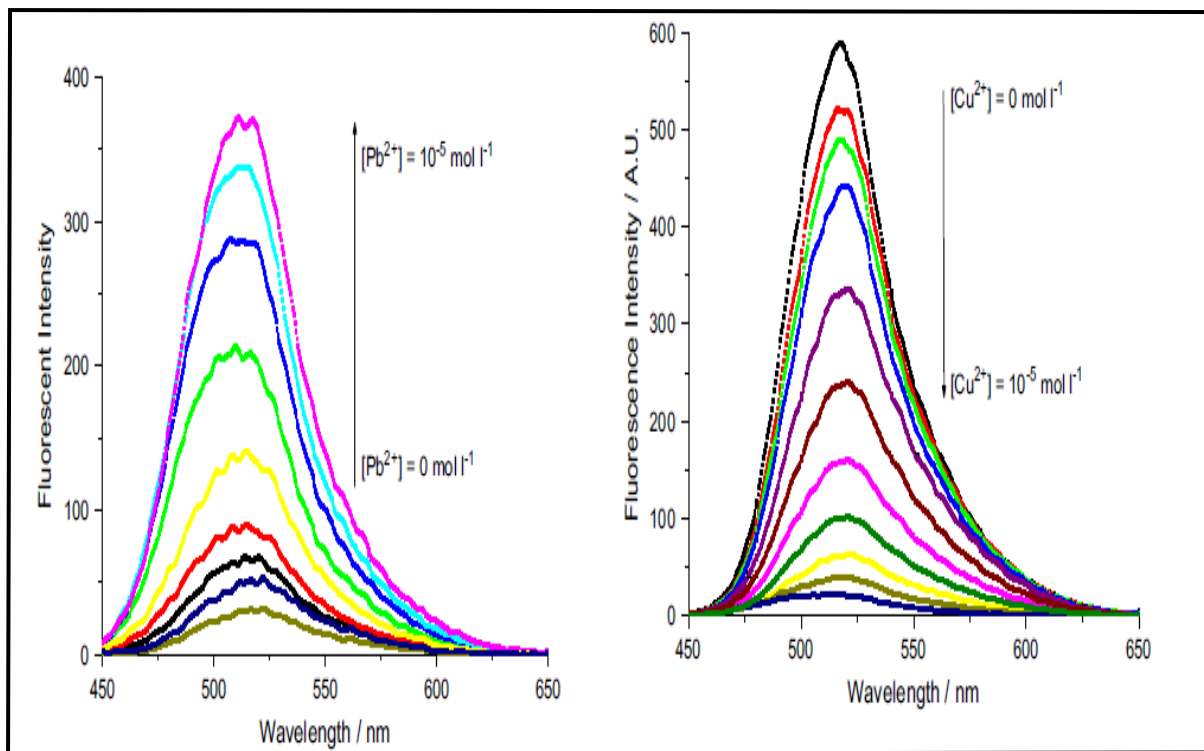
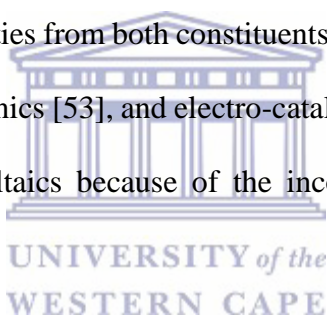


Figure 2. 3: Fluorescence spectra of PPI in acetonitrile at different concentrations of (A)  $\text{Pb}^{2+}$  (B)  $\text{Cu}^{2+}$  [44]

### 2.3.3. Nanoparticle-functionalized PPI dendrimers

In recent years, considerable attention from both fundamental and applied research has been paid to synthesizing and characterizing inorganic nanoparticles functionalized with PPI dendrimers. The shift has been based on nanoparticles because of their great unique properties such as optical, mechanical, and electrical [45-46]. Other nanoparticles such as carbon nanotubes (CNTs) have gained significant attention because they exhibit metallic conductivity, chemical and thermal stability, high tensile strength, and elasticity [46]. However, a major constrain experienced by nanoparticles is their poor solubility and processability [47]. Hence,

considerable efforts have been made to functionalize nanoparticles with PPI dendrimers to enhance solubility and processing. Therefore, PPI dendrimers with their highly branched 3D structural architecture and surface functionality makes them suitable to act as potential templates to host inorganic nanoparticles by forming intra-dendrimer complexes. This is enabled by the peripheral amine groups of the PPI dendrimers that provide a reactive handle for immobilizing the nanoparticles on the surface of the polymer [48]. Recently most studied nanoparticles functionalized with PPI dendrimers for various applications include multiwalled carbon nanotubes (MWCNTs) [46, 49-50], Silver nanoparticles (Ag) [49-50], Palladium nanoparticles [50], and Zirconia [51]. Therefore, the introduction of the nanoparticles onto the surface of PPI dendrimers generate new nanostructures with excellent functions and properties as a result of the combined properties from both constituents, thus increasing their applicability in the fields of optics [52], electronics [53], and electro-catalysis [54]. Hence in this project the application is based on photovoltaics because of the incorporation of ZnSe QD onto the dendritic star copolymer.



## **2.4. Factors that affect the luminescence properties of functionalised PPI dendrimers**

### **2.4.1. Influence of pH on the fluorescence properties**

It is of great interest to investigate the influence of pH on the fluorescence intensity of PPI dendrimers. Grabchev *et al* (2007) [44] investigated the fluorescence intensity in a pH range of 3.4-10.6. In his results, it was observed that the fluorescence intensity increases rapidly in acidic conditions, that is very low pH values of less than 6. The increase in fluorescence intensity at low pH values was further supported by Wang *et al* (2007) [55], Tsuda *et al* (2000) [56], and Grabchev *et al* (2008) [34], as similar observations were reported. The increase in fluorescence intensity at low pH values is due to the protonation of the tertiary nitrogen atoms

in the PPI dendrimer, thus weakening the photo-induced electron transfer (PET) process [34, 44, 56]. The protonated sites results in the increase in the electrostatic repulsions, thus successive neutralization of the amine sites allows the fluorescence to change over a wide pH scale. **Figure 2.4** below is an exemplary plot of pH against fluorescence intensity.

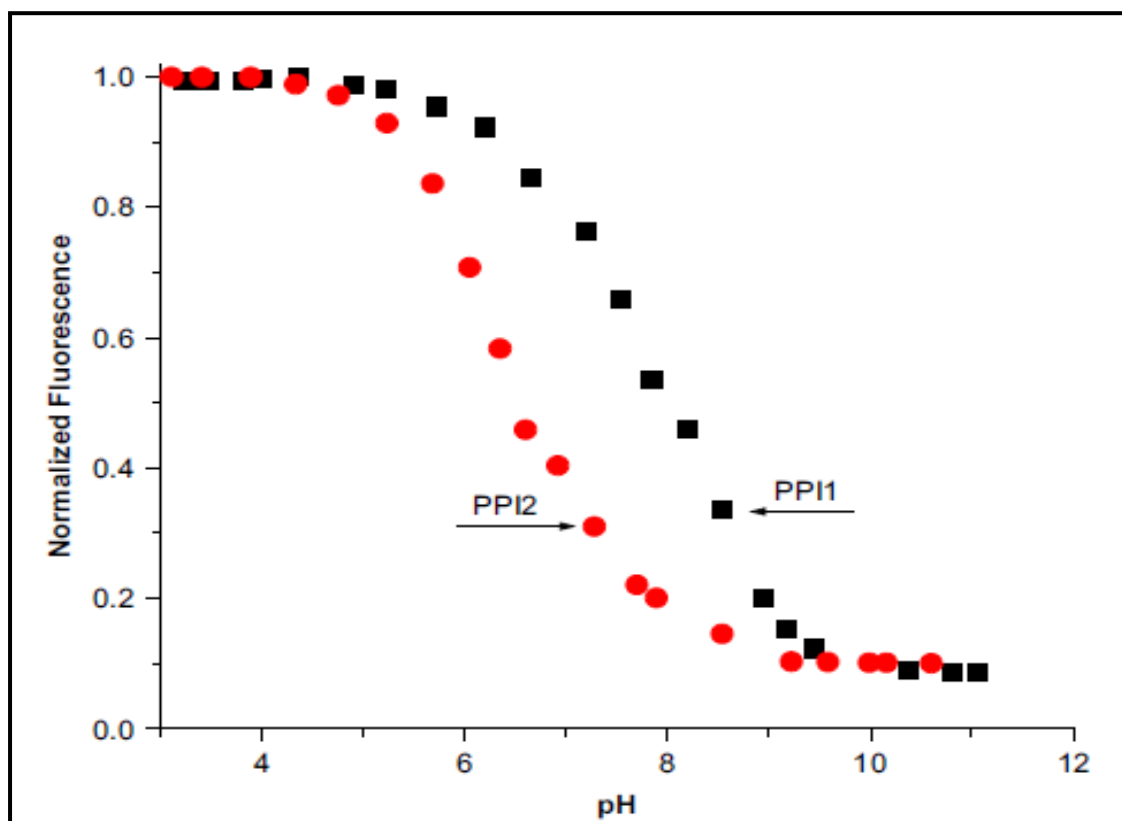


Figure 2. 4: pH dependence of normalised fluorescence intensity for PPI dendrimers [34, 44]

### 2.4.2. Influence of temperature on the fluorescence properties

It is of great interest to investigate the influence of temperature on the fluorescence intensity of PPI dendrimers. Wang *et al* (2007) [55] investigated the fluorescence intensity in a temperature range of 0-45 °C. In his results, the fluorescence intensity increased fast at 45 °C and very low at low temperature values. The results indicate that the higher the temperature, the better the fluorescence intensity. This could be probably due to the massive increase in energy absorbance, thus resulting in the increase in electron excitement as the temperature goes up.

### 2.4.3. Influence of solvent on the fluorescence properties

It is of great interest to investigate the influence of solvent on the fluorescence properties of PPI dendrimers. Grabchev *et al* (2007, 2008) [34, 44] studied the fluorescence characteristics of PPI dendrimers in solvents of different polarity with regards to elucidation of the PET processes. The results obtained showed that the fluorescence quantum yield depends exclusively on the solvent polarity. The results are presented in **table 2.1** below.

Solvent	$\lambda_A$ (nm)	$\lambda_F$ (nm)	$\epsilon(\text{mol}^{-1}\text{cm}^{-1})$	$\nu_A-\nu_F$ ( $\text{cm}^{-1}$ )	$\Phi_F$
Methanol	438	528	44,600	3892	0,022
Ethanol	438	527	44,300	3856	0,031
Propanol	436	526	45,100	3924	0,024
Acetonitrile	434	523	44,800	3921	0,019
DMF	436	526	44,200	3924	0,018
Acetone	432	518	45,600	3843	0,511
Dichloromethane	428	508	45,800	3679	0,601
Chloroform	426	504	45,800	3633	0,861
Tetrahydrofurane	426	505	45,900	3553	0,839

Table 2. 1: Photophysical properties of PPI in different organic solvents [34, 44]

It is said that the PET process accelerates in polar organic solvents, thus leading to lower fluorescence quantum yield.



#### 2.4.4. Influence of concentration on the fluorescence properties

It is of great interest to investigate the influence of concentration on the fluorescence properties of PPI dendrimers. Wang *et al* (2007) [55] studied the fluorescence characteristics of PPI dendrimers at different concentrations. It was indicated that the emission intensity increased linearly with the concentration. Similar results were reported by Grabchev *et al* (2007, 2008) [34, 44]. The results are presented in **figure 2.5** below.

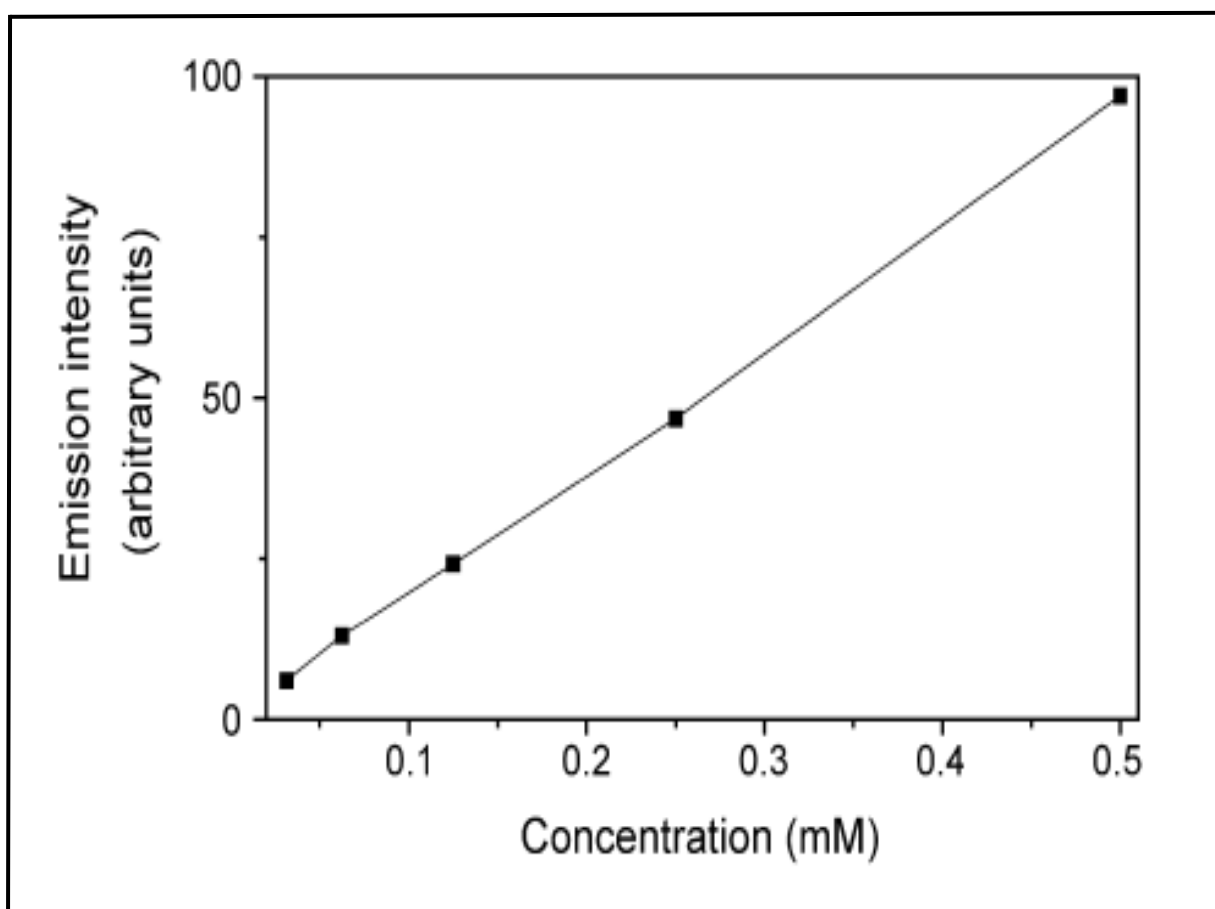


Figure 2. 5: Fluorescence intensity as a function of concentration [55].

## 2.5. References

- [1]- E. Abbasi, S. F. Aval, A. Akbarzadeh, M. Milani, H. T. Nasrabadi, S. W. Joo, Y. Hanifehpour, K. Nejati-Koshki, R. Pashaei-Asl. *Dendrimers: synthesis, applications, and properties*. Nanoscience Research Letters 9 (2014) 247.
- [2]- F. Vögtle, S. Gestermann, R. Hesse, H. Schwierz, B. Windisch. *Functional dendrimers*. Progress in Polymer Science 25 (2000) 987-1041.
- [3]- J. Breitenbach. Spektrum der Wissenschaft/Digest: Moderne Chemie (1998).
- [4]- E. Buhleier, W. Wehner, F. Vogtle. *Cascade - and non-skid-chain-like synthesis of molecular cavity topologies*. Synthesis 55 (1978) 155-158.
- [5]- D. A. Tomalia, H. Baker, J. Dewald, M. Hall, G. Kallos, S. Martin, J. Roeck, J. Ryder, P. Smith. *A New class of polymers: starburst-dendritic macromolecules*. Polymer Journal 17 (1985) 117-132.
- [6]- G. R. Newkome, Z. Yao, G. R. Baker, V. K. Gupta. *Micelles. Part 1. Cascade molecules: a new approach to micelles. A [27]-arborol*. The Journal of Organic Chemistry 50 (1985) 2003-2004.
- [7]- E. R. Gilles, J. M. J. Frechet. *Dendrimers and dendritic polymers in drug delivery*. Drug Discovery Today 9 (2005) 35-43.
- [8]- S. E. Stiriba, H. Frey, R. Haag. *Dendritic polymers in biomedical applications: from potential to clinical use in diagnostics and therapy*. Angewandte Chemie International Edition in English 9 (2002) 1329-1334.
- [9]- G. Spataro, F. Malecaze, C. O. Turrin, V. Soler, C. Duhayon, P. P. Elena. *Designing dendrimers for ocular drug delivery*. European Journal of Medicinal Chemistry 9 (2010) 326-334.
- [10]- D. Boris, M. Rubinstein. *A self-consistent mean field model of a starburst dendrimers: dense core vs. dense shells*. Macromolecules 9 (1996) 7251-7260.

- [11]- J. M. J. Frechet, D.A. Tomalia. *Dendrimers and Other Dendritic Polymers*. Chichester: Wiley (2001).
- [12]- G. R. Newkome, C. N. Moorefield, F. Vögtle. *Dendrimers and Dendrons: Concepts, Syntheses, Applications*. Wiley Weinheim (2001).
- [13]- P. Hodge. *Polymer science branches out*. Nature 9 (1993) 18–19.
- [14]- U. Hahn, M. Gorka, F. Vogtle, V. Vicinelli, P. Ceroni, M. Maestri, V. Balzani. *Light-harvesting dendrimers: Efficient intra- and intermolecular energytransfer processes in a species containing 65 chromophoric groups of four different types*. Angewandte Chemie International Edition 41 (2002) 3595.
- [15]- M. Wells, R. M. Crooks. *Interactions between organized, surface confined monolayers and vapor-phase probe molecules 10. Preparation and properties of chemically sensitive dendrimer surfaces*. Journal of the American Chemical Society 118 (1996) 3988-3689.
- [16]- J. Bu, Z. M. A. Judeh, C. B. Ching, S. Kawi. *Epoxidation of olefins catalysed by Mn(II) salen complex anchored on PAMAMSiO<sub>2</sub> dendrimer*. Catalysis Letters 85 (2003) 183-187.
- [17]- B. D. Viers, B. J. Bauer, Y. Akpalu, F. Groehn, D. Liu, G. Kim. *Hydrogels formed by end-linking peg to dendrimer cross-link agents*. Polymer Preprints 41 (2000) 728-729.
- [18]- I. Majoros, A. Myc, T. Thomas, C. Mehta, J. B. Jr. *PAMAM dendrimer-based multi-functional engineered nano-device for cancer therapy II: Synthesis, characterization, and functionality*. Biomacromolecules 7 (2006) 579-579.
- [19]- J. D. Eichman, A. U. Bielinska, J. F. Kukowska-Latallo, J. R. Baker. *The use of PAMAM dendrimers in the efficient transfer of genetic material into cells*. Pharmaceutical Science & Technology Today 3 (2000) 232-245.
- [20]- H. Kobayashi, S. Kawamoto, T. Saga, N. Sato, A. Hiraga, T. Ishimori, Y. Akita, M. H. Mamede, J. Konishi, K. Togashi, M. W. Brechbiel. *Novel liver macromolecular MR contrast agent with a polypropylenimine diaminobutyl dendrimer core: Comparison to the vascular MR*

*contrast agent with the polyamidoamine dendrimer core.* Magnetic Resonance in Medicine 46 (2001) 795-802.

[21]- A. Baleg, N. Jahed, Anne. Yonkeu, N. Njomo, G. Mbambisa, K. M. Molapo, X. G. Fuku, G. Fomo, H. Makelane, A. Tsegaye, T. T. Waryo, P. Baker, S. Vilakazi, R. Tshikhudo, E. I. Iwuoha. *Impedimetry and microscopy of electrosynthetic poly(propylene imine)-copolypyrrole conducting dendrimeric star copolymers.* Electrochimica Acta 128 (2014) 448-457.

[22]- A. A. Baleg, N. M. Jahed, O. A. Arotiba, S. N. Mailu, N. R. Hendricks, P. G. Baker, E. I. Iwuoha. *Synthesis and characterization of poly(propylene imine) dendrimer-poly(pyrrole) conducting star copolymer.* Journal of Electroanalytical Chemistry 652 (2011) 18-25.

[23]- I. Mishra. *Dendrimer: a novel drug delivery system.* Journal of Drug Delivery and Therapeutics 2 (2011) 70-74.

[24]- M J. Hembade, M. R. Kangane, A. G. Mansuk, H. R. Lukkad. *Dendrimers: as promising nanocarriers for drug delivery.* International Journal of Pharmaceutical and Biological Archive 2 (2013) 61-70.

[25]- D. Kaur, K. Jain, N. K. Mehra, P. Kesharwani, N. K. Jain. *A review on comparative study of PPI and PAMAM dendrimers.* Journal of Nanoparticle Research 18 (2016) 146.

[26]- P. Kesharwani, R. K. Tekade, N. K. Jain. *Formulation development and in vitro–in vivo assessment of the fourth-generation PPI dendrimer as a cancer-targeting vector.* Nanomedicine 9(15) (2014) 1–18.

[27]- P. Kesharwani, R. K. Tekade, N. K. Jain. *Generation dependent cancer targeting poly(propyleneimine) dendrimer.* Biomaterials 35 (2014) 5539–5548.

[28]- N. Shao, Y. Su, J. Hu, J. Zhang, H. Zhang, Y. Cheng. *Comparison of generation 3 polyamidoamine dendrimer and generation 4 polypropyleneimine dendrimer on drug loading,*

*complex structure, release behaviour and cytotoxicity*. International Journal of Nanomedicine 6 (2011) 3361.

[29]- H. M. Marvaniya, P. K. Parikh, V. Patel, K. N. Modi, D. J. Sen. *Dendrimer versatile vectors in gene delivery*. Journal of Chemical and Pharmaceutical Research 2 (2010) 97–108.

[30]- P. Kesharwani, K. Jain, N. K. Jain. *Dendrimer as nanocarrier for drug delivery*. Polymer Science 39 (2014) 268–307.

[31]- S. Pyreddy, P. D. Kumar, P. V. Kumar. *Polyethylene glycolated PAMAM dendrimers-conjugates*. International Journal of Pharmaceutical Investigation 4 (2014) 15.

[32]- U. Gupta, S. K. D. Dwivedi, H. K. Bid, R. Konwar, N. Jain. *Ligand anchored dendrimers based nanoconstructs for effective targeting to cancer cell*. International Journal of Pharmaceutics 393 (2010) 186–197.

[33]- M. Fischer, F. Vogtle. *Dendrimers: From design to application - a progress report*. Angewandte Chemie International Edition 38 (1999) 885-905.

[34]- I. Grabchev, S. Dumas, J. Chovelon, A. Nedelcheva. *First generation poly(propylene imine) dendrimers functionalised with 1, 8-naphthalimide units as fluorescence sensors for metal cations and protons*. Tetrahedron 64 (2008) 2113-2119.

[35]- R. A. Olowu, P. M. Ndangili, A. Baleg, C. O. Ikpo, N. Njomo, P. Baker, E. I. Iwuoha. *Spectroelectrochemical dynamics of dendritic poly(propylene imine)-poly(thiophene) star copolymer aptameric 17 $\beta$ -estradiol biosensor*. International journal of Electrochemical Science 6 (2011) 1686-1708.

[36]- C. Rassie, J. V. Wyk, L. Wilson, H. R. Makelane, U. Feleni, U. Sidwaba, S. Mapolie, P. Baker, E. Iwuoha. *Microscopy and electroanalysis of a first generation copper-poly(propylene imine) metallodendrimer system*. International Journal of Electrochemical Science 10 (2015) 432-444.

- [37]- K. W. Pollak, J. W. Leon, J. M. J. Frechet, M. Maskus, H. D. Abruna. *Effects of dendrimer generation on site isolation of core moieties: electrochemical and fluorescence quenching studies with metalloporphyrin core dendrimers*. Chemistry of Materials 10 (1998) 30-38.
- [38]- C. C. Mak, H. F. Chow. *Dendritic catalysis-reactivity and mechanism of the dendritic Bis (oxazoline) metal complex-catalyzed diels-alder reaction*. Macromolecules 30 (1997) 1228-1230.
- [39]- A. W. Bosman. *Dendrimers in action: structure, dynamics and functionalization of poly(propylene imine) dendrimers Eindhoven*: Technische Universiteit Eindhoven (1999) DOI: 10.6100/IR523548.
- [40]- M. Slany, M. Bardajf, M. J. Casanove, A. M. Caminade, J. P. Majoral, B. Chaudret. *Dendrimer surface chemistry. Facile route to polyphosphines and their gold complexes*. Journal of the American Chemical Society 117 (1995) 9764--9765.
- [41]- J. F. G. A. Jansen, E. W. Meijer. *The dendritic box: Shape selective liberation of encapsulated Guests*. Journal of the American Chemical Society 117 (1995) 4417-4418.
- [42]- M. A. Alam, A. Jahan, M. W. Khan. *A review on dendrimers and metallodendrimers, the important compounds as catalyst in material chemistry*. Advances in Materials 6 (2017) 52-56.
- [43]- S. M. Grayson, J. M. J. Fre'chet. *Convergent dendrons and dendrimers: from synthesis to applications*. Chemical Reviews 101 (2001) 3819-3868.
- [44]- I. Grabchev, P. Bosch, M. Mckenna, A. Nedelcheva. *Synthesis and spectral properties of new green fluorescent poly(propylene imine) dendrimers modified with 1, 8-naphthalimide as sensors for metal cations*. Polymer 48 (2007) 6755-6762.
- [45]- X. Sun, S. Dong, E. Wang. *One-step preparation and characterization poly(propylene imine) dendrimer protected-silver nanoclusters*. Macromolecules 37 (2004) 7105-7108.

- [46]- E. Murugan, S. Arumugam, P. Panneerselvam. *New nanohybrids from poly(propylene imine) dendrimer stabilized silver nanoparticles on multiwalled carbon nanotubes for effective catalytic and antimicrobial applications*. International Journal of Polymeric Materials and Polymeric Biomaterials 65 (2016) 111-124.
- [47]- J. H. T. Luong, S. Hrapovic, D. Wang, F. Bensebaa, B. Simard. *Solubilization of multiwalled carbon nanotubes by 3-aminopropyltriethoxysilane towards the fabrication of electrochemical biosensors with promoted electron transfer*. Electroanalysis 16 (2004) 132-139.
- [48]- Y. Zhou, R. Ma, Y. Ebina, K. Takada, T. Sasaki. *Multilayer hybrid films of Titania semiconductor nanosheet and silver metal fabricated via layer-by-layer self-assembly and subsequent UV irradiation*. Chemistry of Materials 18 (2006) 1235-1239.
- [49]- E. Murugan, G. Vimala. *Effective functionalization of multiwalled carbon nanotube with amphiphilic poly(propylene imine) dendrimer carrying silver nanoparticles for better dispersability and antimicrobial activity*. Journal of Colloid and Interface Science 357 (2011) 354-365.
- [50]- E. Murugan, G. Vimala. *Synthesis, characterization, and catalytic activity for hybrids of multi-walled carbon nanotube and amphiphilic poly(propyleneimine) dendrimer immobilized with silver and palladium nanoparticle*. Journal of Colloid and Interface Science 396 (2013) 101–111.
- [51]- S. K. Shukla, A. K. Mishra, B. B. Mamba, O, A. Arotiba. *Zirconia-poly(propylene imine) dendrimer nanocomposite based electrochemical urea biosensor*. Enzyme and Microbial Technology 66 (2014) 48–55.
- [52]- P. V. Kamat. *Photophysical and photocatalytic aspects of metal nanoparticles*. Journal of Physical and Chemistry B 106 (2002) 7729-7744

[53]- R. Neuendorf, M. Quenten, U. Kreibig. *Optical bistability of small heretogeneous clusters*. Journal of Physical and Chemistry A 104 (1996) 6348-6354.

[54]- T. Sasaki, Y. Ebina, K. Fukuda, T. Tanaka, M. Harada, M. Watanabe. *Titania nanostructured films derived from a Titania nanosheet/polycation multilayer assembly via heat treatment and UV irradiation*. Chemistry of Materials 14 (2002) 3524-3530.

[55]- D. Wang, T. Imae, M. Miki. *Fluorescence emission from PAMAM and PPI dendrimers*. Journal of Colloid and Interface Science 306 (2007) 222-227.

[56]- K. Tsuda, G. C. Dol, T. Gensch, J. Hofkens, L. Latterini, J. W. Weener. *Fluorescence from Azobenzene functionalized poly(propylene imine) dendrimers in self-assembled supramolecular structures*. Journal of the American Chemical Society 122 (2000) 3445-3452.





# CHAPTER THREE

## 3. Experimental

---

This chapter describes the materials and synthetic procedures used for the chemically synthesised two-dimensional and three-dimensional dendritic star copolymers on the basis of innovative dendrimer chemistry, and the synthesis of the quantum dot. The theory of all the analytical techniques used for characterization and interpretation such as Fourier-Transform Infrared Spectroscopy (FTIR), Nuclear Magnetic Resonance (NMR), UV-Visible spectroscopy (UV-Vis), X-ray Diffraction (XRD), Photoluminescence (PL), Transmission Electron Microscopy (TEM), Energy Dispersive Spectroscopy (EDS), Scanning Electron Microscopy (SEM), Thermal Gravimetric Analysis (TGA), and Cyclic Voltammetry (CV) is thoroughly discussed.

### 3.1. Materials and Reagents

Chemical polymerization of the parent materials, PEDOT and G2PPT, together with the dendritic star copolymers, PPT-co-PEDOT and PPT-co-PEDOT-PSSA, was achieved by the use of 3, 4-ethylenedioxythiophene (EDOT, 97%), ferric chloride ( $\text{FeCl}_3$ , reagent grade, 97%), chloroform anhydrous ( $\text{CHCl}_3$ ,  $\geq 99\%$ ), dichloromethane (DCM, anhydrous,  $\geq 99.8\%$ ), methanol anhydrous ( $\text{CH}_3\text{OH}$ , 99.8%), 2- thiophene carbaxaldehyde (2Th, 98%), poly(4-styrene sulfonic acid) solution (PSSA, 18wt% in  $\text{H}_2\text{O}$ ), and second generation poly(propylene imine) dendrimer ( G2PPI). All the above listed chemicals were purchased from Sigma-Aldrich, South Africa except G2PPI which was purchased from Symo-Chem, Eindhoven,

Netherlands. Organo-metallic synthesis of the quantum dot (QD) was achieved by using zinc acetate ( $\text{Zn}(\text{OAc})_2$  99.99% trace metal basis), oleic acid (tested according to ph. Eur), 1-octadecene (technical grade, 90%), selenium powder (Se, 99.99% trace metal basis), trioctylphosphine ( $\text{p}(\text{oct})_3$ , TOP, 97%), and toluene anhydrous ( $\text{C}_7\text{H}_8$ , 99.8%). All the chemicals for quantum dot synthesis were purchased from Sigma-Aldrich, South Africa. Certain characterization techniques were performed by using dimethyl sulfoxide (DMSO,  $\geq 99.5\%$  GC, plant cell cultured), DMSO- $d_6$  (99.9 atom% D), chloroform-d ( $\text{CDCl}_3$  99.8 atom% D), and tetrabutylammonium perchlorate (TBAP, for electrochemical analysis,  $\geq 99.0\%$ ). Deionized water and ethanol (absolute,  $\geq 99.9\%$  GC) were used in all experiments for purification unless otherwise stated.

### 3.2. Chemical synthesis of Poly(3, 4-ethylenedioxythiophene) (PEDOT)

Prior to the synthesis of the homo-polymer, a round bottom flask (250 mL) and a volumetric flask (100 mL) were washed, rinsed and dried for 2 h for complete removal of moisture. Then the glass wares were cleaned with Nitrogen gas ( $\text{N}_2$ ). Poly(3, 4-ethylenedioxythiophene) was prepared by oxidative chemical polymerization of 3, 4-ethylenedioxythiophene (EDOT) monomer following the literature about chemical synthesis of PEDOT with slight modification [1]. Typically, ferric chloride ( $\text{FeCl}_3$ , 0.5677 g, 0.0035 mol) as an oxidising agent and chloroform ( $\text{CHCl}_3$ , 25 mL) were added in a round bottom flask (250 mL) and left to stir for 1h in order for the oxidising agent to be properly dispersed. On the other hand, the monomer EDOT (370  $\mu\text{L}$ , 0.0035 mol) and chloroform ( $\text{CHCl}_3$ , 20 mL) were added in a volumetric flask (100 mL) and allowed to sonicate for 1 hour for the solution to be properly mixed. Immediately after 1 h, the EDOT solution was added dropwise to the oxidant solution to initiate polymerization. The resultant mixture was allowed to proceed for 48 h at 60 °C. Thereafter, the content of the mixture was centrifuged for 30 min to separate the product from the solvent. The remaining content (product) was washed several times with ethanol and water through repeated

centrifugation and then dried at 60 °C for 24 h to evaporate the solvent and remaining volatile compounds.

### **3.3. Chemical synthesis of Poly(3, 4-ethylenedioxythiophene)-poly(4-styrene sulfonic acid) (PEDOT-PSSA)**

Prior to the synthesis of the hetero-polymer, a round bottom flask (250 mL) and a volumetric flask (100 mL) were washed, rinsed and dried for 2 h for complete removal of moisture. Then the glass wares were cleaned with Nitrogen gas (N<sub>2</sub>). PEDOT-PSSA was prepared by *in-situ* oxidative chemical polymerization of EDOT monomer in the presence of PSSA following the literature about chemical synthesis of PEDOT with slight modification [1]. Typically, ferric chloride (FeCl<sub>3</sub>, 0.5677 g, 0.0035 mol) as an oxidising agent and chloroform (CHCl<sub>3</sub>, 25 mL) were added in a round bottom flask (250 mL) and left to stir for 1 h in order for the oxidising agent to be properly dispersed. On the other hand, the monomer EDOT (370 μL, 0.0035 mol), PSSA (1.34 mL), and chloroform (CHCl<sub>3</sub>, 20 mL) were added in a volumetric flask (100 mL) and allowed to sonicate for 1 h for the solution to be properly mixed. Immediately after 1 hour, the EDOT-PSSA solution was added dropwise to the oxidant solution to initiate polymerization. The resultant mixture was allowed to proceed for 48 h at 60 °C. Thereafter, the content of the mixture was centrifuged for 30 min to separate the product from the solvent. The remaining content (product) was washed several times with ethanol and water through repeated centrifugation and then dried at 60 °C for 24 h to evaporate the solvent and remaining volatile compounds.

### **3.4. Synthesis of thiophene-functionalized generation 2 poly(propylene imine) dendrimer (G2PPT)**

Prior to the synthesis of the functionalized dendrimer, a 3-necked round bottom flask (100 mL) was washed, rinsed and dried for 2 h for complete removal of moisture. Then the glass ware was cleaned with Nitrogen gas (N<sub>2</sub>). The synthesis of G2PPT dendrimer proceeded through a Schiff base condensation reaction of G2PPI with 2-thiophe carbaxalydehyde following a reported method [2-4] with modifications. A reaction mixture of poly(propylene imine) generation 2 dendrimer (0.5055 g, 0.6539 mmol) and 2-thiophe carbaxalydeyde (0.5867 g, 5.2316 mmol) in dry methanol (50 mL) was magnetically stirred in a positive pressure of nitrogen gas for 2 days in a three-necked round bottom flask (100 mL). Then methanol was taken out by using rotary evaporation, the remaining oil was dissolved in dichloromethane (DCM) (50 mL), and the organic phase was then washed with water (6 × 50 mL) to remove monomers that did not react. The DCM was then taken out by using rotary evaporation and yielded the desired product as an orange oil.

### **3.5. Chemical oxidative polymerization of EDOT from functionalized G2PPT to form star copolymer G2PPT-co-PEDOT**

Prior to the synthesis of the copolymer, a round bottom flask (250 mL) and a volumetric flask (100 mL) were washed, rinsed and dried for 2 h for complete removal of moisture. Then the glass wares were cleaned with Nitrogen gas (N<sub>2</sub>). G2PPT-co-PEDOT was prepared by *in-situ* oxidative chemical polymerization of EDOT monomer on the surface of G2PPT following the literature about chemical synthesis of PEDOT with slight modification [1]. Typically, ferric chloride (FeCl<sub>3</sub>, 0.5677 g, 0.0035 mol) as an oxidising agent and chloroform (CHCl<sub>3</sub>, 25 mL) were added in a round bottom flask (250 mL) and left to stir for 1 h in order for the oxidising agent to be properly dispersed. On the other hand, the monomer EDOT (370 μL, 0.0035 mol),

G2PPT (0.3382 g, 0.0004375 mol), and chloroform ( $\text{CHCl}_3$ , 20 mL) were added in a volumetric flask (100 mL) and allowed to sonicate for 1 h for the solution to be properly mixed. Immediately after 1 h, the EDOT-PPT solution was added dropwise to the oxidant solution to initiate polymerization. The resultant mixture was allowed to proceed for 48 h at 60 °C. Thereafter, the content of the mixture was centrifuged for 30 min to separate the product from the solvent. The remaining content (product) was washed several times with ethanol and water through repeated centrifugation and then dried at 60 °C for 24 h to evaporate the solvent and remaining volatile compounds.

### **3.6. Incorporation of PSSA to G2PPT-co-PEDOT to form G2PPT-co-PEDOT-PSSA**

Prior to the synthesis of the copolymer, a round bottom flask (250 mL) and a volumetric flask (100 mL) were washed, rinsed and dried for 2 h for complete removal of moisture. Then the glass wares were cleaned with Nitrogen gas ( $\text{N}_2$ ). G2PPT-co-PEDOT-PSSA was prepared by *in-situ* oxidative chemical polymerization of EDOT monomer on the surface of G2PPT in the presence of PSSA following the literature about chemical synthesis of PEDOT with slight modification [1]. Typically, ferric chloride ( $\text{FeCl}_3$ , 0.5677 g, 0.0035 mol) as an oxidising agent and chloroform ( $\text{CHCl}_3$ , 25 mL) were added in a round bottom flask (250 mL) and left to stir for 1 h in order for the oxidising agent to be properly dispersed. On the other hand, the monomer EDOT (370  $\mu\text{L}$ , 0.0035 mol), G2PPT (0.3382 g, 0.0004375 mol), PSSA (1.34 mL), and chloroform ( $\text{CHCl}_3$ , 20 mL) were added in a volumetric flask (100 mL) and allowed to sonicate for 1 hour for the solution to be properly mixed. Immediately after 1 h, the EDOT-PPT-PSSA solution was added dropwise to the oxidant solution to initiate polymerization. The resultant mixture was allowed to proceed for 48 h at 60 °C. Thereafter, the content of the mixture was centrifuged for 30 min to separate the product from the solvent. The remaining content

(product) was washed several times with ethanol and water through repeated centrifugation and then dried at 60 °C for 24 h to evaporate the solvent and remaining volatile compounds.

### **3.7. Synthesis of Zinc selenide quantum dot (ZnSe QD)**

Zinc selenide quantum dot was synthesized following a reported procedure [5] based on organic synthesis of zinc selenide quantum dot. Briefly, a solution precursor of zinc was prepared by mixing zinc acetate (1.2 g, 6.540 mmol), oleic acid (1.2 mL), and 1-octadecene (20 mL) in a flask and heated up to 290 °C. On the hand, a selenide precursor solution was prepared by mixing elemental selenium (0.1 g, 1.266 mmol), trioctylphosphine (1 mL), and 1-octadecene (10 mL) in a separate flask and heated up to 225 °C. Then the selenide solution was injected into the hot zinc solution and was allowed to react for 5 min. After injection for ZnSe QD growth, the mixture was stopped and immediately quenched and cooled down by pouring toluene (10 mL). Methanol (5 mL) was then poured into the mixture to precipitate the quantum dot. The product was washed several times using ethanol and water through repeated centrifugation and dried at 45 °C overnight to evaporate the solvent and other volatile compounds.

### **3.8. Preparation of the active layer: G2PPT-co-PEDOT-PSSA: ZnSe QD**

2.3 mg/mL of G2PPT-co-PEDOT-PSSA was prepared by dissolving 23 mg of the star copolymer in DMSO (10 mL) and sonicated for 1 h. On the other hand, 2.3 mg/mL of ZnSe QD was also prepared by dissolving 23 mg of ZnSe in toluene (10 mL) and sonicated for 1 h. Then the blends or active layers were prepared in five different ratios by mixing:

- 1 mL of G2PPT-co-PEDOT-PSSA solution with 1 mL ZnSe solution ( 1:1 layer)
- 1 mL of G2PPT-co-PEDOT-PSSA solution with 2 mL ZnSe solution ( 1:2 layer)
- 1 mL of G2PPT-co-PEDOT-PSSA solution with 3 mL ZnSe solution ( 1:3 layer)
- 2 mL of G2PPT-co-PEDOT-PSSA solution with 1 mL ZnSe solution ( 2:1 layer)

- 3 mL of G2PPT-co-PEDOT-PSSA solution with 1 mL ZnSe solution ( 3:1 layer)

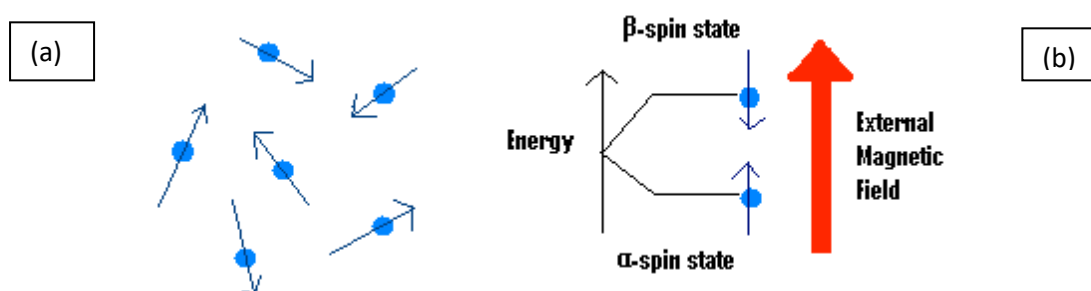
The resultant mixtures were further sonicated for a period of 24 h.

### 3.9. Analytical Techniques

Analytical methods are set of techniques which are used to determine the chemical, physical or optical nature of a material and also to quantify certain species within the material under study. The following analytical techniques were employed in this work.

#### 3.9.1. Proton Nuclear Magnetic Resonance spectroscopy ( $^1\text{H}$ NMR)

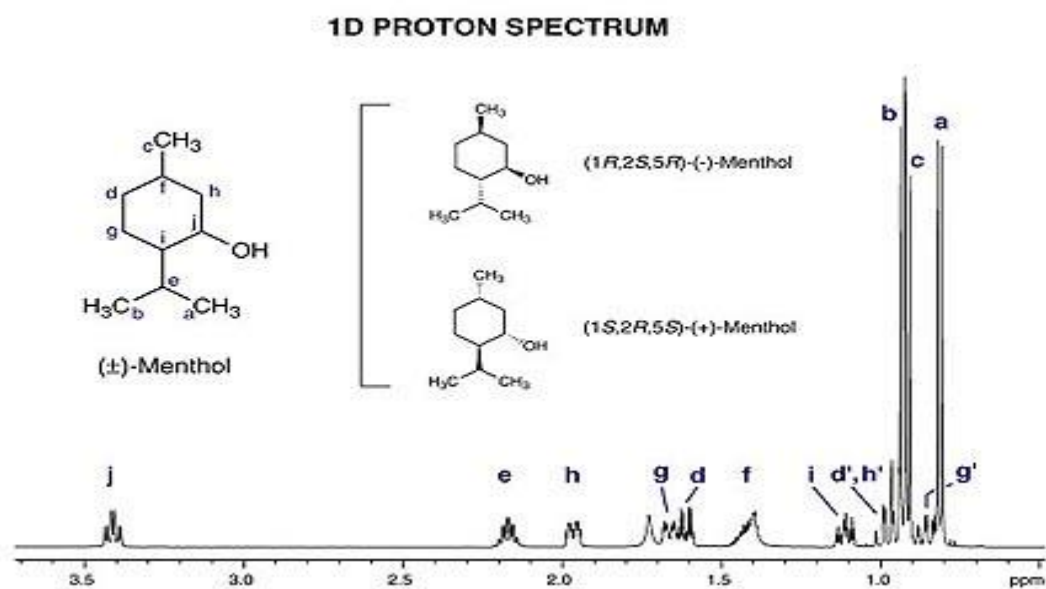
NMR spectroscopy is a technique employed to detect a compound's distinctive structure with respect to hydrogen-1 nuclei. It distinguishes the carbon-hydrogen interaction of an organic compound. In general, the principle revolves around the atomic nucleus spin when subjected to an applied external magnetic field. Without an external applied magnetic field, the nucleus spin are unsystematic or unspecific and spin in unspecific directions. But, when an external magnetic field is present, the nuclei line-up either with or against the field of the external magnet (see scheme 3.1).



Scheme 3. 1: (a) No applied external magnetic field, (b) external magnetic field is applied.

However, the energy difference ( $\Delta E$ ) between two spin states increases as the strength of the applied magnetic field increases. Now, for  $^1\text{H}$  NMR to give signals, the nuclei must undergo relaxation. Relaxation is when the nuclei returns to their original state after being subjected to

an external magnetic field. During this process, they emit electromagnetic signals whose frequencies are dependent on the difference in energy between two spin states.  $^1\text{H}$  NMR then reads these signals and plot them on a graph of signal frequency versus intensity (see scheme 3.2). It should be well stated that simple NMR spectra are recorded in solution, and solvent protons must not be allowed to interfere. With this being said, deuterated (often symbolised as D) solvents are preferred.



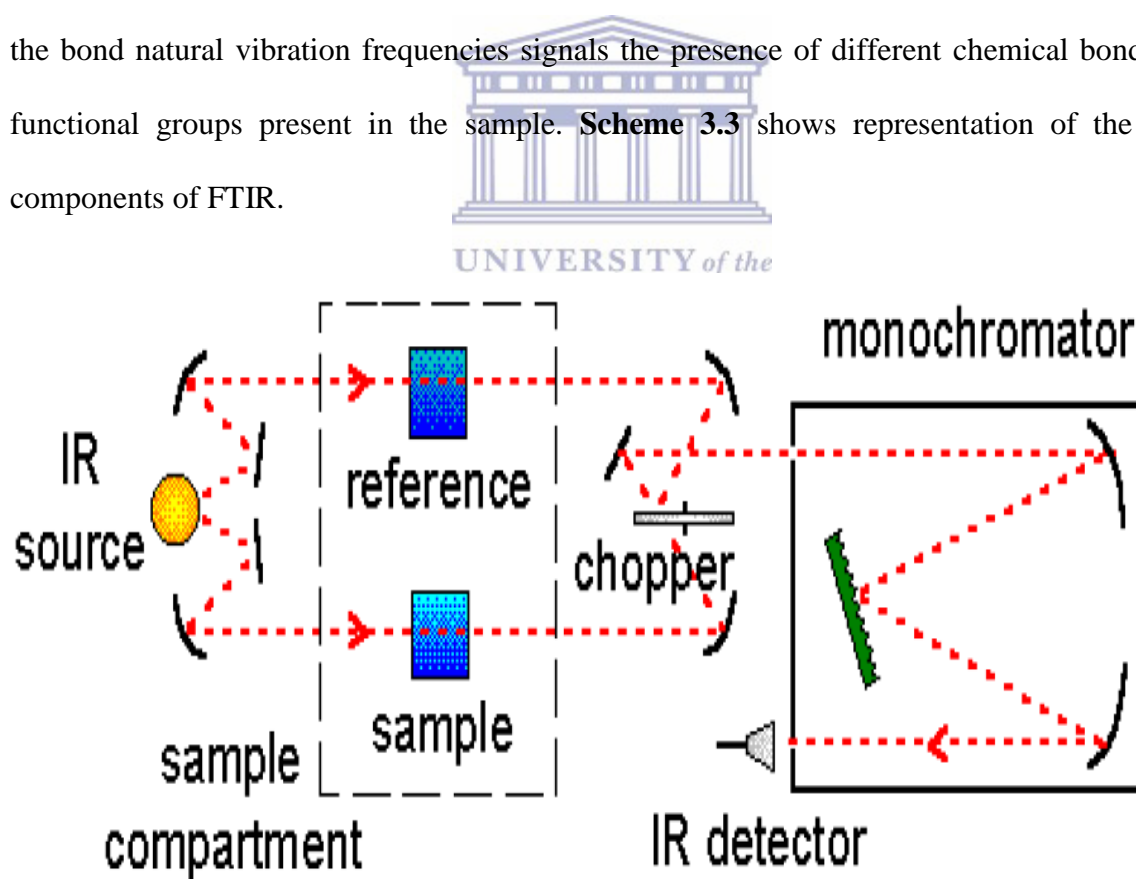
Scheme 3. 2: Typical 1-dimensional proton spectrum.

In this work,  $^1\text{H}$  NMR was employed to confirm the chemical structures of G2PPT, PEDOT, PEDOT-PSSA, G2PPT-co-PEDOT, and G2PPT-co-PEDOT-PSSA. In order to achieve that,  $^1\text{H}$  NMR spectra were recorded on a 200 MHz, Varian Gemini XR200 spectrometer, using  $\text{CDCl}_3$  and  $\text{DMSO-d}_6$  as solvents.



### 3.9.2. Fourier Transform Infrared Spectroscopy (FTIR)

Fourier transform infrared spectroscopy (FTIR) is a technique which is employed to acquire an infrared spectrum of absorption or emission of a liquid, solid, or a gas. FTIR depends on the certainty that almost all molecules absorb light in the infra-red region of the electromagnetic spectrum [6-7]. This absorption coincide precisely with the functional groups present in the molecule. The frequency values are denoted as wave numbers usually over the range 4000 – 400  $\text{cm}^{-1}$ . The background emission spectrum of the IR source is first measured which is used to rectify the spectra recording of analytes, followed by the emission spectrum of the IR source with the sample in place [8]. The ratio of the sample spectrum to the background spectrum is directly related to the sample's absorption spectrum. The resultant absorption spectrum from the bond natural vibration frequencies signals the presence of different chemical bonds and functional groups present in the sample. **Scheme 3.3** shows representation of the basic components of FTIR.

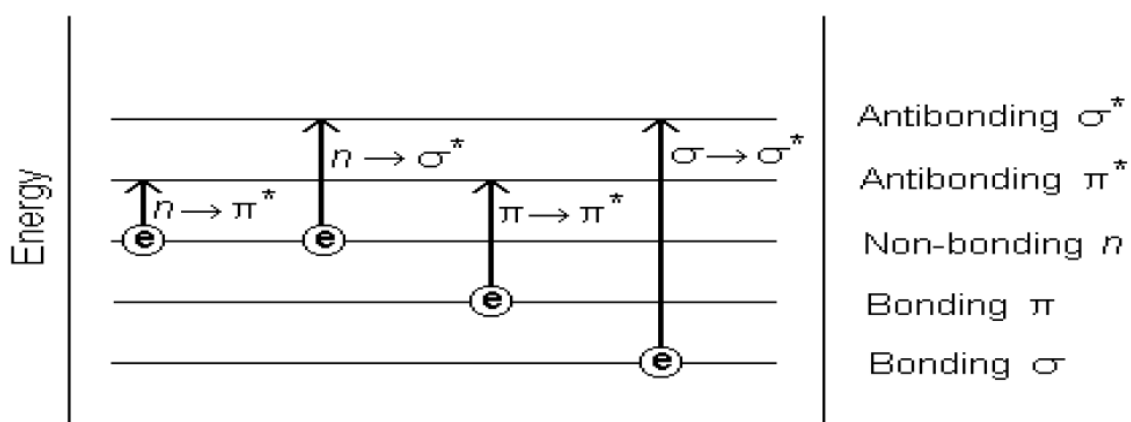


Scheme 3. 3: Simplified schematic illustration of a dispersive IR spectrometer [9].

FTIR is mainly used for qualitative analysis in which the functional groups of the sample is determined. In this work FTIR was used to observe functional groups present in G2PPT, PEDOT, G2PPT-co-PEDOT, PEDOT-PSSA, and G2PPT-co-PEDOT-PSSA. In order to achieve that, FTIR spectra were recorded using a PerkinElmer Spectrum 100 FTIR spectrometer at a range of 400-4000  $\text{cm}^{-1}$  wavenumber. The powder samples were mixed with KBr prior to analysis.

### 3.9.3. Ultraviolet-Visible Spectroscopy (UV-Vis)

UV-Vis refers to the reflectance or absorption spectroscopy in the ultraviolet-visible region. This implies that it utilises light in the visible and adjacent (near-UV and near-infrared) ranges. Basically, it is used to study the electronic transitions that molecules undergo. It is routinely used in analytical chemistry for qualitative and quantitative analysis such as (i) characterizing aromatic compounds and conjugated olefins, and (ii) to find out the molar concentration of the solute under study. In principle, light is irradiated on a molecule. The  $\pi$  electrons or non-bonding electrons absorb the energy from the oncoming radiation in the form of ultraviolet or visible light and are thus excited from ground state to higher energy state [6, 10]. The transitions are summarised in the **Scheme 3.4** below.



Scheme 3. 4: Possible electronic transitions of  $\pi$ ,  $\sigma$ , and  $n$  electrons [10]

The absorbed energy to excite the electrons is equal to the energy separation between the filled valence band and the empty or partially filled conduction band. This energy separation is known as the band gap. Its mathematical relation is as follows:

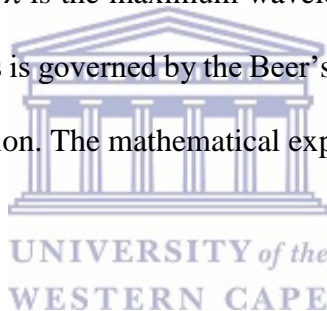
$$\Delta E = h\nu \quad 3.1$$

Where  $\Delta E$  is the difference in energy between the valence and conduction band,  $h$  is Planck's constant, and  $\nu$  is the photon frequency. However, since the relationship between frequency and wavelength is known ( $\nu \propto 1/\lambda$ ) then equation 3.1 rearranges to:

$$\Delta E = \frac{hc}{\lambda} \quad 3.2$$

Where  $c$  is the speed of light and  $\lambda$  is the maximum wavelength at which the sample absorbs at. The whole principle of UV-Vis is governed by the Beer's Law which relates the absorbance and the concentration of the solution. The mathematical expression of the law is as follows:

$$A = \epsilon bc \quad 3.3$$

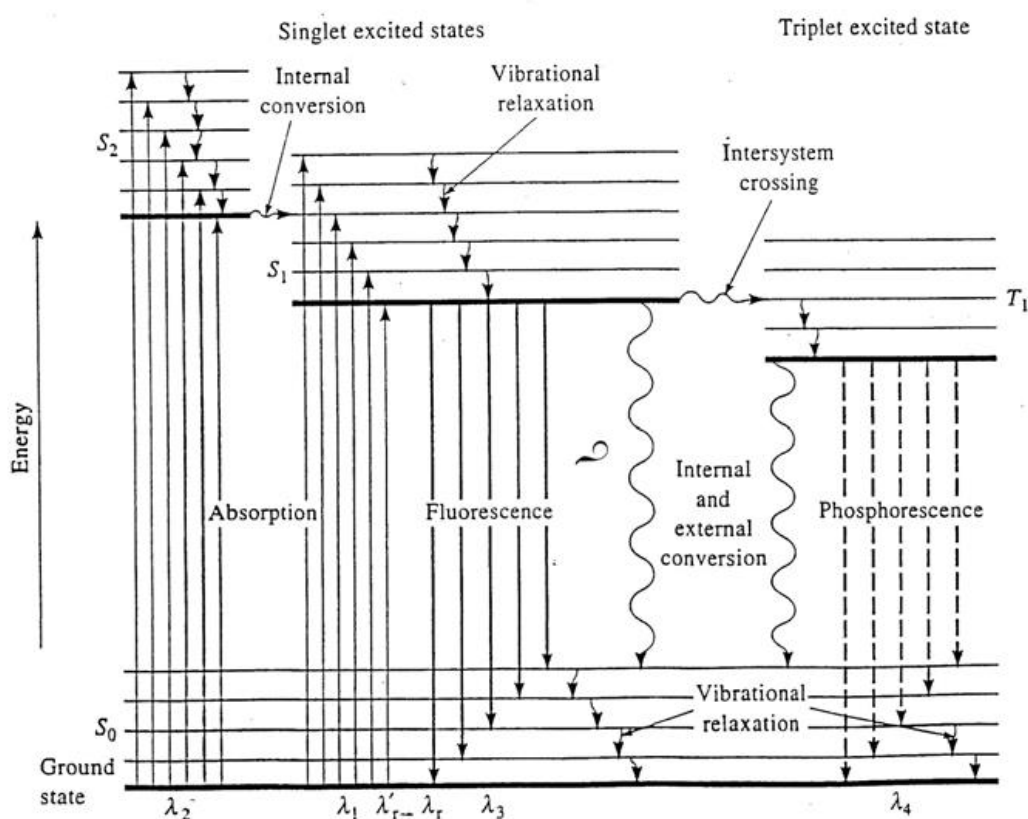


Where  $\epsilon$  is the molar absorptivity of the material,  $b$  is the path length of the cell, and  $c$  is the concentration of the sample under study. In this work, UV-Vis was employed to study the possible electronic transitions which enabled the determination of the optical band gap of the as synthesized materials. In order to achieve this, UV-Vis measurements were recorded using a Nicolet Evolution 100 UV-Visible spectrometer (Thermo electron, UK) at a range of 200-1000 nm wavelength.

#### **3.9.4. Fluorescence/ Photoluminescence Spectroscopy (PL)**

Fluorescence is an analytical technique that in principle is more similar to ultraviolet-visible spectroscopy. Briefly, fluorescence is a spectrochemical technique that is normally employed to excite molecules or atoms of a particular analyte by irradiating them at a certain fixed wavelength of interest but emit photons of different wavelength, usually longer wavelength

(low energy). This technique provides both qualitative and quantitative information about the analyte. When light of an appropriate wavelength is absorbed (i. e excitation), the transition of the molecule changes the electronic state from the ground state, usually denoted as  $S_0$ , to the excited state ( $S_1$ - $S_n$ ), particularly to the vibrational levels in the excited states. Therefore, once the molecule is in this excited state, relaxation can occur through several processes. Fluorescence is one of these processes and results in the emission of light. The whole processes are summarised using the Jablonski diagram in **scheme 3.5** below.



Scheme 3. 5: Jablonski diagram showing the electronic transition levels [6].

In this work, photoluminescence was employed to investigate the emission of the samples which is an important technique especially for solar cells application. In order to achieve this, Fluorescence properties of the samples were recorded using Horiba NanoLog™ - TRIAX (USA), with double grating excitation and emission monochromators with a slit width of 5 nm.

### 3.9.5. X-Ray Diffraction (XRD)

X-ray Diffraction (XRD) is a versatile, non-destructive technique which renders comprehensive information about the chemical composition and crystallographic structure of many kind of materials; natural and manufactured. It is therefore an indispensable technique in material characterization. These technique is based on constructive interference of monochromatic X-rays and a crystalline sample of which interaction of the incident rays with the sample induces constructive interference such that Bragg's law is satisfied. The mathematical expression of the law is as follows [8]:

$$n\lambda=2d\sin\theta \quad 3.4$$

Where  $\lambda$  designates the wavelength of the radiation beam,  $d$  is the interplanar spacing between two diffracting lines,  $\theta$  is the diffraction angle, and  $n$  is an integer usually equal to 1. XRD is extensively employed for the detection or determination of unknown crystalline materials such as inorganic compounds and minerals, measurements of sample purity, characterisation of crystalline materials, and determination of unit cell dimensions [7]. The technique possesses numerous advantages such as being powerful and rapid (<20 min) for identification of unknown materials and data analysis is relatively easy. However, its disadvantage is that peak overlay may occur and worsens for high angle reflections and that for fixed materials, detection limit is ~2% of sample [11]. In this study, XRD was used for phase identification and material crystallinity. In order to achieve this, XRD measurements were recorded using a Bruker AXS D8 Advance diffractometer (voltage 40 KV; current 40 mA) at a range 10-90 degrees.

### 3.9.6. Thermogravimetric Analysis (TGA)

TGA is a method that is normally employed to monitor changes in chemical and physical properties of samples when subjected to increasing temperature conditions but at constant rate of heating. It reveals information about physical phenomena such as vaporization, sublimation, adsorption, and desorption. Likewise, it also reveals information about chemical phenomena such as chemisorption, desolvation, and decomposition [8]. TGA is commonly utilised to deduce selected features of materials that display either mass gain or loss due to oxidation, decomposition, or loss of volatiles (such as moisture). Its common applications are (i) determination of organic content in a sample, and (ii) studies of reaction kinetics and degradation mechanisms [8]. Again, TGA can be utilized to assess the thermal stability of a material. In simple terms, there will be no observed mass changes if a material under study is thermally stable. Advantages of this method are that it provides very little room for instrumental error and does not require a series of standards for calculation of an unknown. Its disadvantage is that it only provides for the analysis of a single element, or a limited group of elements at a time. In this work, TGA was employed to estimate the thermal stability of the materials particularly after the introduction of PSSA on the star copolymer back bone. In order to achieve this, the thermal stability was performed using a Perkin-Elmer TGA 4000 instrument connected to a PolyScience digital temperature controller under N<sub>2</sub> gas purged at a flow rate of 20 ml/min. The calibration of the instrument was performed using indium (melting point =156.6 °C) and aluminium (melting point = 660 °C). Samples ranging between 1–4 mg were heated from 30-900 °C at a constant heating rate of 10 °C /min. The data was collected and analysed using Pyris software®.

### **3.9.7. Scanning Electron Microscopy (SEM)**

SEM is a type of scanning probe microscopy. Briefly, scanning electron microscope is a muscular microscope that utilises electrons instead of light to produce an image of objects such as foreign particles and residues, fractured metal components, biological samples, and polymers. It utilises a focused beam consisting of high energy electrons (approximately 20 KV) to create a diversity of signals at the surface of solid samples. The signals arise from the interaction of the electron and the sample and show information about the sample including chemical composition, external morphology (texture), crystalline structure and orientation of materials making up the sample. The advantages related with SEM involve, among others, its capability to perform analyses of selected point locations on the sample. Areas ranging from approximately 1 cm to 5 microns can also be imaged in a scanning mode using conventional SEM techniques (magnification ranging from 20× to approximately 30,000×, and a spatial resolution of 50 to 100 nm) [12]. In this work, SEM was employed to investigate the surface morphological properties of the materials. In order to achieve this, the SEM images were recorded using a SEM Gemini LEO 1525 Model microscope.

### **3.9.8. High-Resolution Transmission Electron Microscopy (HRTEM)**

HRTEM is an electron probe microscopy. Basically, it is an imaging mode of TEM that permits for direct imaging of the sample's atomic structure. It is widely used by most scientists to study or investigate atomic scale properties of materials such as nanoparticles, semiconductors, metals, and sp<sup>2</sup>-bonded carbon like graphene. In principle, a beam of electrons is transmitted through the sample (with an accelerating voltage of 300 KV), interacting with it as it passes through. Then an image is formed from the interaction of the electrons through the sample. The transmitted beam contains information about electron density, periodicity, and phase. The quantum mechanical properties of electrons are such that the electron has a wavelength defined by de Broglie relationship:

$$\lambda = \frac{h}{p} = \frac{h}{\sqrt{2M_0E}} \quad 3.5$$

Where  $h$  is the Planck constant,  $M_0$  is the rest mass of electron, and  $E$  is the acceleration voltage. But because electrons in TEM are known to be moving at a very high speed defined by the accelerating voltage of the electron gun, then the equation rearranges to the relativistic version as follows:

$$\lambda = \frac{hc}{\sqrt{2EE_0 + E^2}} \quad 3.6$$

Where  $E_0$  is the rest energy and  $c$  is the speed of light. In this work, HRTEM was employed to investigate the internal composition, shape and size of the materials. In order to achieve this, HRTEM images were recorded using a FEI Tecnai G2 20 transmission electron microscope (TEM) coupled with EDX, operating at an accelerating voltage of 200 kV.

### 3.9.9. Cyclic Voltammetry (CV)

Cyclic voltammetry (CV) is an electrochemical method that estimates the current that evolves in an electrochemical cell under conditions where potential is in surplus of that speculated by the Nernst equation [7, 11, 13]. CV (**Figure 3.1**) is performed by cycling the potential of a working electrode, and estimating the resulting current. In this technique, it is compulsory to have a working, reference, counter electrode, and an electrolytic solution to be added to the sample solution to make sure that conductivity is sufficient [13]. It is frequently utilised to study or investigate a diversity of redox processes, the involvement of intermediates in redox reactions, to detect the stability of reaction products, electron transfer kinetics and the reversibility of a reaction [11]. During CV experiment, the potential of the working electrode is ramped linearly against time. The potential of the working electrode is inverted when cyclic voltammetry reaches a potential that is fixed, and this inversion can occur numerous times in only one experiment. The peak potentials ( $E_{pc}$ ,  $E_{pa}$ ) and the peak currents ( $I_{pc}$ ,  $I_{pa}$ ) are the



important parameters in a recorded cyclic voltammogram for the anodic and cathodic scans, respectively. An electrochemically reversible reaction occurs when the electron transfer is faster than other processes such as diffusion. The peak separation is given by the equation:

$$\Delta E_p = |E_{pa} - E_{pc}| = 2.303 RT/nF \quad 3.7$$

Where  $\Delta E_p$  is the peak separation (V),  $E_{pa}$  is the anodic peak potential (V),  $E_{pc}$  is the cathodic peak potential (V),  $n$  is the number of electrons,  $F$  is the Faraday constant (96486,3365 C mol<sup>-1</sup>),  $R$  is the gas constant (8.314 J mol<sup>-1</sup> K<sup>-1</sup>) and  $T$  is the absolute temperature of the system (298 K). Therefore, the number of electrons ( $n$ ) involved in the electrochemical process can be measured from the above equation. Thus, for a reversible redox reaction at 25 °C (298 K) with  $n$  electrons,  $\Delta E_p$  should be 0.0592/ $n$  V or about 60 mV for one electron.

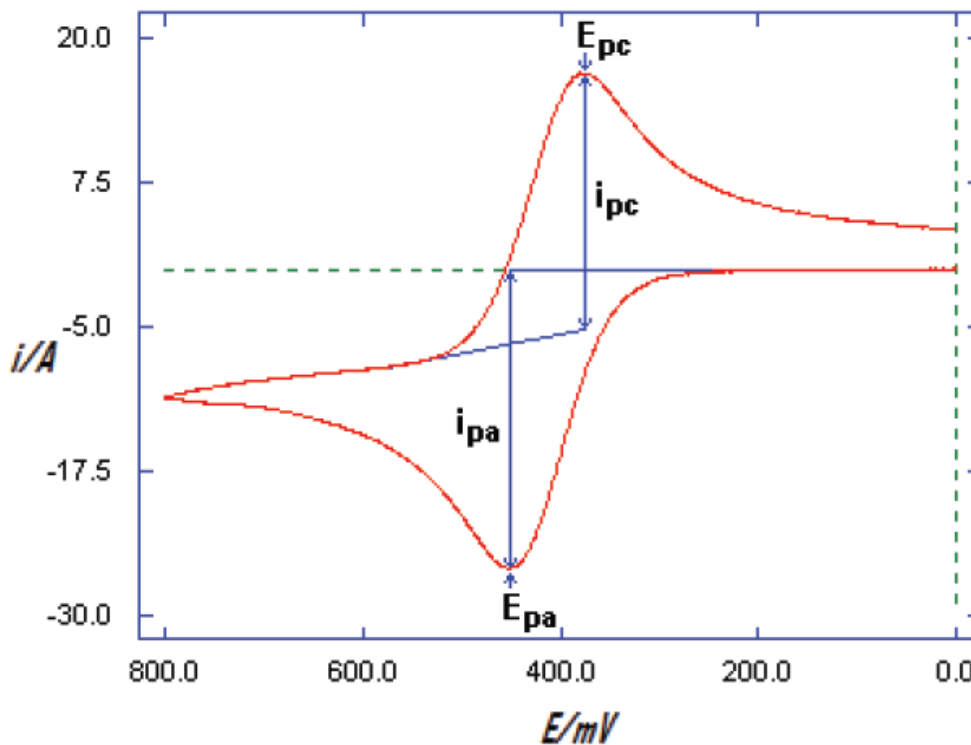


Figure 3. 1: Typical cyclic voltammogram showing the peak cathodic and anodic current respectively for a reversible reaction [14].

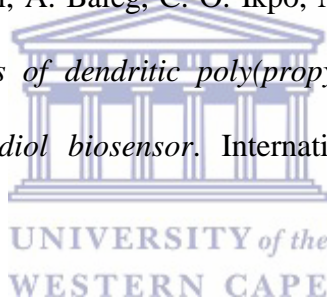
In this work, CV was utilised to evaluate the electrochemical parameters such as HOMO and the LUMO of the materials. In order to achieve this, the information was recorded using a traditional three-electrode set-up with glassy carbon electrode (3 mm diameter, 0.071 cm<sup>2</sup> area) as a working electrode, Pt wire as a counter electrode and Ag/AgCl wire as a reference electrode. Repetitive scanning of polymers (2 mg/mL in 0.1 M TBAP/DMSO) was measured from -0.3 to +0.7 V at the scan rate of 0.01-0.10 Vs<sup>-1</sup>. Electrochemical experiments were performed in 5 ml of 0.1 M TBAP/DMSO electrolytic system.

### **3.9.10. Square Wave Voltammetry (SWV)**

Square wave voltammetry (SWV) is a form of linear potential sweep voltammetry which has found plenty of applications in diverse fields. In SWV experiments, the current at a working electrode is estimated while the potential between the reference electrode and working electrode is swept linearly in time. Its advantage is that it can be used to perform an experiment much faster than the other electrochemical techniques [13]. SWV suppresses background currents much more productively than cyclic voltammetry. In this work, the SWV was used to support the CV analysis for investigation of electrochemical properties of the materials. The experiments were performed following the same procedure as in CV above.

### 3.10. References

- [1]- C. Jianga, G. Chen, X. Wang. *High-conversion synthesis of poly(3, 4-ethylenedioxythiophene) by chemical oxidative polymerization*. Synthetic Metals 162 (2012) 1968-1971.
- [2]- A. Baleg, N. Jahed, Anne. Yonkeu, N. Njomo, G. Mbambisa, K. M. Molapo, X. G. Fuku, G. Fomo, H. Makelane, A. Tsegaye, T. T. Waryo, P. Baker, S. Vilakazi, R. Tshikhudo, E. I. Iwuoha. *Impedimetry and microscopy of electrosynthetic poly(propylene imine)-co-polypyrrole conducting dendrimeric star copolymers*. Electrochimica Acta 128 (2014) 448-457.
- [3]- R. A. Olowu, P. M. Ndangili, A. Baleg, C. O. Ikpo, N. Njomo, P. Baker, E. I. Iwuoha. *Spectroelectrochemical dynamics of dendritic poly(propylene imine)-poly(thiophene) star copolymer aptameric 17 $\beta$ -estradiol biosensor*. International journal of Electrochemical Science 6 (2011) 1686-1708.
- [4]- A. A. Baleg, N. M. Jahed, O. A. Arotiba, S. N. Mailu, N. R. Hendricks, P. G. Baker, E. I. Iwuoha. *Synthesis and characterization of poly(propylene imine) dendrimer-poly(pyrrole) conducting star copolymer*. Journal of Electroanalytical Chemistry 652 (2011) 18-25.
- [5]- L. Chen, Y. Jiang, C. Wang, X. Liu, Y. Chen, J. Jie. *Green chemical approaches to ZnSe quantum dots: preparation, characterisation and formation mechanism*. Journal of Experimental Nanoscience 5 (2010) 106-117.
- [6]- D. A. Skoog, D. M. West, F. J. Holler. *Fundamentals of Analytical Chemistry*, 8th Edition, Saunders College Publishing (1992).
- [7]- <http://www.chemicool.com/img1/graphics/ir.gi>.
- [8]- J. McMurry., *Organic Chemistry*, 7th Edition Brooks/Cole, Thomson Learning, Inc (2008).
- [9]- <http://lab-training.com/wp-content/uploads/2013/03/AAS-Diagram.png>.



[10]- M. Clugston, R Flemming, D. Vogt. *Chemistry: An introduction for southern African students*, 1<sup>st</sup> Edition, Oxford University Press (2002).

[11]- A. J. Bard, L. R. Faulkner. *In: Electrochemical Methods: Fundamentals and applications*. 2nd edition, John Wiley & Sons Inc (2001).

[12]- J. Bindell. *Scanning electron microscopy, in Encyclopaedia of materials characterization: Surfaces, interfaces, thin films*, R. Brundle, C. Evans, editors. (1992), Greenwich: Manning Publication Company.

[13]- [https://openi.nlm.nih.gov/imgs/512/389/2871148/PMC2871148\\_ijms-11-01956f1.png](https://openi.nlm.nih.gov/imgs/512/389/2871148/PMC2871148_ijms-11-01956f1.png).

[14]- A. Baleg. *Synthesis and electrochemistry of novel conducting dendrimeric star copolymers on poly (propylene imine) dendrimer*. PhD Thesis, Department of Chemistry, University of the Western Cape, (2011).



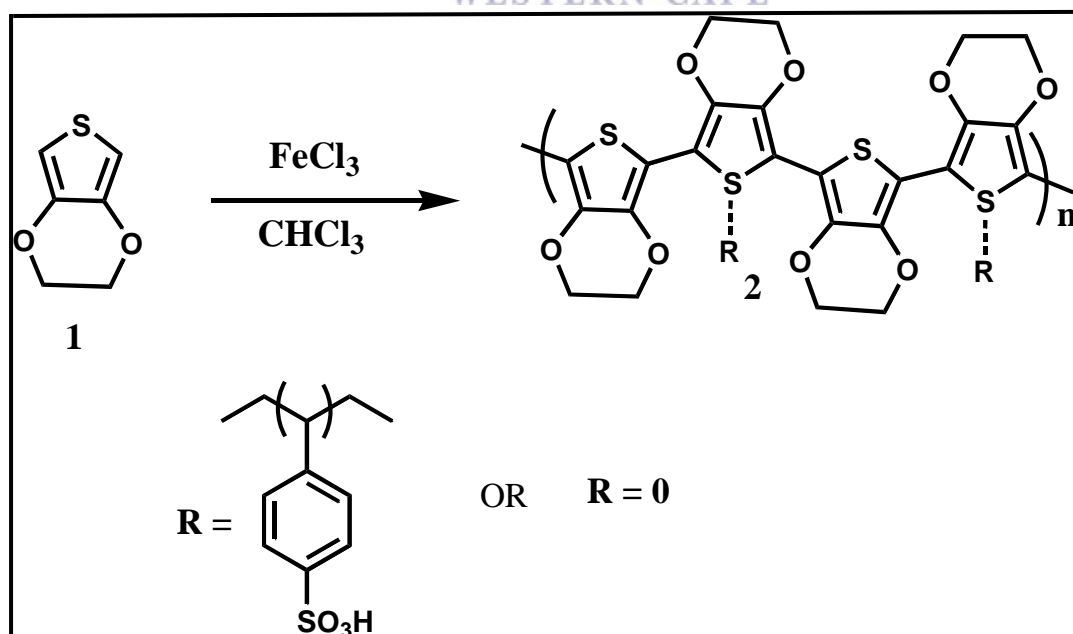
# CHAPTER FOUR

## 4. Results and Discussion

### 4.1. Synthesis and Characterisation of polymers

#### 4.1.1. Synthesis

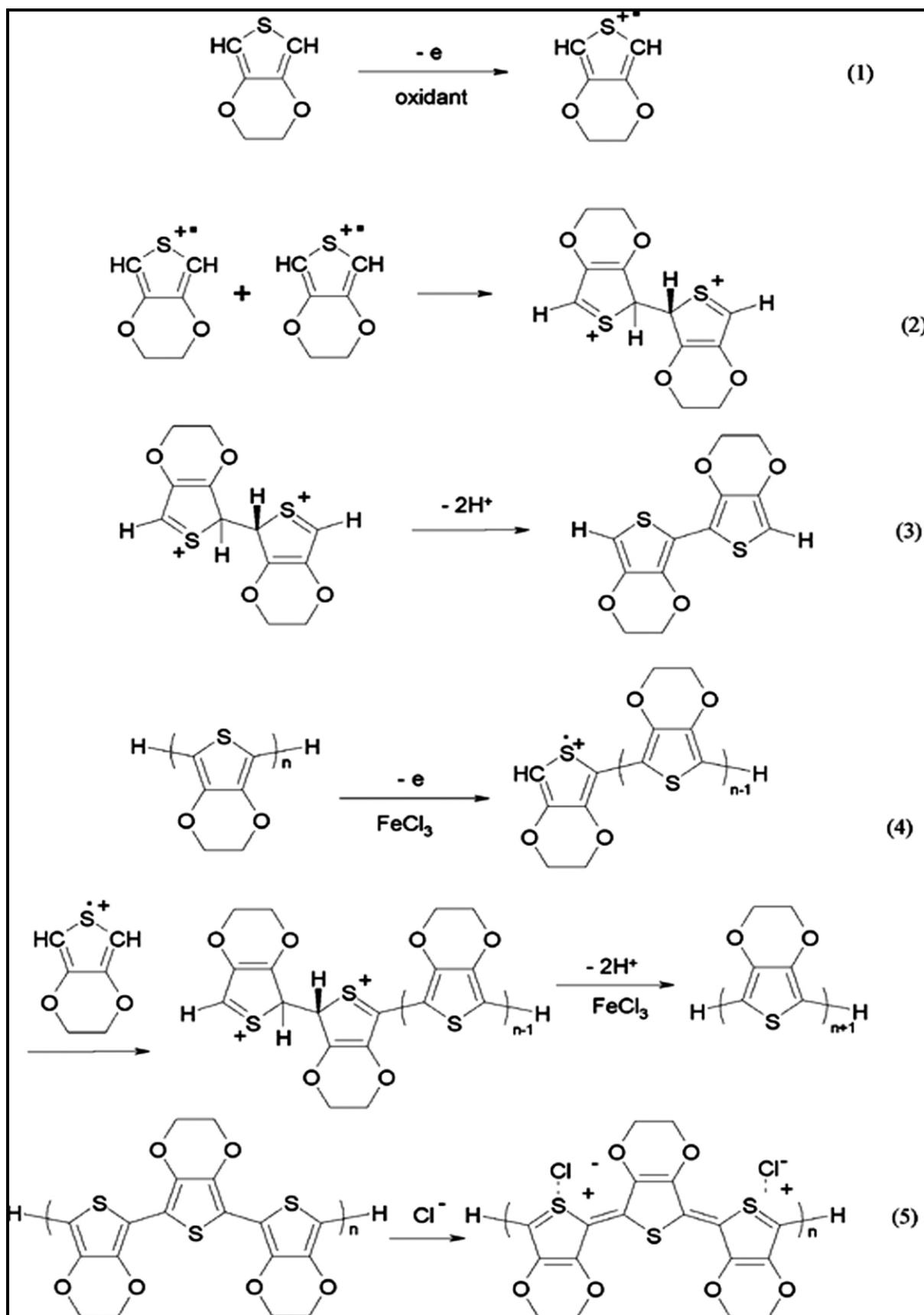
**Scheme 4.1** below illustrates the synthesis of PEDOT (**2**, R= 0). Compound (**2**) was prepared as described in the previous chapter, section 3.2. Compound (**2**) was synthesized according to literature [1] as shown in **scheme 4.1** through oxidative polymerization, using (**1**) as a monomer to yield (**2**) as a polymer. The conversion of compound (**1**) to (**2**) was achieved using FeCl<sub>3</sub> as an oxidant which went on to proceed for 48 h. A dark blue precipitate was obtained and further washed with ethanol and water to remove unreacted monomer.



Scheme 4. 1: Synthetic pathway to PEDOT via oxidative polymerization of EDOT monomer.

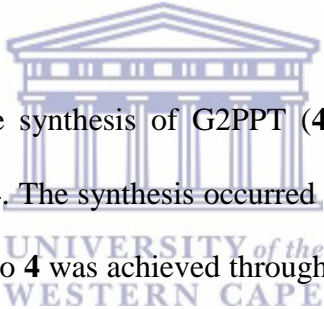
The polymerization mechanism of the formation of compound (2) is well documented [2]. **Scheme 4.2** illustrates the mechanism of PEDOT polymerization. The mechanism involves the formation of EDOT cation radical (step 1) as a result of oxidation induced by the introduction of the oxidant ( $\text{FeCl}_3$ ). Once oxidation has occurred, the cation radicals combine via  $\alpha - \alpha$  coupling (step 2), followed by the formation of conjugation by deprotonation (step 3). From this point, polymerization continues from n-mer to (n + 1)-mer (step 4) till the undoped or doped state of compound (2) (step 5).





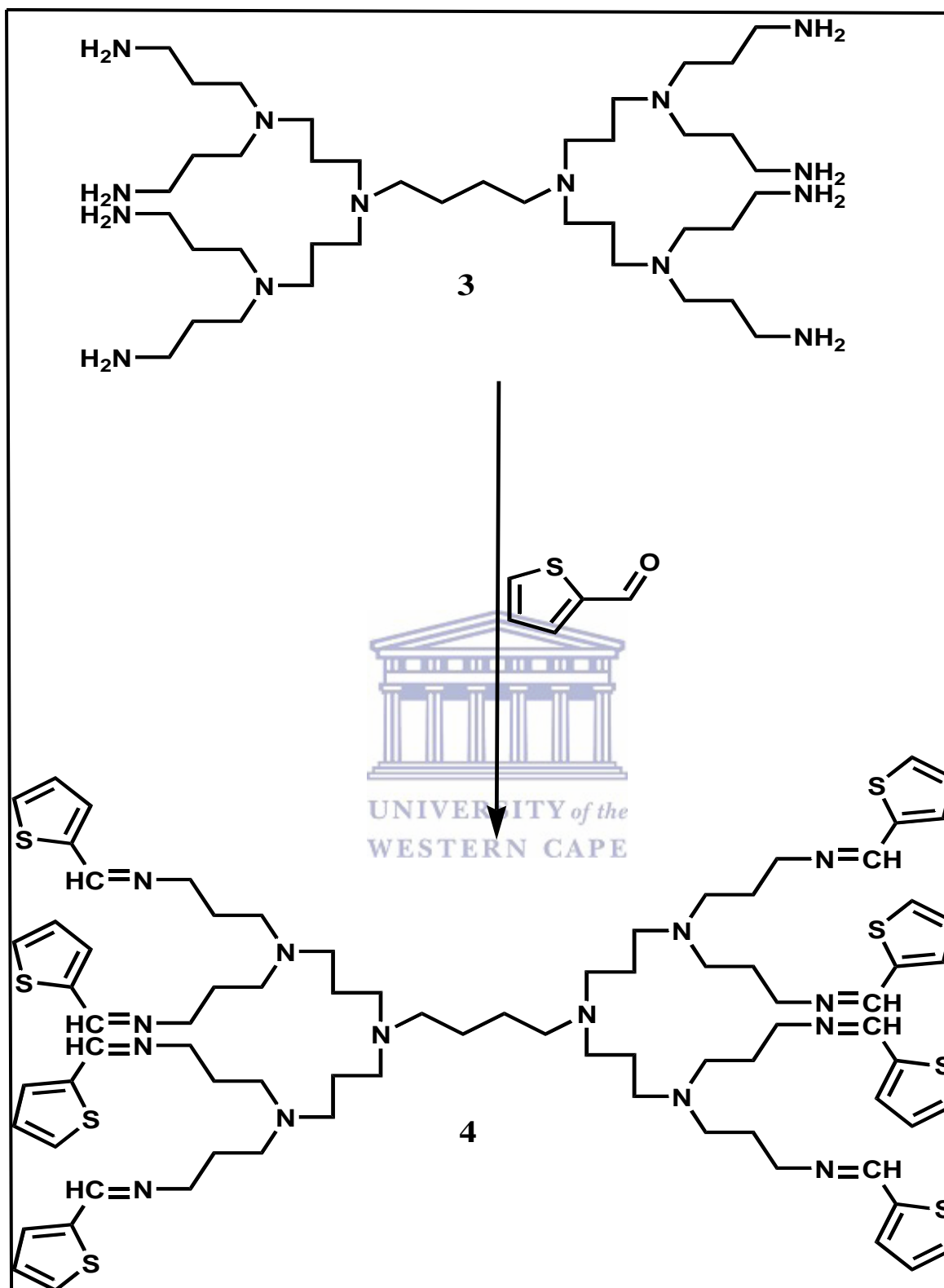
Scheme 4. 2: Polymerization mechanism of the formation of PEDOT via step (1-5) [2].

During oxidative polymerization of compound (1), PSSA is also added *in-situ* to form PEDOT-PSSA (R= PSSA) as shown in **scheme 4.1** above. The incorporation of PSSA is described in the previous chapter, section 3.3. The incorporation of PSSA into the PEDOT polymer is as a result of the electrostatic interaction between the negatively charged oxygen atom in the PSSA (after the –OH dissociated to H<sup>+</sup>) and the positively charged sulphur atom in the EDOT (during oxidation processes, S<sup>+</sup>, step 1 in scheme 4.2) [3, 5]. However, according to [4-5], the bond formation is weak, hence represented as dotted lines. The PSSA was incorporated into the PEDOT chain for two functions: (1) act as a counter ion or dopant, and (2) stabilises or enhances the solubility. This in turn brings several other advantages such as low oxidation potential, moderate band gap with very good stability, and excellent environmental stability [5].



**Scheme 4.3** below illustrates the synthesis of G2PPT (4). Compound 4 was prepared as described in chapter 3, section 3.4. The synthesis occurred as reported in literature [6-8]. The functionalization of compound 3 to 4 was achieved through a condensation reaction, which is the reaction between the primary amine group from the dendrimer moiety and the carbonyl group from the aldehyde resulting in the release of water. The obtained product is a yellow oil-like substance.

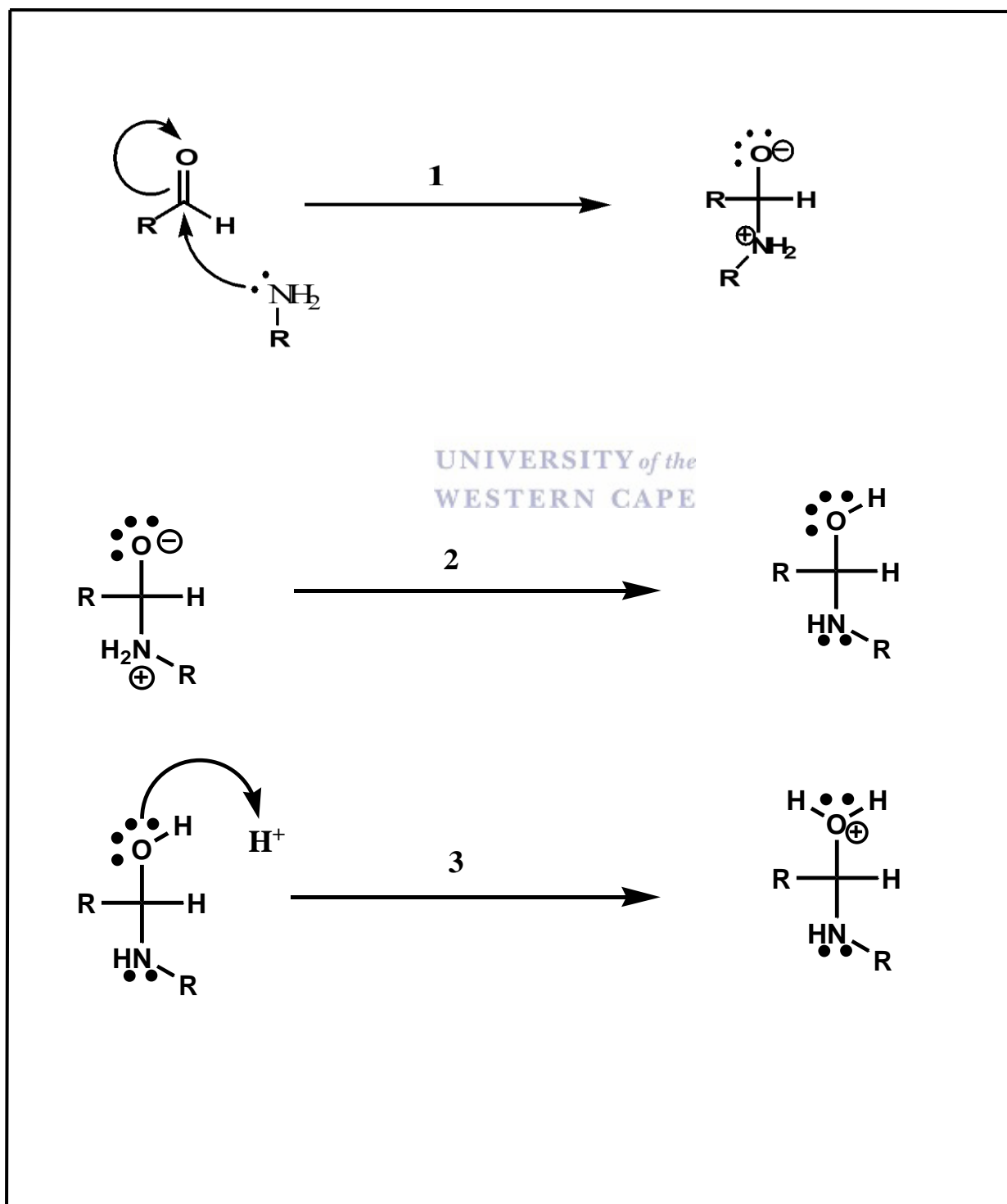


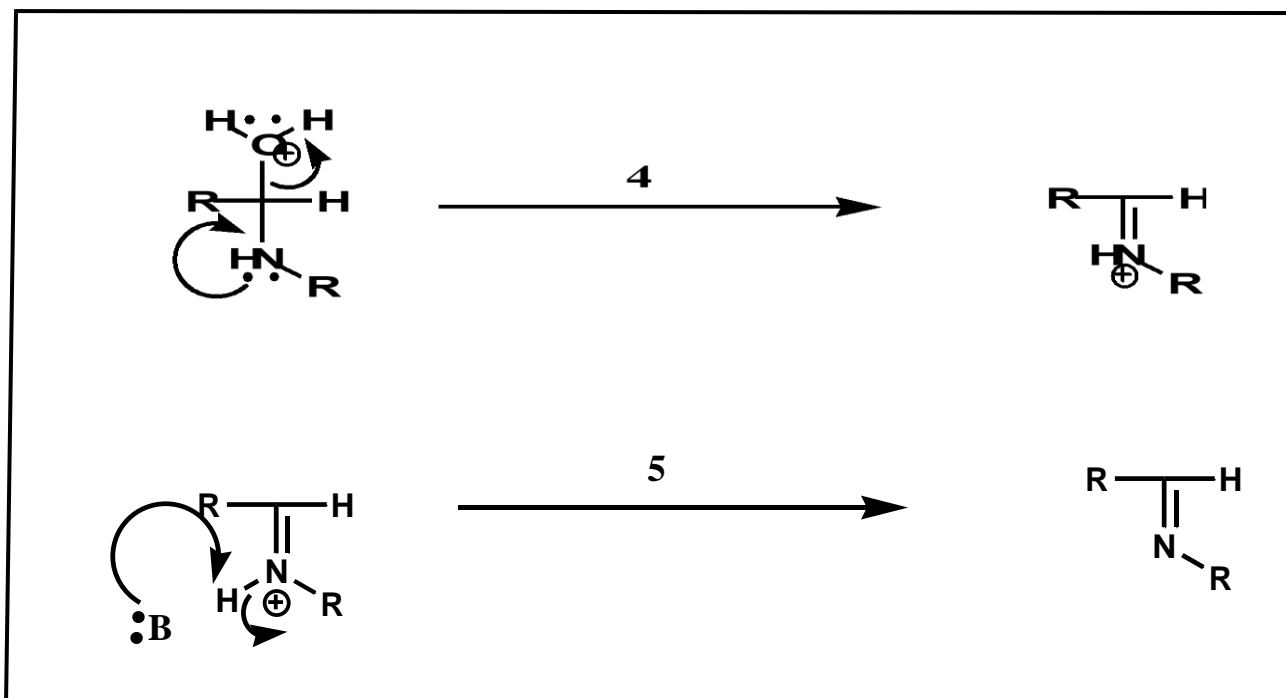


Scheme 4. 3: Functionalization of G2PPI to G2PPT through a condensation reaction.

The mechanism of the reaction between the primary amine and the carbonyl group is illustrated in **scheme 4.4**. The mechanism proceeds via five steps, which involves the nucleophilic attack

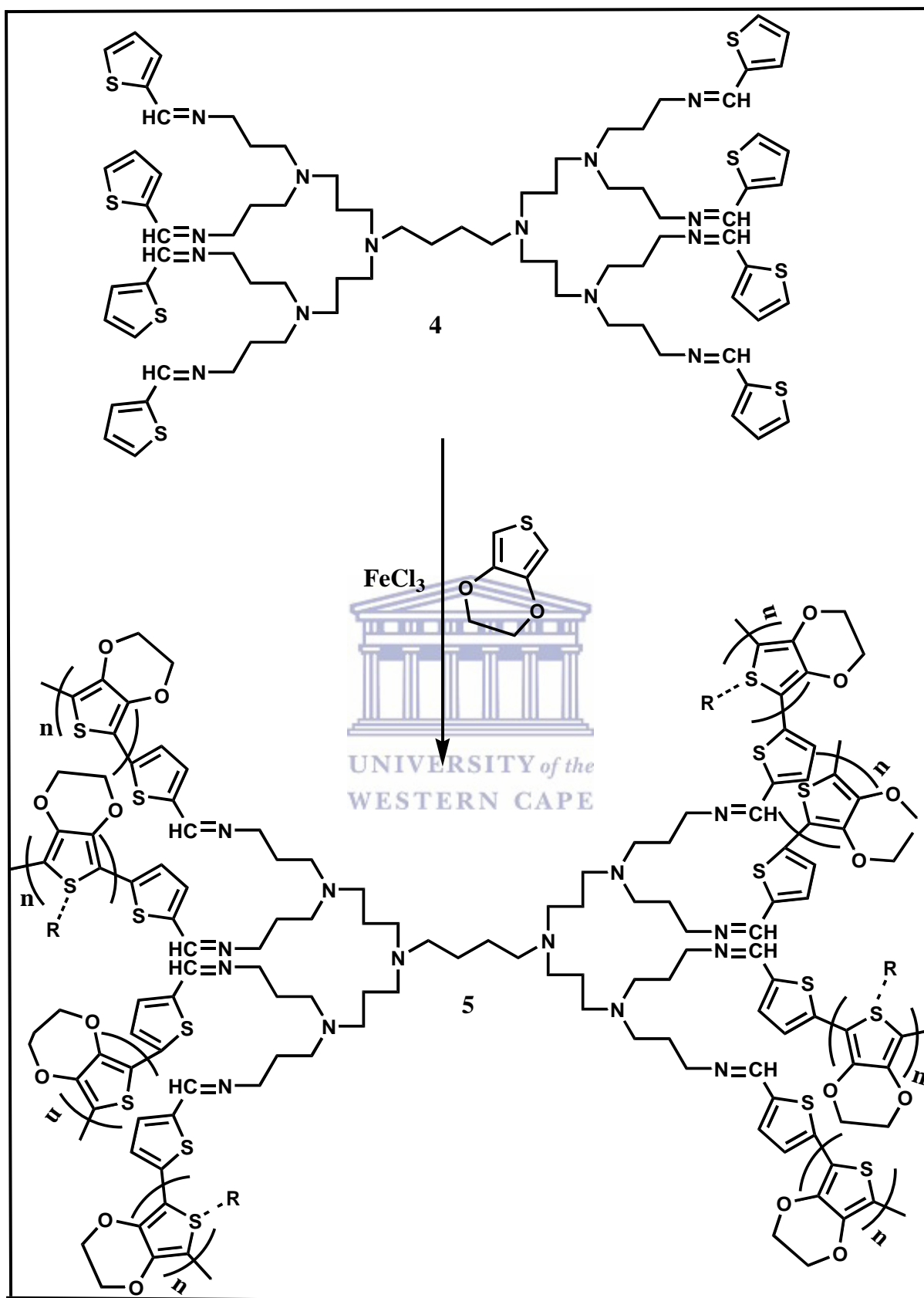
(step 1) of the amine nitrogen in  $\text{RNH}_2$  (through the lone pair on the nitrogen) on the electron deficient carbonyl carbon of the aldehyde, followed by a proton transfer (step 2) resulting in the rearrangement of the position of the proton. Once this is done, protonation of OH (step 3) occurs with the help of the solvent thus enabling the removal of water (step 4) leaving behind a cationic primary imine. The cationic primary imine is then neutralised by deprotonation to form the resultant new imine bond ( $\text{C}=\text{N}$ ).





Scheme 4. 4: G2PPT formation mechanism between the primary amine of the dendrimer and the carbonyl group of the aldehyde via step (1-5).

**Scheme 4.5** below illustrates the formation of G2PPT-co-PEDOT (**5**) (R=0). Compound **5** was synthesized as described in chapter 3, section 3.2 [1]. The formation of compound **5** from compound **4** follows the same synthetic procedure and mechanism as explained in scheme 4.1 and scheme 4.2 above, respectively. The difference is that a 3-dimensional star copolymer is formed by polymerising PEDOT chains on the surface of the dendrimer, which is enabled by the presence of the thiophene group after functionalisation. The growth of PEDOT on the surface of the dendrimer results in the star copolymer being a core-shell polymer, with the dendrimer being a core and the PEDOT being the shell. Likewise, G2PPT-co-PEDOT-PSSA (R=PSSA) is formed according to the explanation based on PEDOT-PSSA formation above.



Scheme 4. 5: Synthetic pathway to G2PPT-co-PEDOT via oxidative polymerization of EDOT monomer on the surface of G2PPT.

## 4.1.2. Structural Characterisation

### 4.1.2.1. Proton Nuclear Magnetic Resonance ( $^1\text{H}$ NMR)

To examine the functionalisation completeness or process and recognition of any functionality changes on G2PPI after being embedded with 2Th,  $^1\text{H}$  NMR was employed for analysis using  $\text{CDCl}_3$  as a solvent. The results are presented in **figure 4.1** (A-C) below. Figure 4.1 (A) is the proton spectrum of 2Th. The results show three signals resonating at around 7.1, 7.8, and 9.8 ppm chemical shifts respectively. The signals at 7.1 and 7.8 ppm are attributed to the protons labelled 1, 2, and 3 on the structure while the signal at 9.8 ppm which is more deshielded is attributed to proton 4 on the structure. Figure 4.1 (B) represents pristine G2PPI. The results show three intense signals resonating at around 1.5, 2.3, and 2.7 ppm corresponding to proton 3, 2, and 1 on the structure respectively.

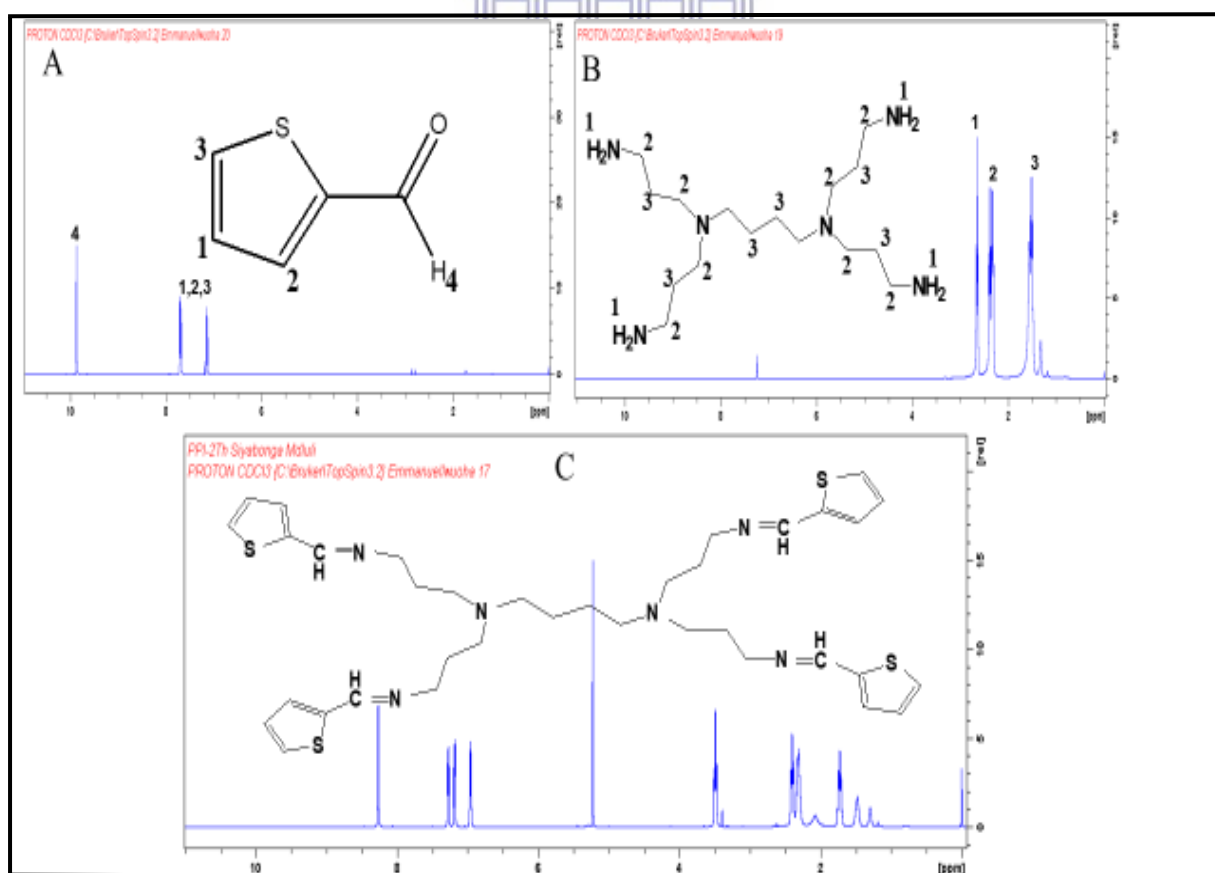


Figure 4. 1:  $^1\text{H}$  NMR of (A) 2Th, (B) pristine G2PPI, and (C) G2PPT.

Figure 4.1 (C) represents the proton spectrum of functionalised G2PPI with 2Th. Comparing (A) and (C) it is quite noticeable that proton 4 observed in (A) is not observed in (C) while protons 1, 2, and 3 observed in (A) are still observed in (C). The disappearance of proton 4 confirms successful completion of the condensation reaction. Moreover, a new signal in (C) resonating at 8.3 ppm is observed which is attributed to the formation of the new functionality (N=CH). All signals observed in (B) are also observed in (C) confirming the presence of the dendrimer in the newly synthesised compound. These results are in accordance to the results obtained by [6-8] which shows successful functionalisation of the dendrimer with the aldehyde.

To examine the polymerization process and recognition of any functionality changes on EDOT with and without the presence of PSSA,  $^1\text{H}$  NMR was employed for analysis using DMSO- $d_6$  as a solvent. The results are presented in **figure 4.2** (A-C) below.

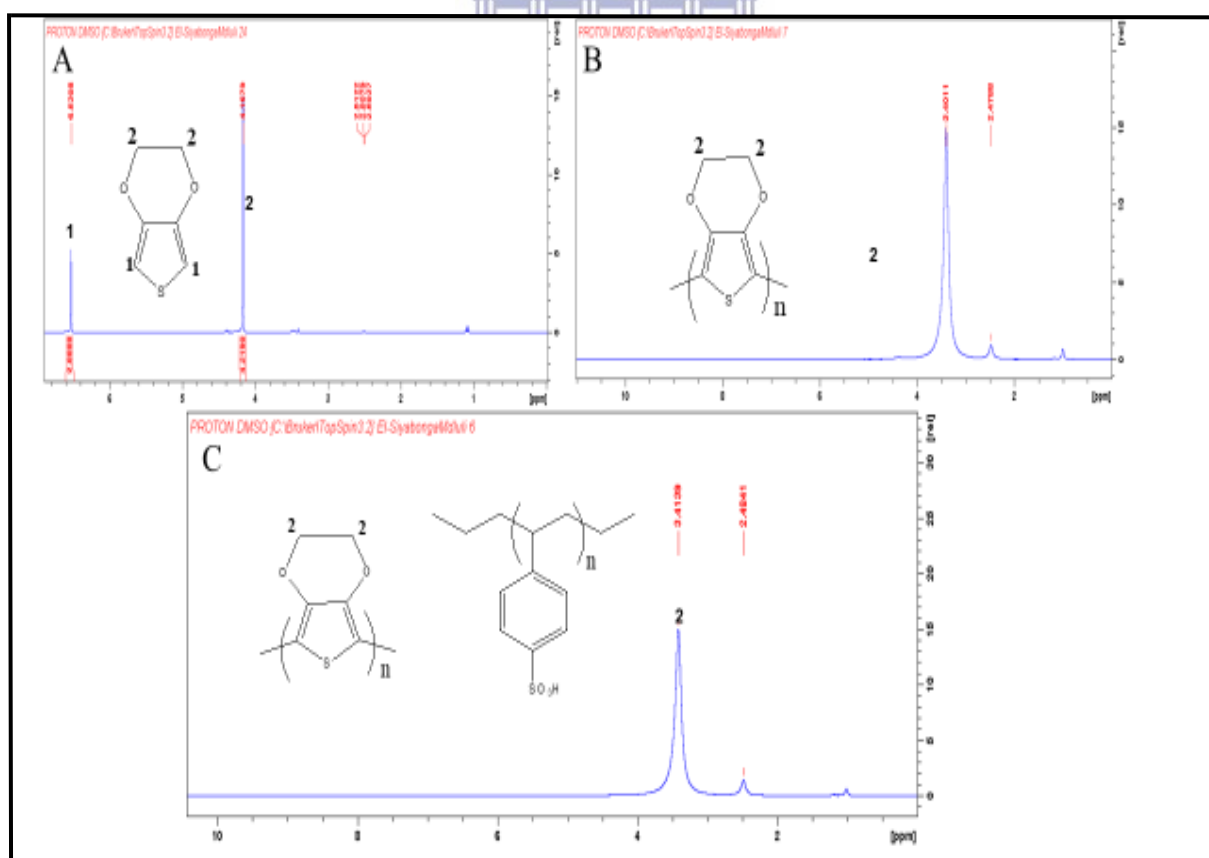


Figure 4. 2:  $^1\text{H}$  NMR of (A) EDOT, (B) PEDOT, and (C) PEDOT-PSSA.

In figure 4.2 (A) the results show two signals resonating around 4.2 and 6.6 ppm respectively. The signal at 4.2 ppm is attributed to proton 2 on the structure while the more deshielded signal is attributed to proton 1 on the structure. In (B), only one signal is observed at around 2.6 ppm which again is attributed to proton 2 with the only difference being that it now appears more shielded than in (A). The change in the position of the signal could be a symbol that an entirely new compound has been formed. Proton 1 which is observed in (A) is not observed in (B). The disappearance of it confirms that EDOT has been polymerized to PEDOT through  $\alpha - \alpha$  coupling. There are no observed functional changes in (C) in comparison with (B). However, it is not surprising to observe no changes as no additional functionality was expected as [4-5] explained the weak bondage existing between the oxygen atom from PSSA and the sulphur atom from the thiophene ring in PEDOT.

To examine the polymerization process and recognition of any functionality changes on the growth of PEDOT on the surface of the dendrimer with and without the presence of PSSA,  $^1\text{H}$  NMR was employed for analysis using  $\text{DMSO-d}_6$  as a solvent. The results are presented in **figure 4.3** (A-B) below. In (A) the signal at 8.3 ppm which was observed in figure 4.1 (C) above is also observed. The protons labelled 2 in figure 4.2 (A and B) arising from PEDOT and the  $\text{CH}_2$  protons in figure 4.1 (B) arising from the dendrimer are also observed. This confirms the successful growth of PEDOT on the surface of the dendrimer to form core-shell G2PPT-co-PEDOT. Just like explained in figure 4.2 (C), figure 4.3 (B) shows a similar behaviour with the only difference being that the signals are better pronounced, especially the  $\text{N}=\text{CH}$  signal.

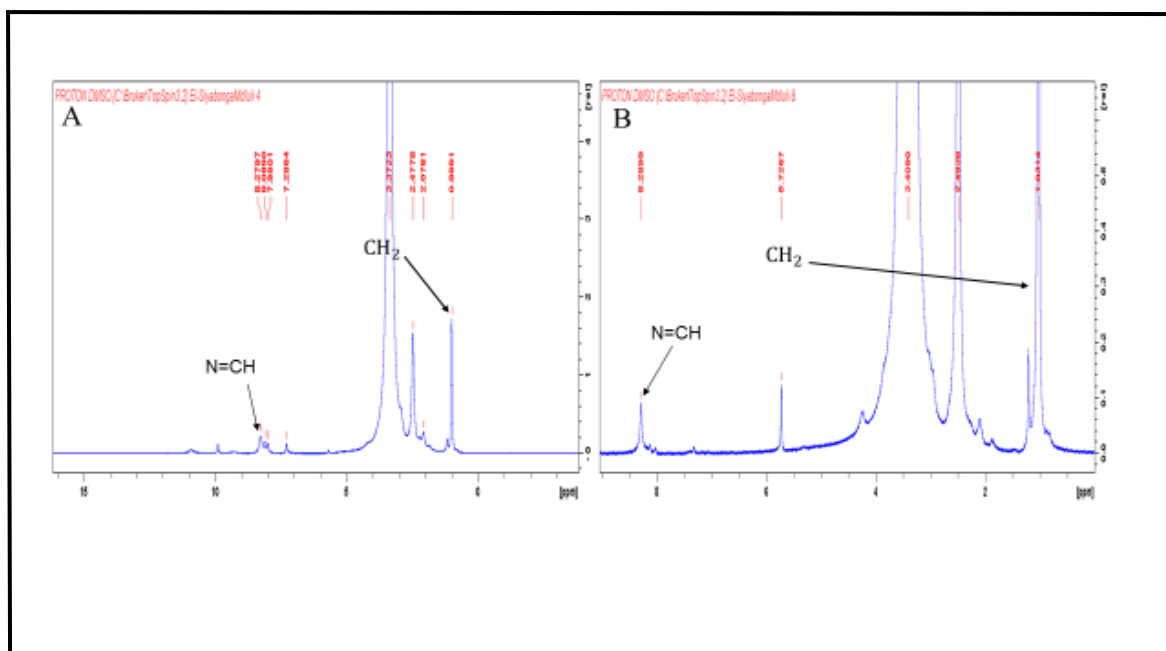


Figure 4. 3:  $^1\text{H}$  NMR of (A) G2PPT-co-PEDOT and (B) G2PPT-co-PEDOT-PSSA.

#### 4.1.2.2. Fourier Transform Infrared Spectroscopy (FTIR)

To further examine the polymerization process and recognition of any functionality changes on G2PPT after being incorporated with PEDOT and PSSA, FTIR analysis was employed in the range of  $400\text{-}4000\text{ cm}^{-1}$  and the results are presented in **figure 4.4 (A-C)** below. Figure 4.4 (A) below compares the FTIR spectra of the monomer EDOT and the resultant polymer PEDOT polymerized at  $60\text{ }^\circ\text{C}$  for 48 h. The spectra (blue line) shows all the characteristic peaks of PEDOT at  $1524, 1473, 1202, 1133, 1050,$  and  $1048\text{ cm}^{-1}$ . The bands at approximately  $1524$  and  $1473\text{ cm}^{-1}$  are assigned to the asymmetric stretching modes of  $\text{C}=\text{C}$  and inter-ring stretching mode of  $\text{C}-\text{C}$  respectively. The bands appearing at  $1202$  and  $1133$  are attributed to the stretching of  $\text{C}-\text{O}-\text{C}$  vibrations, while the bands at  $1050,$  and  $1048\text{ cm}^{-1}$  are characteristic bands of the  $\text{C}-\text{S}-\text{C}$  stretching mode in the thiophene ring, which suggest successful formation of the PEDOT in this polymerization reaction. These results are similar to the results reported by [1, 9-10]. In the case of EDOT (black line), all the vibrational bands observed in PEDOT are also observed. The only difference is that the band at  $889\text{ cm}^{-1}$  assigned to the out of plane



bending of C-H [7] located at the  $\alpha$ -position of the thiophene ring in EDOT does not appear in PEDOT indicating the conversion of EDOT to PEDOT through  $\alpha - \alpha$  coupling. The results are in agreement to the results observed on  $^1\text{H}$  NMR.

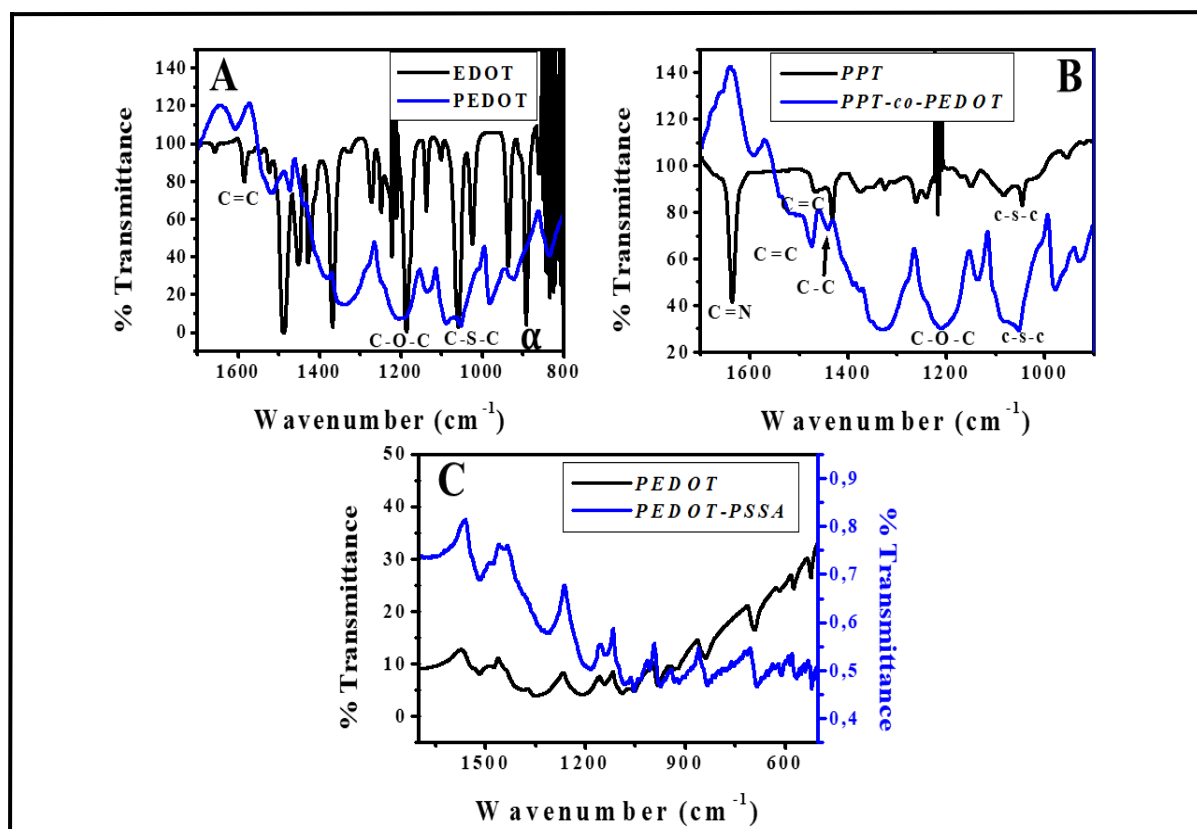


Figure 4. 4: FTIR of (A) EDOT and PEDOT, (B) G2PPT and G2PPT-co-PEDOT, and (C) PEDOT and PEDOT-PSSA.

The FTIR spectra of the functionalized dendrimer G2PPT and the copolymer G2PPT-co-PEDOT are all shown in figure 4.4 (B) above. The G2PPT show bands at 1637, 1467, 1432, and 1043  $\text{cm}^{-1}$ . The band at 1637  $\text{cm}^{-1}$  is attributed to the stretching mode of C=N vibrations [6-8] which is clearly absent in the homo-polymer PEDOT in figure 4.4 (A) but present in the G2PPT-co-PEDOT with a small shift. The band at 1467 and 1432  $\text{cm}^{-1}$  originate from the stretching vibrations of C=C and C-C respectively. The C-O-C vibrational bands at 1133 and 1202  $\text{cm}^{-1}$  present in PEDOT in (A) are completely absent in the G2PPT spectrum in (B) implying that the dendrimer was indeed functionalised with thiophene. However, the same

bands C-O-C are present in G2PPT-co-PEDOT showing that the C-H bending from the thiophene has been completely replaced by C-O-C in the G2PPT-co-PEDOT. In addition, all the characteristic vibrational bands of PEDOT are observed in the spectrum of G2PPT-co-PEDOT implying that the growth of PEDOT on the surface of the dendrimer was successfully achieved.

Figure 4.4 (C) above shows the FTIR spectra of pristine PEDOT and doped PEDOT-PSSA. The spectrum of the PEDOT-PSSA looks identical to the spectrum of pristine PEDOT with the changes only being the intensity of transmittance and small shifts in vibration wavenumbers. This small changes are perhaps indicative of an entirely new compound. However, it is not surprising not to see any additional functional groups as a weak bond between the thiophene ring from PEDOT and the sulfonic group from the PSSA has been proven to exist [4]. However, our results are similar to those reported by Reye-Reyes *et al* [11] with some small shifts in vibration wavenumbers. The observed results are in good agreement with what was observed in  $^1\text{H}$  NMR.

#### 4.1.2.3. Ultraviolet-Visible Spectroscopy (UV-Vis)

Electronic transitions together with band gap determination of the materials was achieved by employing UV-Vis spectroscopy at the range of 200-1100 nm in 200 ppm DMSO. The absorption spectra of G2PPI, G2PPT, PEDOT, G2PPT-co-PEDOT, and G2PPT-co-PEDOT-PSSA are all presented in **figure 4.5 (A-B)** below. figure 3.5 (A) presents the comparison between the unfunctionalised dendrimer G2PPI and the functionalised dendrimer G2PPT. The unfunctionalised dendrimer show one absorption peak at 235 nm which corresponds to the  $n-\sigma$  \* transitions of the  $\text{NH}_2$  chromophore on the structure. The functionalised dendrimer G2PPT show two distinct absorption peaks at 259 and 301 nm. The band at 259 nm corresponds to the  $n-\pi$  \* transitions of the C=N chromophore, while the band at 301 nm corresponds to the  $\pi -$

$\pi$  \* transitions of the C=C chromophore on the structure. The red shift of the peak from 235 to 259 nm is indicative of an increase in  $\pi$  conjugation upon functionalisation with thiophene [12] which alters the chromophores responsible for absorption as clearly seen on the resultant structure of G2PPT. Based on this interpretation, it is obvious that the functionalisation of the G2PPI was successful as the same conclusion was conferred by both  $^1\text{H}$  NMR and FTIR.

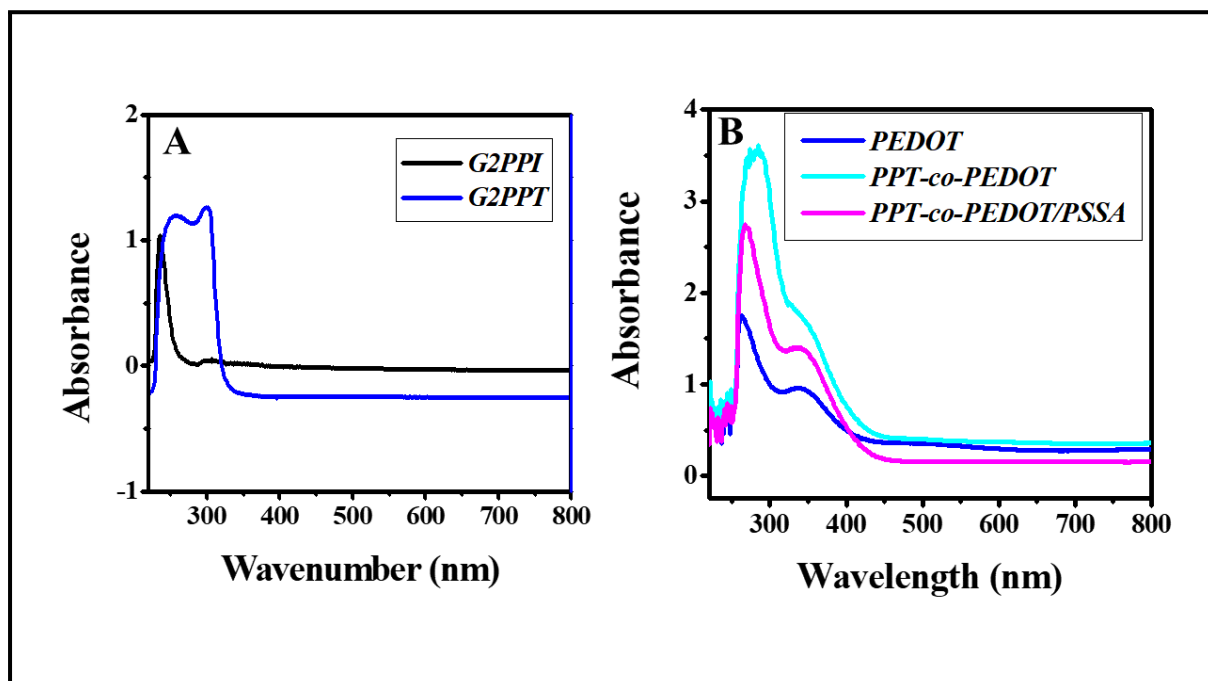


Figure 4. 5: (A) Absorption spectra of G2PPI and G2PPT, (B) Absorption spectra of PEDOT, G2PPT-co-PEDOT, and G2PPT-co-PEDOT-PSSA.

Figure 4.5 (B) presents the comparison between the polymer composites. The pristine PEDOT show two distinct absorption peaks at 264 and 339 nm. The peak at 264 nm corresponds to the  $\pi - \pi$  \* transitions of the benzoid ring, while the peak at 339 nm corresponds to the  $\pi - \pi$  \* transitions of the quinoid rings. However, there is a slight red shift and increase in absorbance upon copolymers formation through the growth of PEDOT on the surface of G2PPT with and without PSSA incorporated. The resultant absorption peaks are observed at 285 and 351 nm when only PEDOT is incorporated with G2PPT and also observed at 264 and 342 nm when incorporated in the presence of PSSA. The shift in the absorption peaks is caused by the

increase in the chain length of the PEDOT on the surface of G2PPT, thus causing an increase in  $\pi$  conjugation [12]. The obvious shift implies successful polymerization of EDOT on the surface of the dendrimer with and without the presence of PSSA as also conferred by both  $^1\text{H}$  NMR and FTIR.

With the help of the optical absorption spectrum (figure 4.5), it is well known that the Tauc relation can be deduced to determine the optical band gap between the transitions as presented in **Figure 4.6 (A-C)**. The Tauc relation is given by the following equation:

$$\alpha h\nu = A[h\nu - E_g]^n \quad 4.1$$

Where  $\alpha$  is the absorption coefficient,  $h\nu$  is the photon energy,  $A$  is the band tailing parameter,  $E_g$  is the optical band gap, and  $n$  is either 2 for direct transitions or  $1/2$  for indirect transitions [12-15]. Hence, the band gap of the absorption peak can be obtained by extrapolating from the Tauc plot of  $(\alpha h\nu)^2$  vs  $h\nu$  to the energy axis (see **figure 4.6**) [12-15].

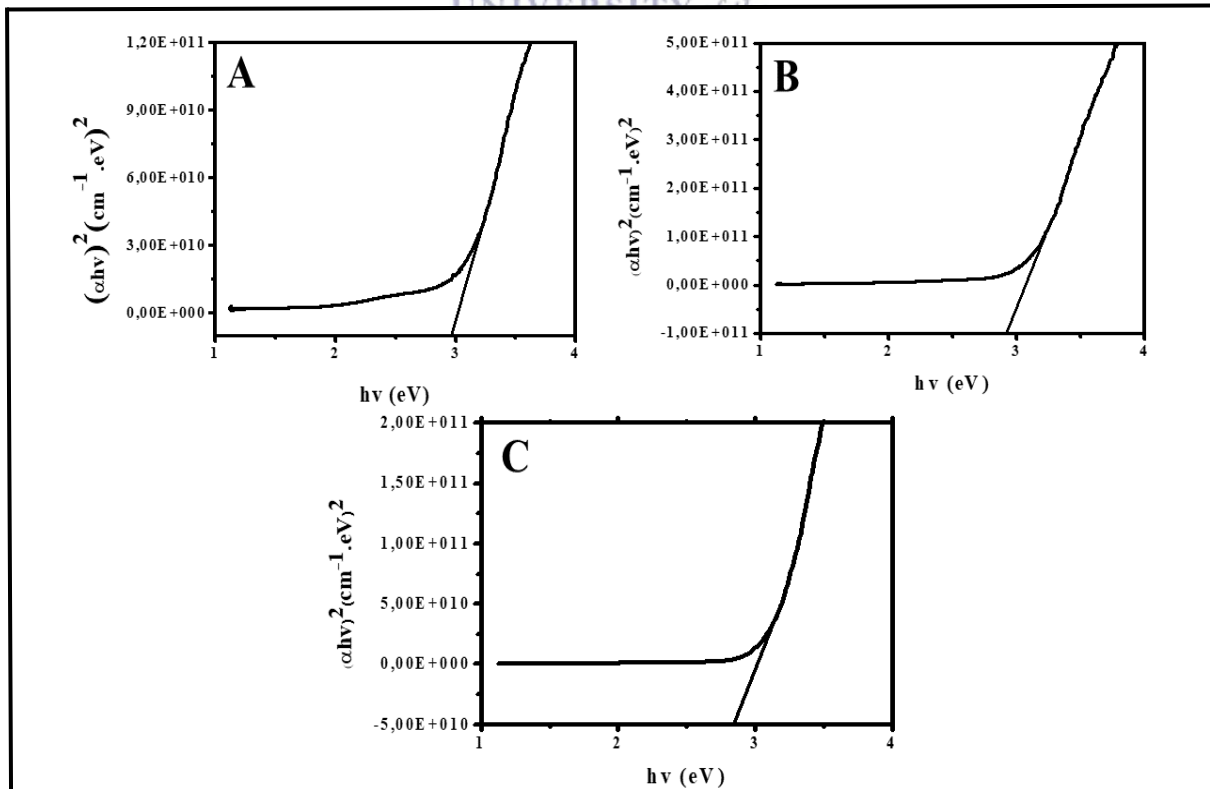


Figure 4. 6: Tauc plot of (A) PEDOT, (B) G2PPT-co-PEDOT, (C) G2PPT-co-PEDOT-PSSA.

The optical band gaps of the materials, PEDOT, G2PPT-co-PEDOT, and G2PPT-co-PEDOT-PSSA were determined to be 2.96, 2.92, and 2.85 eV respectively. The reduction in the band gaps in the case of the copolymers is due to the increase in electron density as conjugation increases [12, 16] compared to the pristine PEDOT. This observation enables the latter copolymer to be promising for use in photovoltaics.

#### 4.1.2.4. Photoluminescence (PL) Spectroscopy

Fluorescence studies of the polymers were achieved with the help of absorption studies obtained from UV-Vis using the same prepared solutions. The results are presented in **figure 4.7 (A-D)** below. Figure 4.7 (A) represents the emission spectrum of PEDOT excited at different excitation wavelength ranging from 300-400 nm at a wavelength difference of 20 nm. The results show that PEDOT emit at 516 nm even though excited at different wavelength. The no change in emission wavelength is indicative of nearly monodispersed particles and narrow size distribution as evident by the narrow-like Gaussian curve. G2PPT (figure 4.7 (B)) was excited at excitation wavelength ranging from 301-360 nm at a wavelength difference of 20 nm. The results reveal that G2PPT emit at 453 nm even though excited at different wavelengths. Again the no change in emission wavelength is indicative of nearly monodispersed particles. However, the Gaussian curve is broader which is indicative of larger particles distributed. The star copolymer G2PPT-co-PEDOT (figure 4.7 (C)) was excited at wavelength similar to those of PEDOT and G2PPT to deduce whether the starting materials preserved their individual properties. Its emission peak is observed at 478 nm which was observed to be an average of its components, designating a kind of hybrid material. A nearly monodispersed size distribution is observed. The introduction of PSSA on the star copolymer (figure 4.7 (D)) backbone blue shift the emission of the star copolymer by 60 nm to 472 nm. According to reports by Gupta *et al* [17], the blue shift is due to the increase in size chains, which alters the torsion angle and

leads to lower conjugation length. This observation is in agreement with the observation seen on UV-Vis measurements above.

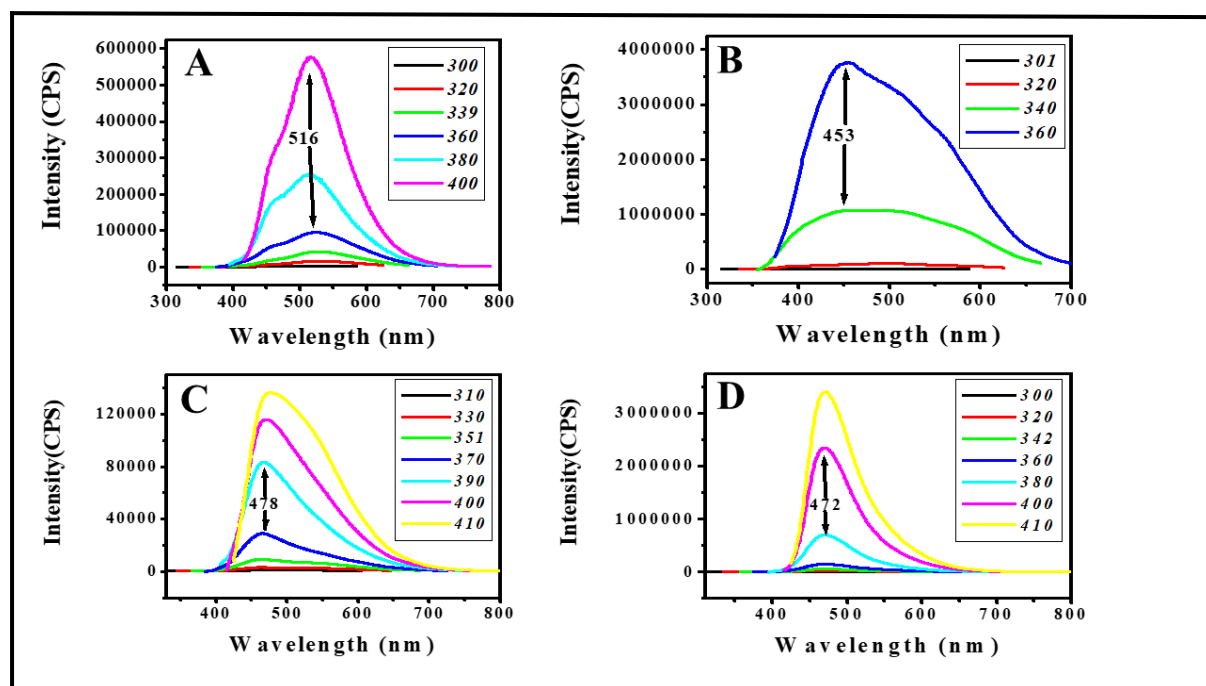


Figure 4. 7: Emission spectra of (A) PEDOT, (B) G2PPT, (C) G2PPT-co-PEDOT, and (D) G2PPT-co-PEDOT-PSSA.

#### 4.1.2.5. X-ray Diffraction (XRD).

The XRD patterns of the as-prepared materials, PEDOT, PEDOT-PSSA, G2PPT-co-PEDOT, and G2PPT-co-PEDOT-PSSA are all shown in **figure 4.8** below. The XRD patterns of PEDOT show two characteristic peaks at nearly  $2\theta \sim 26^\circ$  and  $13^\circ$ . The diffraction peak at  $2\theta \sim 26^\circ$  can be attributed to the inter-chain planar ring stacking [18], corresponding to the plane (400) [19]. It is further mentioned that this diffraction peak indicates that the particle is in nanoscale [20]. The diffraction peak with low intensity at  $2\theta \sim 13^\circ$  is considered to be the distance between the two stacks in the two-dimensional stacking arrangement polymer chains and intervening dopant ions [21], such as the remaining traces of  $\text{FeCl}_3$  salt used during the chemical synthesis of PEDOT.

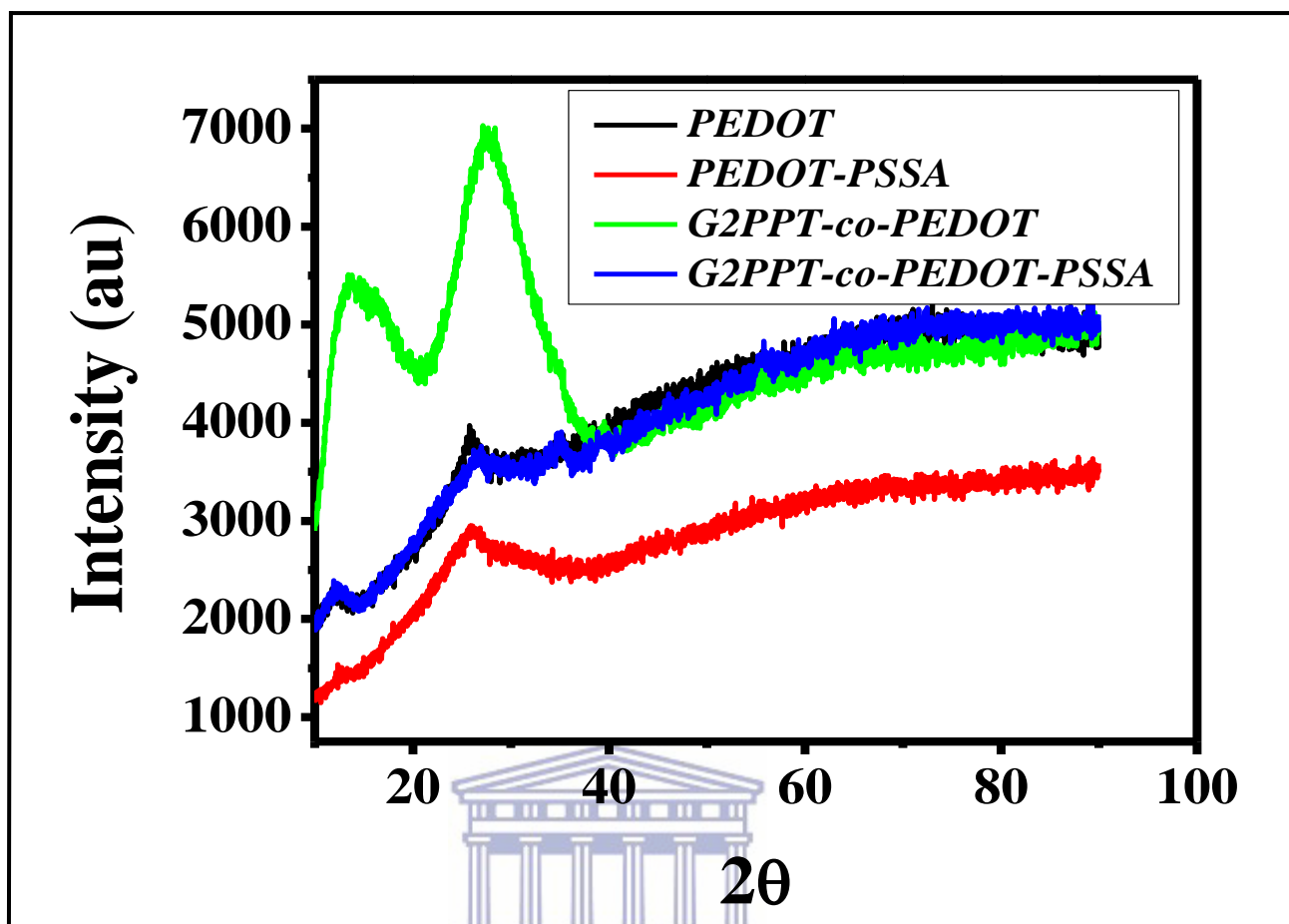


Figure 4. 8: XRD patterns of PEDOT, PEDOT-PSSA, G2PPT-co-PEDOT, and G2PPT-co-PEDOT-PSSA.

The introduction of PSSA on the backbone of PEDOT does not bring any phase changes due to the weak bondage that is known to exist between PSSA and PEDOT. Two new diffraction peaks with low intensities are observed upon star copolymer formation at  $2\theta \sim 35^\circ$  and  $40^\circ$ . These new diffraction peaks are probably due to the unique properties of the dendrimer which further confirms that an entirely new compound was synthesized. This is also evident by the increase in the intensity of the diffraction peaks. However, all the polymers exhibit broad diffraction patterns which is indicative of them being in an amorphous state.

#### 4.1.2.6 Thermal Gravimetric Analysis (TGA)

Thermogravimetric analysis (TGA) is a very significant dynamic method that is utilised to detect the degradation behaviour of the as-synthesized materials when subjected to elevated temperatures. Furthermore, it can be utilised to determine the precise weight loss ratio of each component in a sample. The thermograms of mass loss versus temperature for PEDOT, PEDOT-PSSA, G2PPT-co-PEDOT, and G2PPT-co-PEDOT-PSSA were recorded at a heating rate of 10 °C/ min in a nitrogen atmosphere. The results are presented in **figure 4.9** below.

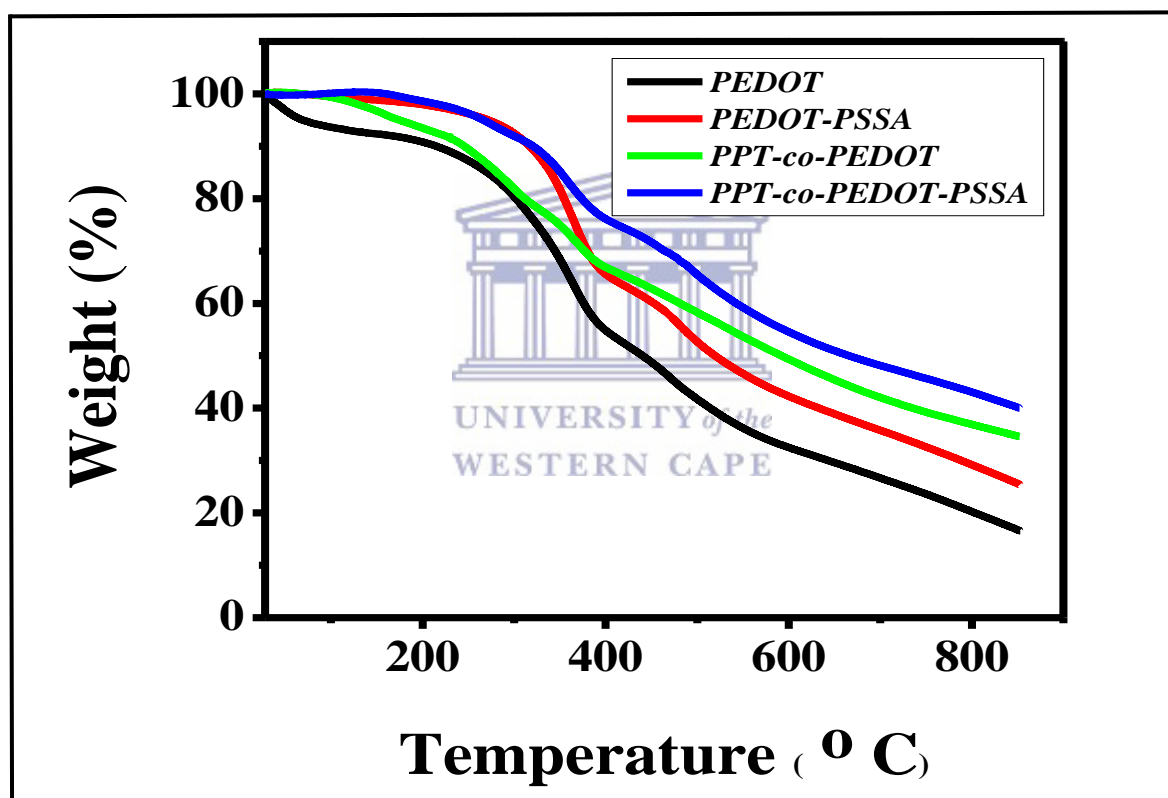


Figure 4. 9: Thermogravimetric plot of PEDOT, PEDOT-PSSA, G2PPT-co-PEDOT, and G2PPT-co-PEDOT-PSSA.

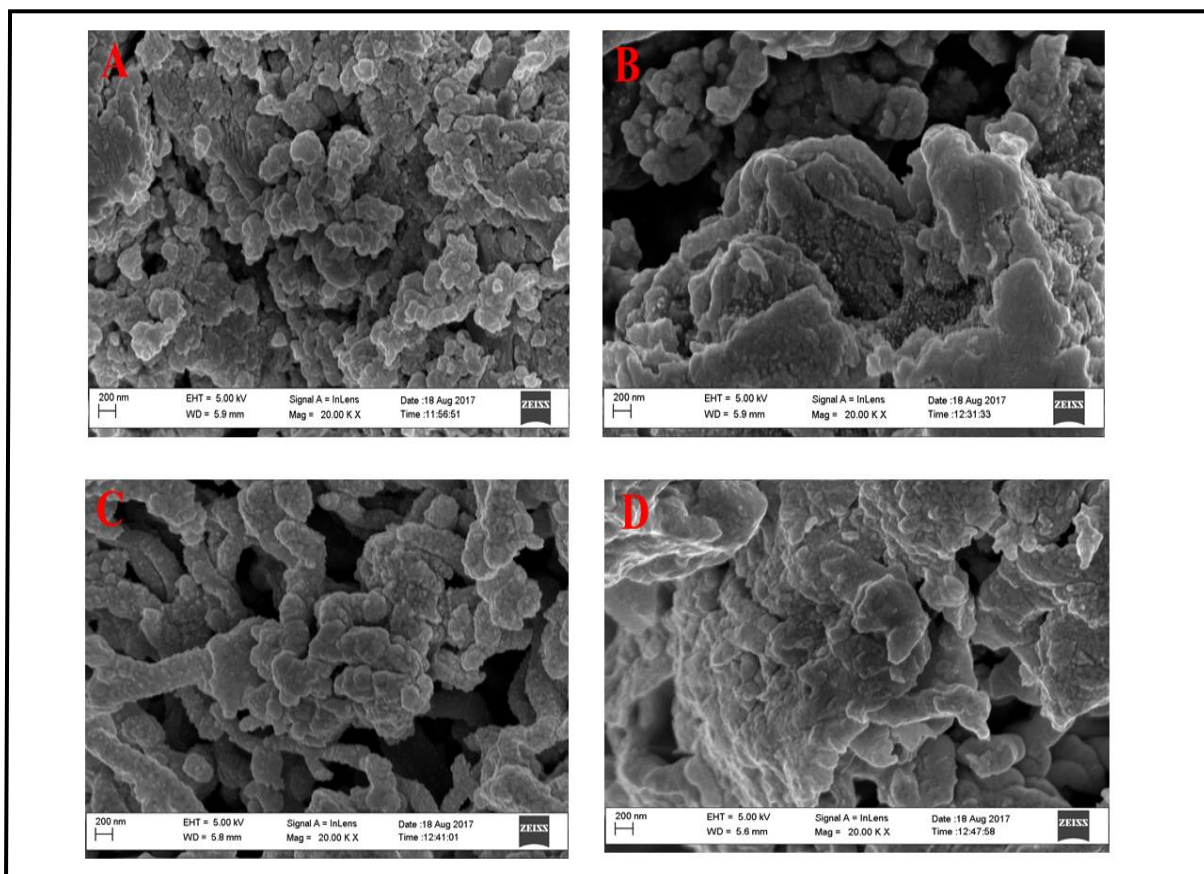
It can be seen that the thermogravimetric plot of pristine PEDOT depicts two thermal degradation steps throughout the entire experimental range of 30- 900°C. The first weight loss up to 150 °C is attributed to the removal of moisture, trapped water molecules, and other volatile



compounds physisorbed on the polymer backbone. The main degradation at 389 °C can be ascribed to the collapse of the polymer chains. These results are similar to the results observed by Chutia *et al* [22]. One of the functions of PSSA is to enhance the thermal stability. This statement has been proven to be correct as we observe an enhancement in the thermal stability due to the introduction of PSSA in the PEDOT backbone. The decreased rate of weight loss in the PEDOT-PSSA with increasing temperature symbolises an internal change in this material, hence it's obvious that a new compound was synthesized. The thermal stability is further enhanced by the introduction of G2PPT as a core to form the star copolymer. The enhancement can be attributed to the increase in conjugation due to increase number of stacking between the polymer chains. In addition, though the thermograms of all the polymers seem to undergo the same two degradation steps, PEDOT exhibit a steeper weight loss as compared to the polymer composites. The slower, less steep degradation in the G2PPT-co-PEDOT-PSSA suggest a higher thermal stability due to the stabilising effects of both G2PPT and PSSA and a changed in morphology upon composites formation. The small amount of the material remaining after thermal decomposition at the entire experimental range was found to be in the order PEDOT (17 %) < PEDOT-PSSA (26 %) < G2PPT-co-PEDOT (35 %) < G2PPT-co-PEDOT-PSSA (41 %). The results demonstrate that the thermal stability is directly proportional to the stacking of the polymers.

#### **4.1.2.7. Scanning Electron Microscopy (SEM)**

The surface morphologies of PEDOT, PEDOT-PSSA, G2PPT-co-PEDOT, and G2PPT-co-PEDOT-PSSA were investigated by SEM. The results are presented in **figure 4.10 (A-D)** below. The SEM image of PEDOT (figure 4.10 (A)) depicted flake-like structures along with a large number of aggregated globular structures, which is in accordance with the observations made by Zhao *et al* [9].



UNIVERSITY of the  
WESTERN CAPE

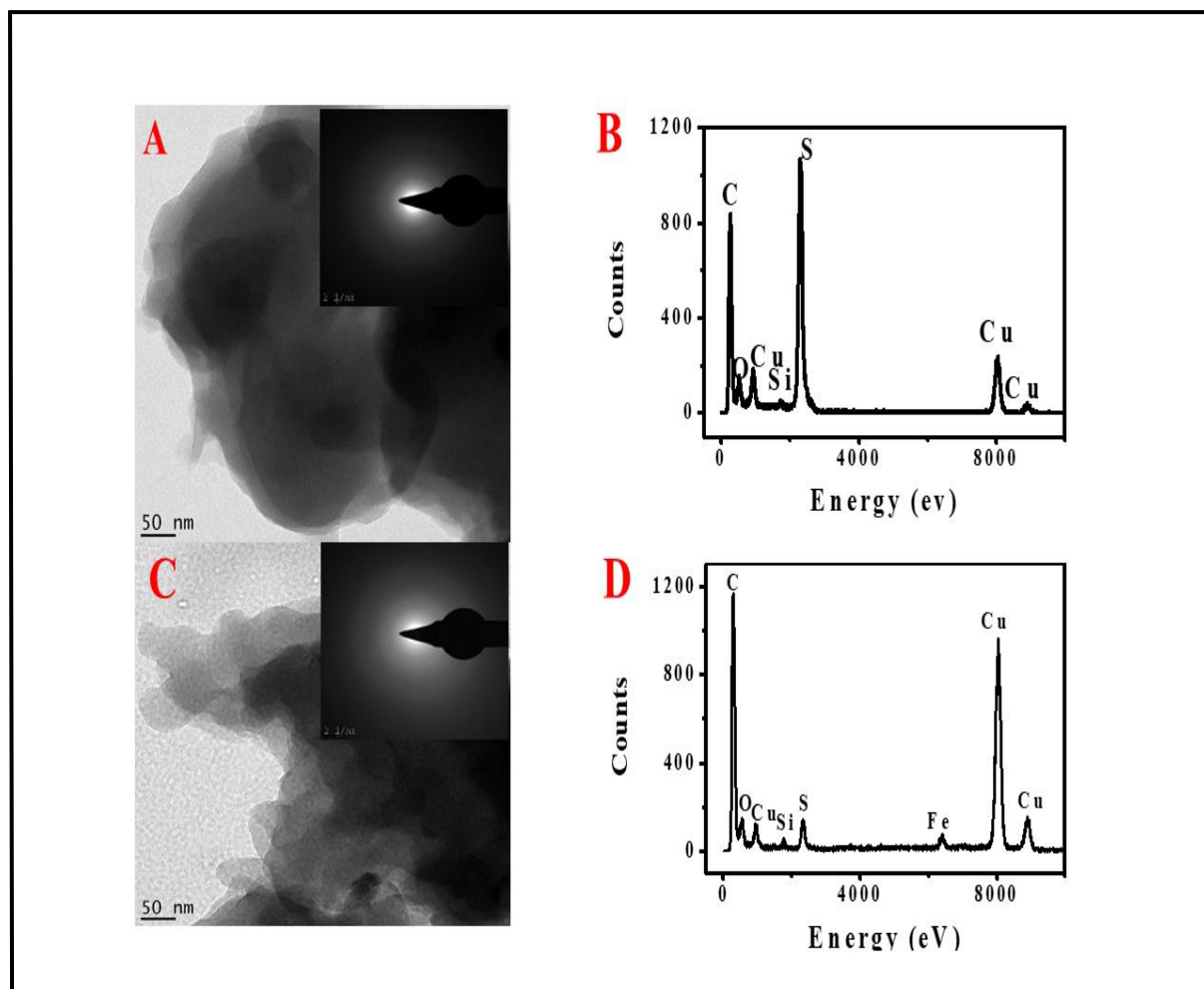
Figure 4. 10: SEM images of (A) PEDOT, (B) PEDOT-PSSA, (C) G2PPT-co-PEDOT, and (D) G2PPT-co-PEDOT-PSSA.

The introduction of PSSA on the backbone of PEDOT shows morphological changes as small particles are observed on the surface of PEDOT (figure 4.10 (B)). This then confirms the presence of PSSA on PEDOT. The image of G2PPT-co-PEDOT (figure 4.10 (C)) shows a coral-like or tubular-like structures with many tentacles which are separated from each other. However, the flake-like structures are also observed demonstrating the presence of PEDOT. This then indicates that the tubular-like structures are due to the unique properties of G2PPT. The same observation seen on the introduction of PSSA to PEDOT is also observed on the introduction of PSSA to G2PPT-co-PEDOT (figure 4.10 (D)), showing the presence of PSSA which results to morphological changes. The effect or morphological structures of G2PPT

might not be clear because of the entire surface coverage of PEDOT to form the core-shell star copolymer. Hence all the images look PEDOT-like morphologies.

#### 4.1.2.8. High Resolution Transmission Electron Microscopy (HRTEM).

The internal morphologies of PEDOT, PEDOT-PSSA, G2PPT-co-PEDOT, and G2PPT-co-PEDOT-PSSA were investigated by employing HRTEM coupled with EDX for elemental analysis. The results are presented in **figure 4.11 (A-H)** together with the inset images of the selected area electron diffraction (SAED) patterns used to determine the crystallinity of the samples.



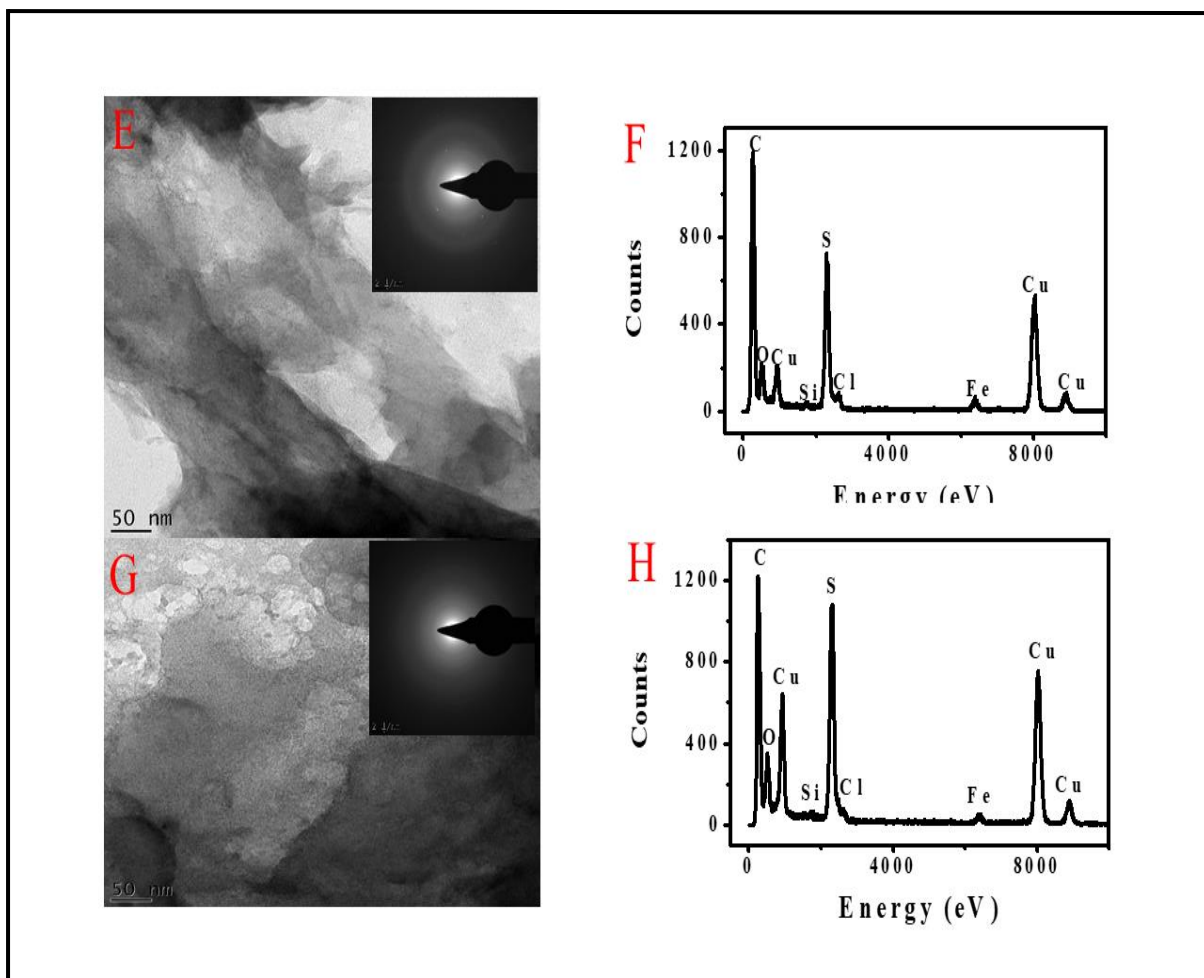


Figure 4. 11: HRTEM images of (A) PEDOT (C) PEDOT-PSSA (E) G2PPT-co-PEDOT (G) G2PPT-co-PEDOT-PSSA, and EDX of (B) PEDOT (D) PEDOT-PSSA (F) G2PPT-co-PEDOT (H) G2PPT-co-PEDOT-PSSA. Inset: SAED of all the samples.

It could be seen that both PEDOT and PEDOT-PSSA (figure 4.11 (A and C)) showed spherical structures. Upon copolymer formations, the morphology was relatively cloudy-like but some microporous structures are observed (figure 4.11 (E and G)). This can be attributed to the growth of PEDOT on the surface of G2PPT forming a core-shell star copolymer upon subsequent polymerisation. The SAED results of PEDOT and PEDOT-PSSA do not show clear ring patterns which suggest amorphous structures as seen from XRD. However, SAED of the star polymers show ring patterns but not that clear suggesting semi-crystalline structures. This crystallinity observation could be attributed to the unique properties brought by G2PPT upon

copolymer formation. The elemental analysis of C, O, S, and N were investigated by EDX presented in figure 4.11 (B, D, F, and H). All expected elements were observed except nitrogen. This is due to the elements of the dendrimer being hidden by the bulky PEDOT elements in its periphery. The presence of Fe and Cl are the remaining traces of the oxidant used during synthesis, while the Cu is from the copper grid.

### 4.1.3. Electrochemical Characterisation

Electrochemistry of functional species is one of the most prominent parameters for potential usage of these materials as semiconductors for photovoltaic applications [23]. In order to decide the possible usage of a material as a semiconductor, its electrochemical response should be generally determined. For these purposes in this work, the electrochemical characterisation of PEDOT, PEDOT-PSSA, G2PPT-co-PEDOT, and G2PPT-co-PEDOT-PSSA was investigated with voltammetric measurements such as cyclic voltammetry (CV) and Square wave voltammetry (SWV) to determine the HOMO and LUMO which leads to the determination of the electrochemical band gap.

#### 4.1.3.1. Cyclic Voltammetry (CV)

**Figure 4.12** below shows the voltammetric responses, current-potential curves of glassy carbon electrode (GCE), PEDOT, PEDOT-PSSA, G2PPT-co-PEDOT, and G2PPT-co-PEDOT-PSSA in 0.1 M TBAP/DMSO electrolytic solution at 100 mV/s scan rate. The cyclic voltammograms consistently displayed one distinctive oxidation and one reduction peak. PEDOT which is known to have a low oxidation potential has an oxidation peak potential ( $E_{pa}$ ) at  $\sim 0.2620V$  and a reduction peak potential ( $E_{pc}$ ) at  $\sim 0.120V$ .

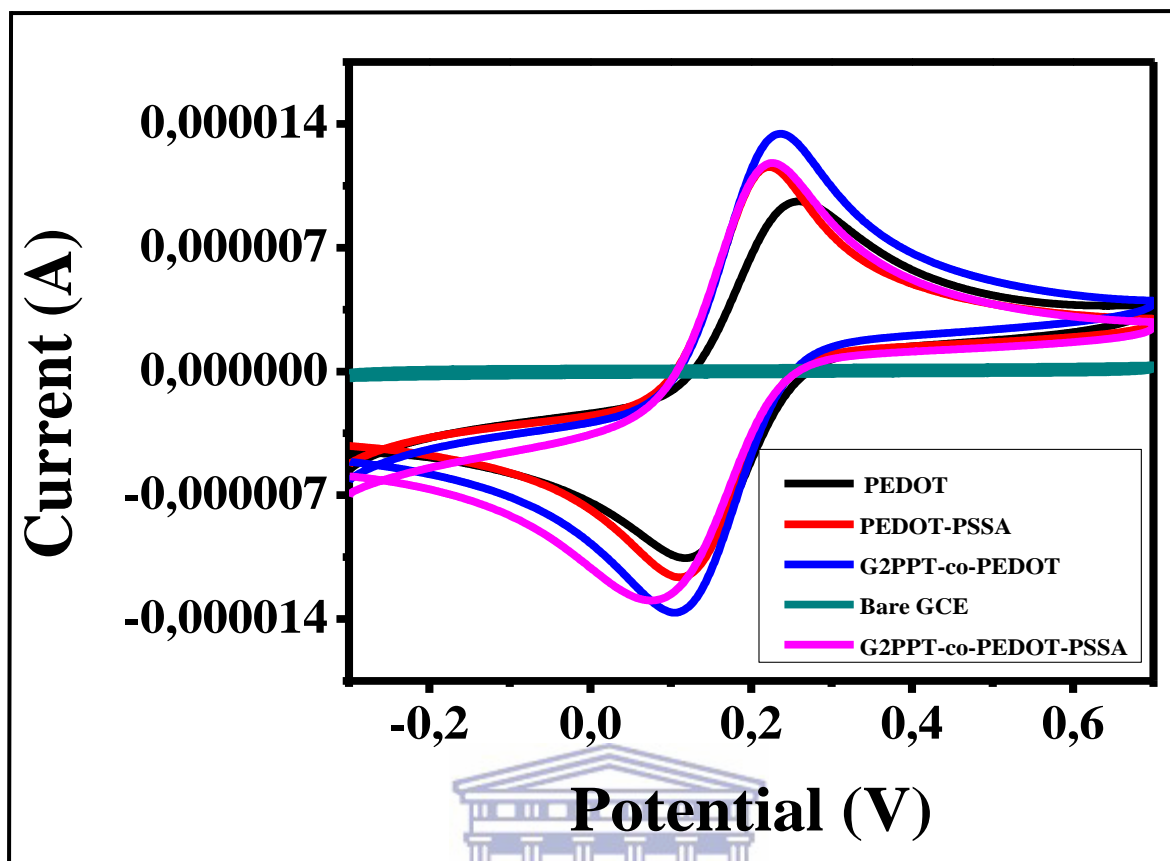


Figure 4. 12: Cyclic voltammograms of PEDOT, PEDOT-PSSA, G2PPT-co-PEDOT, and G2PPT-co-PEDOT-PSSA in 0.1 M TBAP/DMSO electrolyte at 100 mV/s.

The maximum anodic current ( $I_{pa}$ ) was observed to be  $9.8\mu A$  and the maximum cathodic current was observed to be  $-10.2\mu A$ . The voltammogram is symmetrical with the ratio of the anodic to cathodic current ( $I_{pa}/I_{pc}$ ) equal to unity, which is characteristic of a reversible behaviour [24]. However, the introduction of both PSSA and G2PPT to form the star copolymers causes an increase in the conductivity as seen by the increase in current. This could be attributed to the increased electron density and conjugation which promotes fast migration of the  $\pi$  electrons or bipolarons along the polymer chains. The PSSA which acts as a polyelectrolyte increases the diffusional ions thus accelerates the rate at which the ions are inserted and released on the electrode surface, hence resulting in increased current. With the

help of the cyclic voltammograms above, the HOMO and LUMO of the materials were determined and the results are tabulated below (see **table 4.1**).

The determination of the HOMO and LUMO was done using the following equation reported by Dong *et al* [25]:

$$E_{\text{LUMO}} = (E'_{\text{red}} + 4.8) \text{ eV} \quad 4.2$$

$$E_{\text{HOMO}} = (E'_{\text{ox}} + 4.8) \text{ eV} \quad 4.3$$

$$E_{\text{g}} = E_{\text{LUMO}} - E_{\text{HOMO}} \quad 4.4$$

Where  $E'_{\text{red}}$  and  $E'_{\text{ox}}$  are the onset reduction and oxidation potentials.

Material	$E'_{\text{red}}$ (V)	$E'_{\text{ox}}$ (V)	$E_{\text{LUMO}}$ (eV)	$E_{\text{HOMO}}$ (eV)	$E_{\text{g}}$ (eV)
PEDOT	0.307	0.105	5.107	4.905	0.202
PEDOT-PSSA	0.289	0.070	5.094	4.870	0.219
G2PPT-co-PEDOT	0.281	0.078	5.081	4.880	0.201
G2PPT-co-PEDOT-PSSA	0.267	0.068	5.067	4.890	0.199

Table 4. 1: Summary of HOMO, LUMO, and the band gap.

The effect of scan rate on the electrochemical responses of PEDOT, PEDOT-PSSA, G2PPT-co-PEDOT, and G2PPT-co-PEDOT-PSSA was also investigated in 0.1M TBAP/DMSO electrolytic system using GCE as the working electrode. **Figure 4.13** below illustrates the multi-scan voltammograms of the materials at scan rates ranging from 10-100 mV/s. Analysis

of the voltammograms revealed that the peak potentials and corresponding current vary with the scan rates.

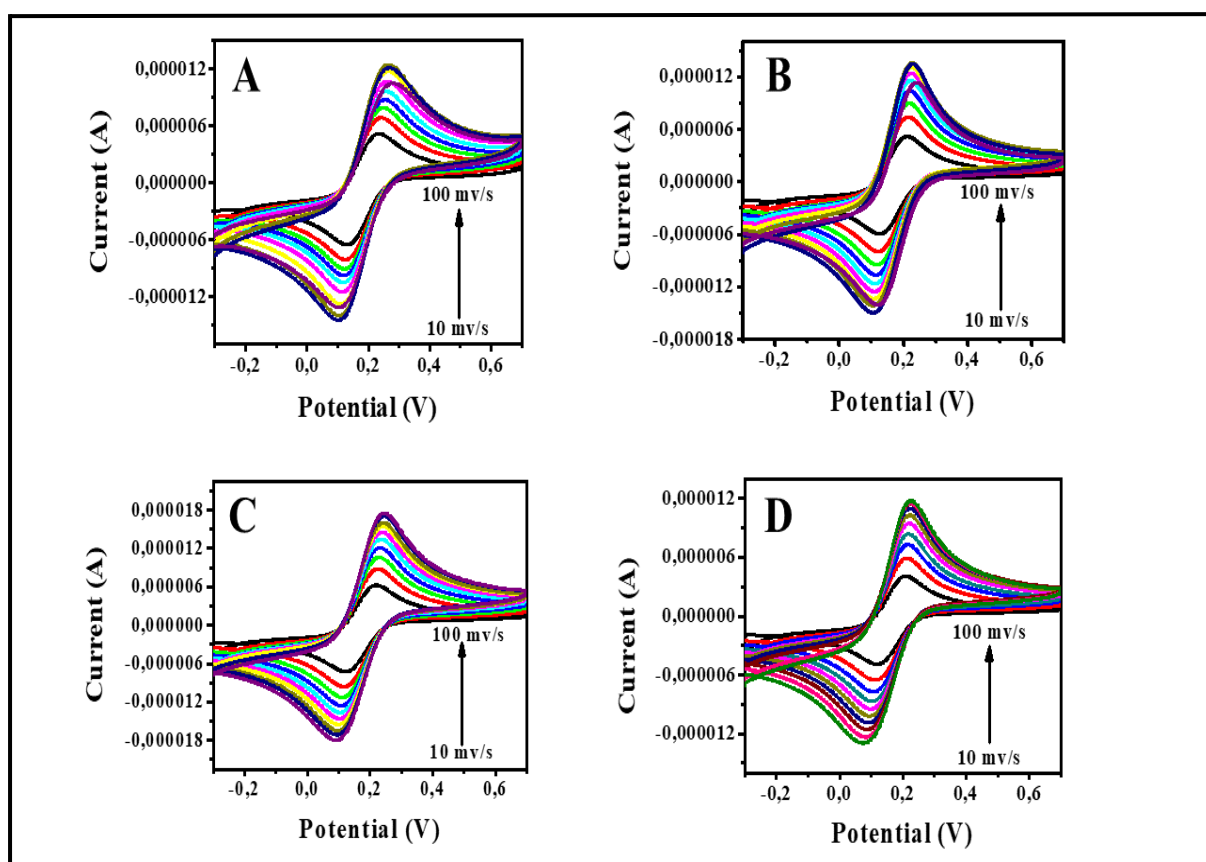


Figure 4. 13: Multi-scan rate cyclic voltammograms of (A) PEDOT, (B) PEDOT-PSSA, (C) G2PPT-co-PEDOT, and (D) G2PPT-co-PEDOT-PSSA at 10-100 mV/s scan rates in 0.1M TBAP/DMSO.

The systems displayed progressive shift in anodic peak towards more positive values coupled with shift in cathodic peak towards less positive values with increase in scan rate. The separations increase progressively from 0.102 V at 10 mV/s to 0.160 V at 100 mV/s, 0.081 V at 10 mV/s to 0.123 V at 100 mV/s, 0.096 V at 10 mV/s to 0.155 V at 100 mV/s, and 0.088 V at 10 mV/s to 0.154V at 100 mV/s for PEDOT, PEDOT-PSSA, G2PPT-co-PEDOT, and G2PPT-co-PEDOT-PSSA respectively and are all coupled with increase in the magnitude of the peak currents with increase scan rates. This indicates that the polymer structures are electro-



active governed by the sulphur atom in the thiophene ring and electron transfer processes are coupled to a diffusion process namely, charge transportation along the polymeric structures [26-27].

With the help and estimation from CV (figure 4.12 and 4.13), the number of electrons transferred for the polymers was calculated using the equation [26]:

$$|E_p - E_{p1/2}| = 2.20RT/nF = 56.5/n \quad 4.5$$

Where  $E_p$  is the maximum peak potential,  $E_{p1/2}$  is half the maximum peak potential,  $R$  is the gas constant (8.314 J.mol.K<sup>-1</sup>),  $T$  is the absolute temperature (298K) of the system,  $F$  is the faraday constant (96.584 C/mol), and  $n$  represents the number of electrons transferred. From the equation, the number of electrons was found to be  $n=2$  (two-electron transfer systems) for all the polymers which is in agreement to the number of electrons ( $n=2$ ) removed during oxidation of two EDOT monomers when being polymerised by the oxidant FeCl<sub>3</sub> (see scheme 4.2). Baleg *et al* also found two electrons being transferred during his studies of G1PPI-co-PPY [28].

Now that the number of electrons transferred is known, the Brown Anson equation was used to estimate the surface concentration ( $\Gamma^*$ ) of the adsorbed electro-active species using the anodic peak current  $I_{pa}$  obtained at 100 mV/s. The equation is as follows [26, 27, 29, 30]:

$$I_p = n^2 F \Gamma^* A v / 4RT \quad 4.6$$

Where  $I_p$  represents the peak current,  $A$  is the surface area of the electrode (0.071 cm<sup>2</sup>),  $v$  is the scan rate (V/s),  $\Gamma^*$  is the surface concentration of the adsorbed electro-active species,  $F$ ,  $R$ ,  $T$ , and  $n$  are the same as in equation 4.5. The surface concentration of PEDOT, PEDOT-PSSA, G2PPT-co-PEDOT, and G2PPT-co-PEDOT-PSSA was found to be  $3.468 \times 10^{-2}$ ,  $4.15 \times 10^{-2}$ ,  $4.30 \times 10^{-2}$  and  $4.841 \times 10^{-2}$  mol/cm<sup>2</sup> respectively.

Now that that surface concentration of each polymer is known, the Randels-Sevcik equation of analysing voltammetric data was used to determine the rate of charge transport coefficient ( $D$ ) along the polymer chains. The Randels-Sevcik behaviour of the cyclic voltammetric peak currents has been used to evaluate  $D$  from the slope of the straight line obtained from the plot of  $I_p$  versus  $v^{1/2}$ . The equation is as follows:

$$I_p = 2.686 \times 10^5 n^{3/2} A \Gamma^* D^{1/2} v^{1/2} \quad 4.7$$

The parameters  $I_p$ ,  $n$ ,  $A$ ,  $D$ ,  $v$ , and  $\Gamma^*$  are the same as in equation 4.6. The plot of  $I_p$  versus  $v^{1/2}$  is presented in **figure 4.14 (A-B)** below.

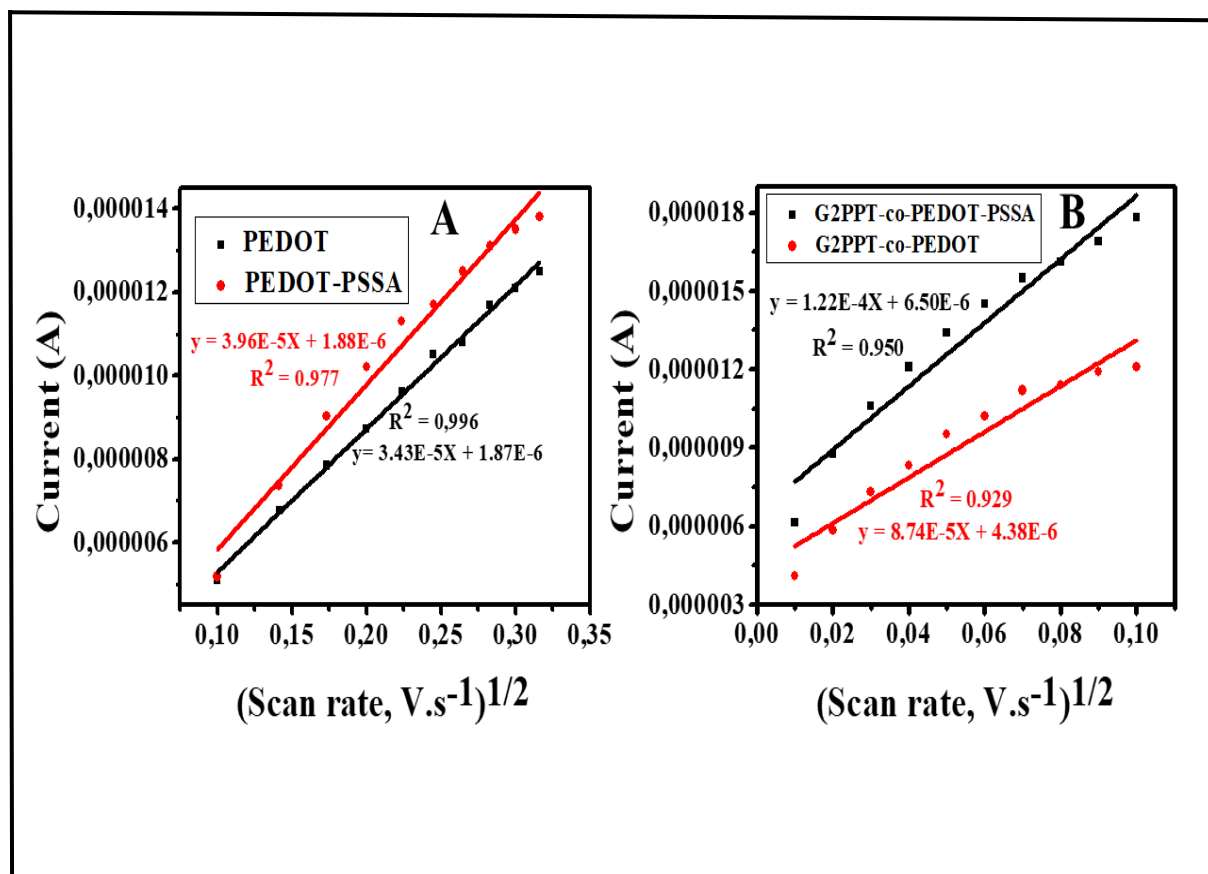


Figure 4. 14: Randels-Sevcik plots for GCE in 0.1M TBAP/DMSO electrolytic system at scan rates range of 10-100 mV/s.

The  $D$  values were determined to be  $3.36 \times 10^{-16}$ ,  $3.13 \times 10^{-16}$ ,  $1.42 \times 10^{-15}$ , and  $2.18 \times 10^{-15}$   $\text{cm}^2/\text{s}$  for PEDOT, PEDOT-PSSA, G2PPT-co-PEDOT, and G2PPT-co-PEDOT-PSSA respectively. The  $D$  value of G2PPT-co-PEDOT-PSSA is a magnitude higher than the  $D$  value of pristine PEDOT and G2PPT-co-PEDOT. This implies that electron transfer processes are occurring at a much faster rate in G2PPT-co-PEDOT-PSSA than in pristine PEDOT and the start polymer without PSSA. This can be attributed to the combination of the unique properties of G2PPT and the conducting polymer PEDOT coupled to PSSA which act as a polyelectrolyte, thus accelerating the rate of flow of ions going in and out of the electrode surface.

The linear regression equations for the anodic peaks which are based on the logarithm of the oxidative peak currents against the logarithm of the scan rate indicating diffusion kinetically controlled reactions for all the polymers in determining the transfer coefficient ( $\alpha$ ) are presented in **figure 4.15 (A-B)** below.

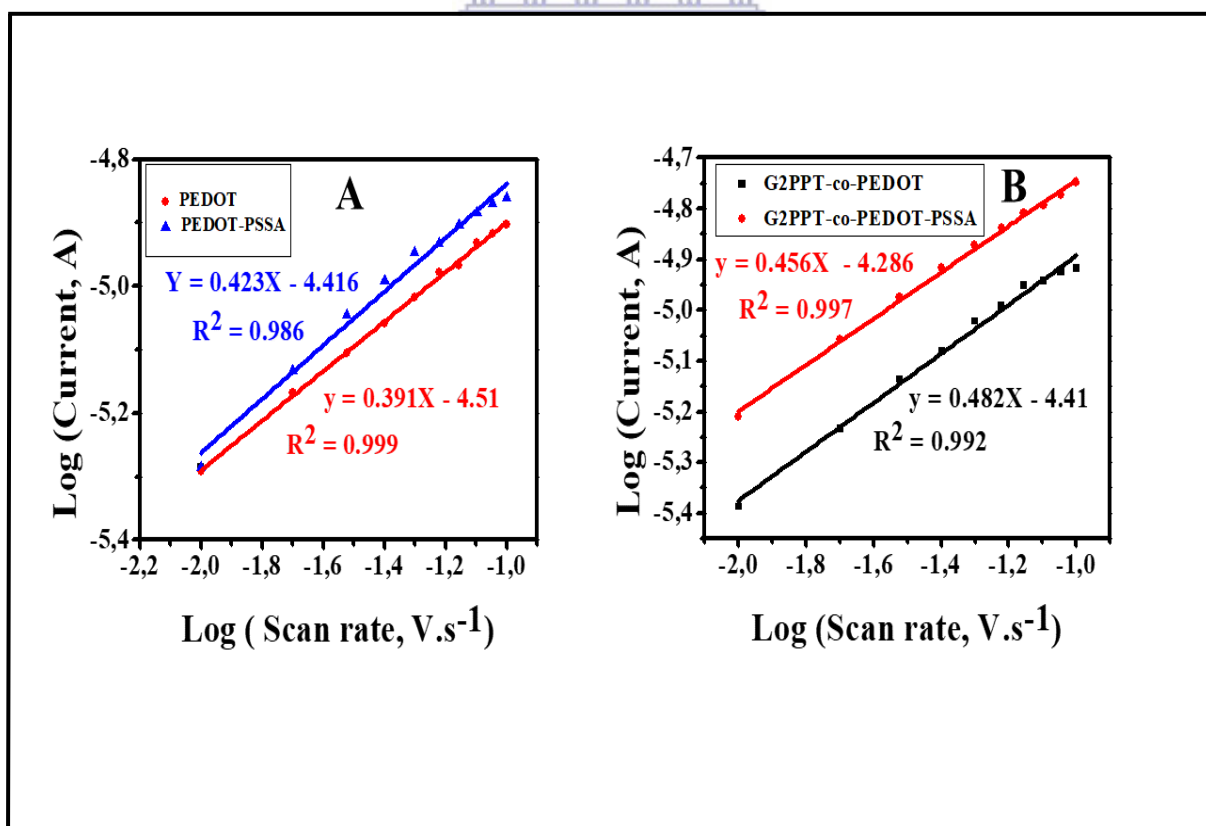


Figure 4. 15: Logarithm plot of peak current vs scan rate for  $\alpha$  determination.

Table 4.2 below presents all the electrochemically determined parameters which are based on diffusion kinetically controlled reactions of the polymers.

Material	Surface concentration, $\Gamma^*$ , (mol/cm <sup>2</sup> )	Diffusion coefficient, $D_e$ , (cm <sup>2</sup> /s)	Transfer coefficient, $\alpha$ .	Number of transferred electrons
PEDOT	$3.468 \times 10^{-2}$	$3.36 \times 10^{-16}$	0.391	2
PEDOT-PSSA	$4.15 \times 10^{-2}$	$3.13 \times 10^{-16}$	0.423	2
G2PPT-co-PEDOT	$4.30 \times 10^{-2}$	$1.42 \times 10^{-15}$	0.482	2
G2PPT-co-PEDOT-PSSA	$4.841 \times 10^{-2}$	$2.18 \times 10^{-15}$	0.456	2

Table 4. 2: Electrochemical parameters of all the polymers.

#### 4.1.3.2. Square Wave Voltammetry (SWV)

The SWV was utilized as the electrochemical probe of the system due to its high sensitivity Faradaic current [31]. Basically, it was used as a support to CV and to confirm that there were no additional or hidden redox couples. Therefore, as presented in **figure 4.16 (A-B)** below, it is clear that no additional redox couples are observed hence confirming that the system undergoes a two-electron process. Moreover, SWV confirmed the reversibility of the redox. The effect of varying scan rates is presented in **figure 4.17 (A-D)** for oxidation and **figure 4.18 (A-D)** for reduction.

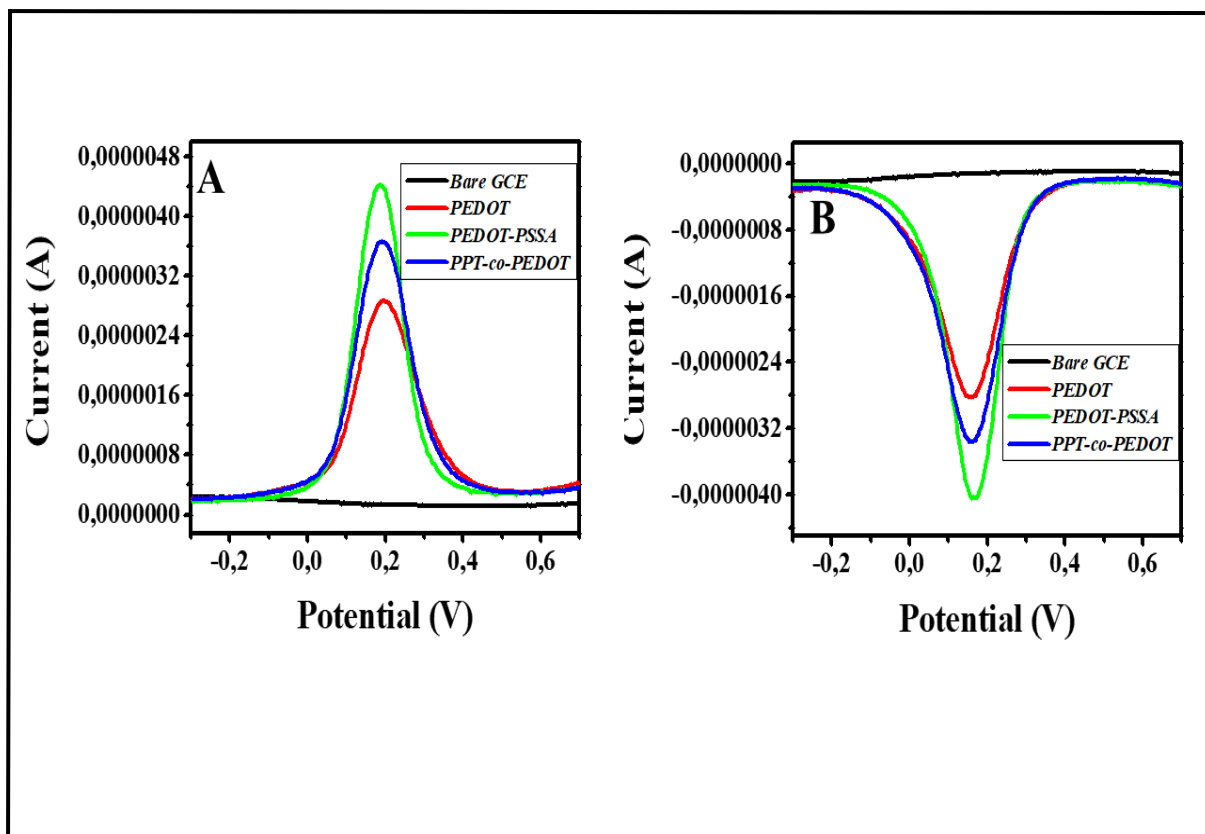


Figure 4. 16: SWV representing (A) Oxidation (B) Reduction of the polymers in 0.1M TBAP/DMSO at 100 mV/s.

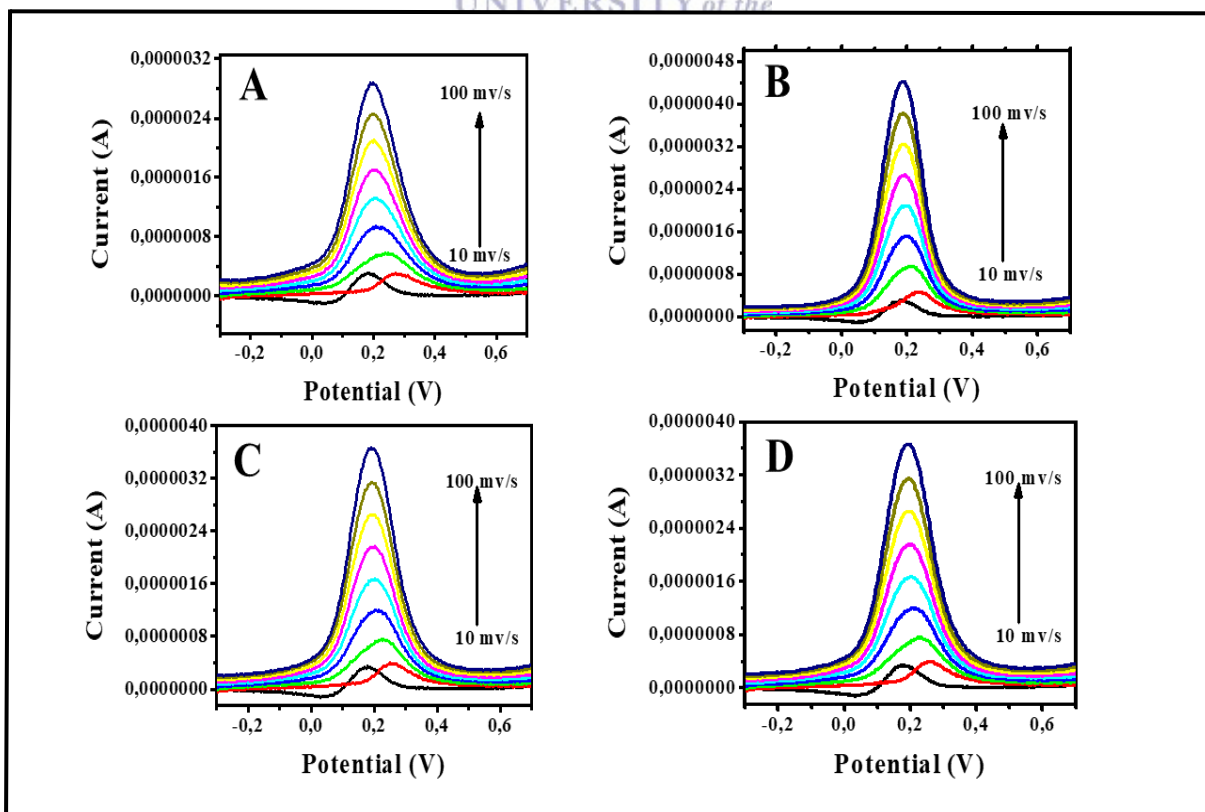


Figure 4. 17: SWV oxidation of (A) PEDOT (B) PEDOT-PSSA (C) G2PPT-co-PEDOT (D) G2PPT-co-PEDOT-PSSA in 0.1M TBAP/DMSO at scan rate range of 10-100 mV/s.

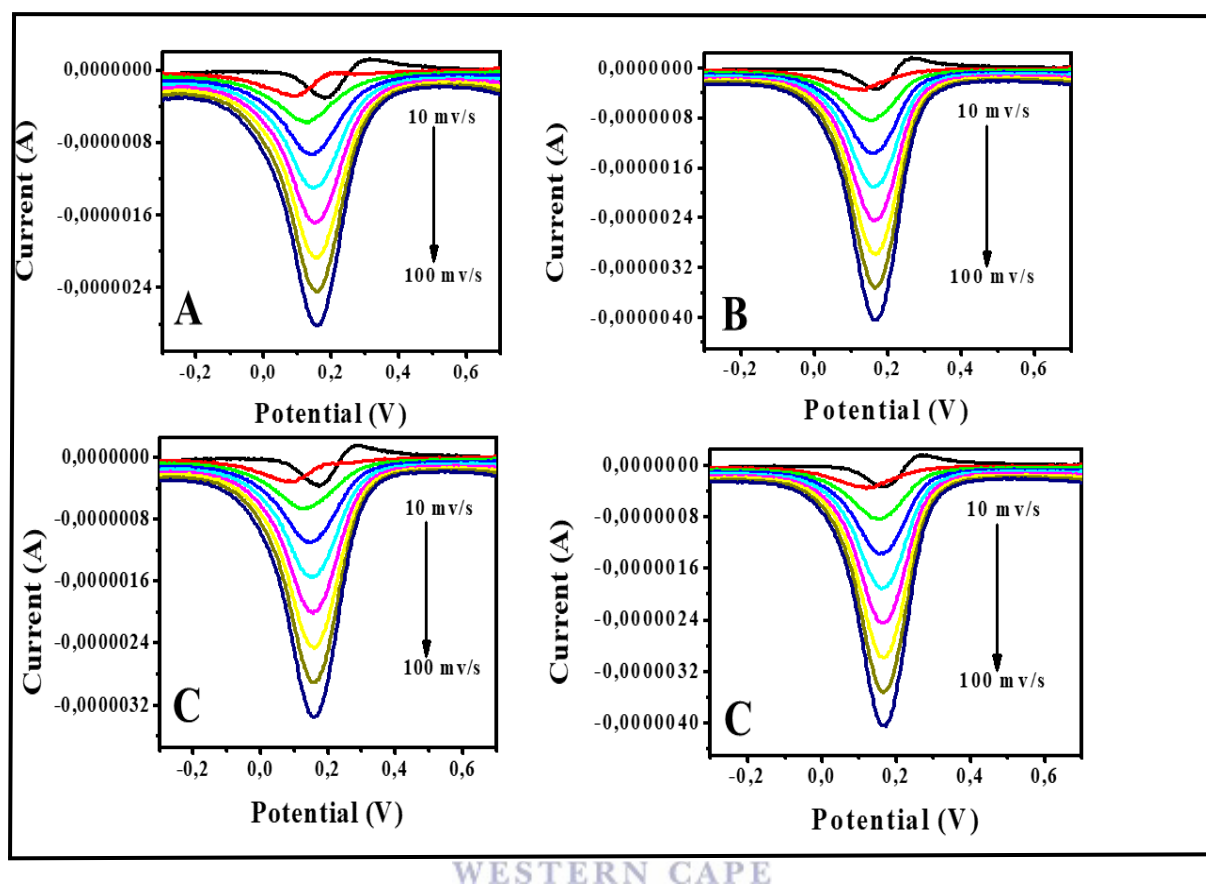


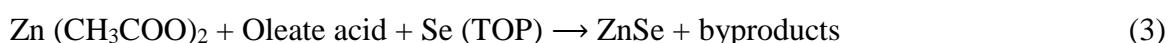
Figure 4. 18: SWV reduction of (A) PEDOT (B) PEDOT-PSSA (C) G2PPT-co-PEDOT (D) G2PPT-co-PEDOT-PSSA in 0.1M TBAP/DMSO at scan rate range of 10-100 mV/s.

## 4.2. Synthesis and Characterisation of ZnSe Quantum Dot (QD)

### 4.2.1. Synthesis

Scheme 4.6 below illustrates the organic synthesis of ZnSe QD. The QD was prepared as described in the previous chapter, section 3.7. The QD was synthesized according to literature [32]. In the experimental procedure, oleic acid (OA) was chosen as the surface binding ligand for stabilising the nanoparticles and cationic precursors. The ligand keep the particles isolated, thus preventing nuclei agglomeration and facilitating homogeneous growth [33-34]. Trioctylphosphine (TOP) act as the coordinating solvent and selenium (Se) powders solvent

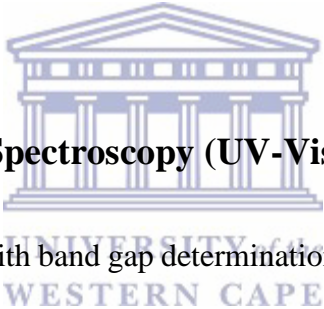
also to provide better size control and surface passivation [33-34]. The QD is formed by first preparing both zinc and selenium precursor solutions and later combine them. The synthesis reaction (scheme 4.6) can be described as follows [32]:



Equation (3) is the general reaction equation of the formation of ZnSe QD in this experiment. Equation (1) is the process of forming Zn-complexes while equation (2) is the process involving dissolution of Se powder in TOP.

## 4.2.2. Characterisation

### 4.2.2.1. Ultraviolet Visible Spectroscopy (UV-Vis)



Electronic transitions together with band gap determination of the ZnSe QD was achieved by employing UV-Vis spectroscopy at the range of 200-1100 nm in 200 ppm toluene. **Figure 4.19** show the absorption spectra of ZnSe nanoparticles. From the figure, the optical absorption wavelength was found to be 416 nm which is close to the absorption wavelength of 412 nm observed by Chen *et al* [32]. However, it is well known that the ligand used to passivate the surface of the particles, the reaction temperature, and the heating time all play a role in determining the rate of growth, and the size of the particles after injection [32, 35-36]. With the help of the absorption spectrum of ZnSe QD, the Tauc relation was employed to determine the optical band gap. The Tauc relation is given by **equation 4.1** above and the results are presented in **figure 4.20** below.

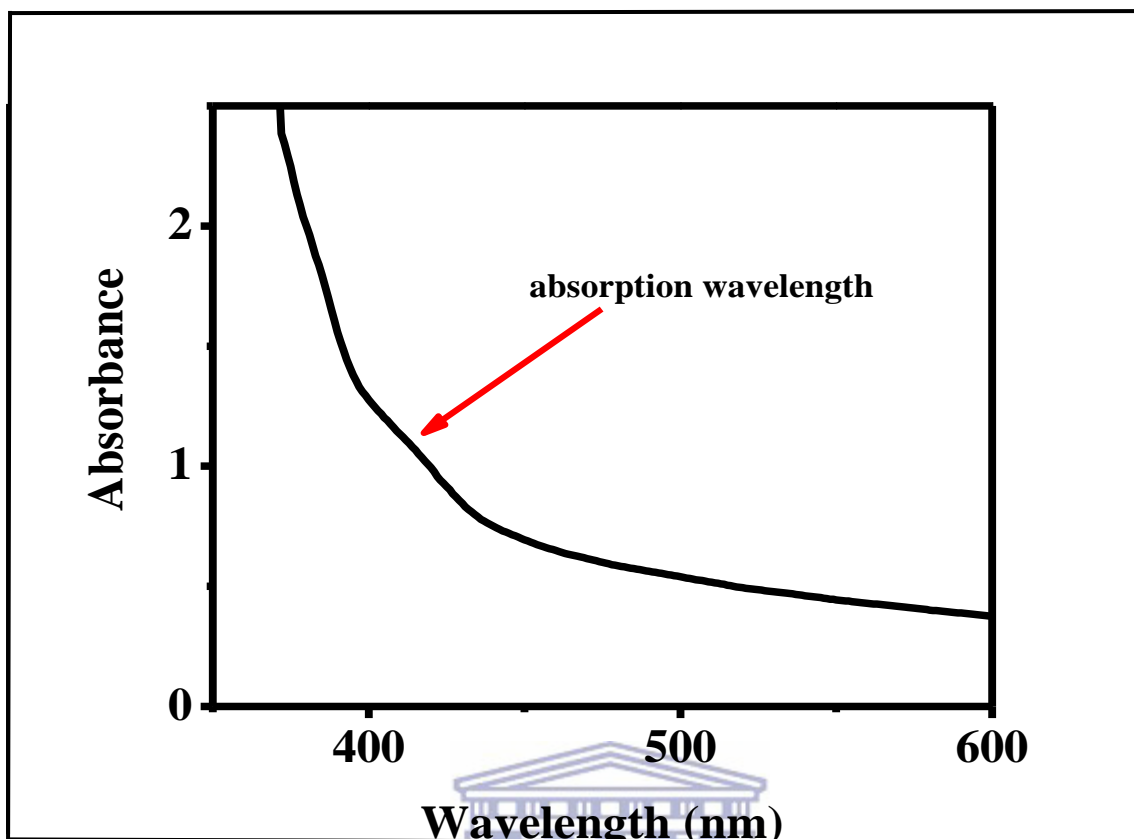


Figure 4. 19: Optical absorption spectrum of ZnSe QD in 200 ppm Toluene.

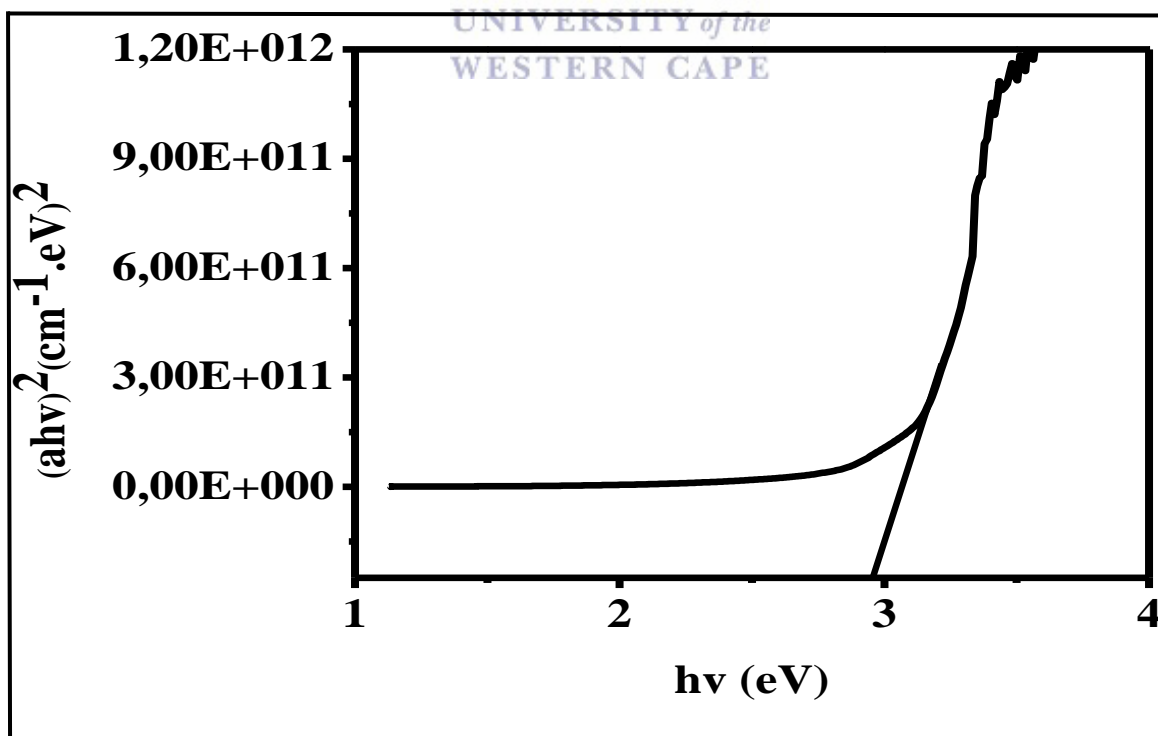


Figure 4. 20: Tauc plot of ZnSe QD for band gap determination.



The optical band energy,  $E_g$ , of ZnSe QD was found to be 2.95 eV which is close to the value of 3.14 eV found by Senthilkumar *et al* [35]. This band gap shows a blue shift of 0.25 eV from the standard bulk band gap at room temperature ( $E_g = 3.7$  eV).

#### 4.2.2.2. Photoluminescence (PL) Spectroscopy

Fluorescence studies of the QD was achieved with the help of absorption studies obtained from UV-Vis using the same prepared solution. The results are presented in **figure 4.21** below.

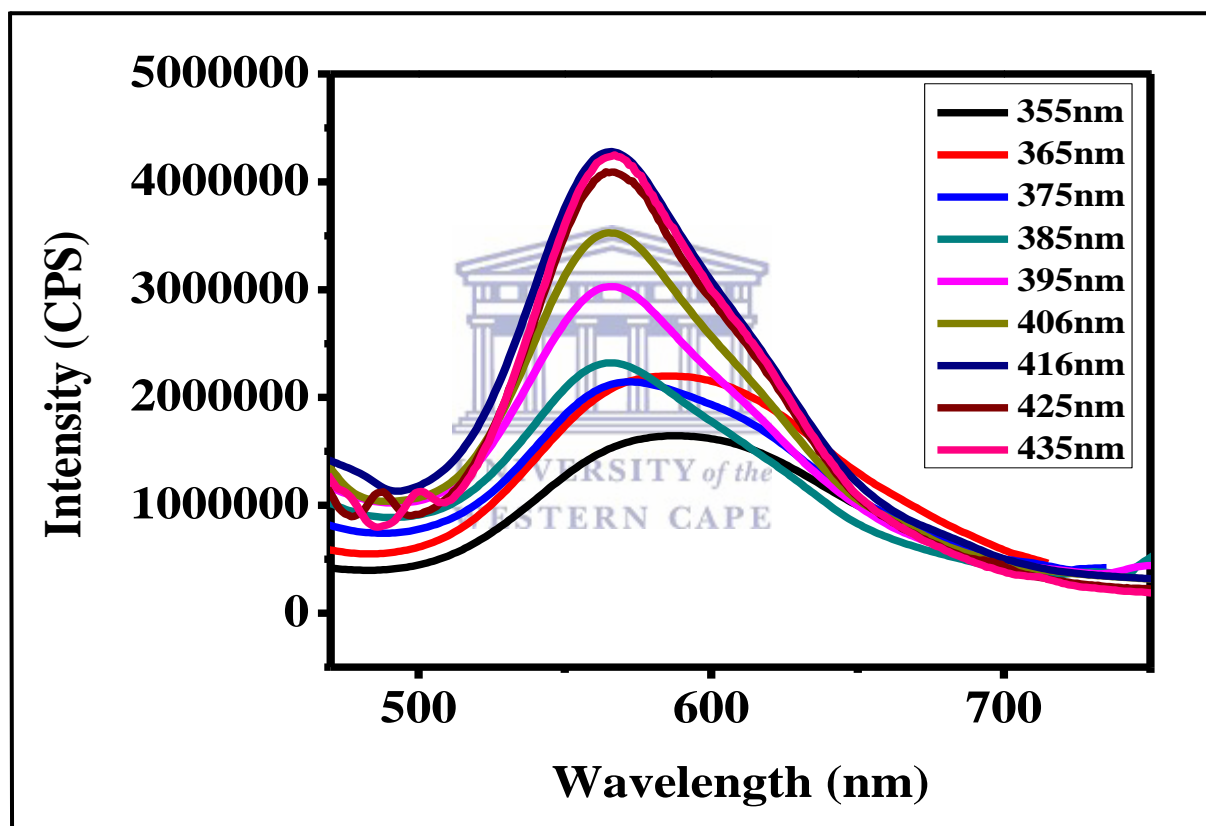


Figure 4. 21: Photoluminescence spectra of ZnSe.

The ZnSe QD is excited at different excitation wavelengths ranging from 355-435 nm at a wavelength difference of 10 nm. Even though the QD is excited at different wavelength, the emission peak is centred at 566 nm which is attributed to the recombination of the excitons. The obtained QD show a stoke shift of 116 and 179 nm with respect to the emission peaks obtained by Chen *et al* [32] and Selthilkumar *et al* [35] respectively. The PL emission spectra

is also a Gaussian shape, which clearly indicates a pure band-gap emission without any significant trap state emission [32]. The narrow emission peak and no change in the emission peak indicates that the QD are monodispersed.

#### 4.2.2.3. High Resolution Transmission Electron Microscopy (HRTEM)

The HRTEM images coupled with EDX of the as-prepared ZnSe QD and the selected area electron diffraction (SAED) are presented in figure 4.22 (A-B) below.

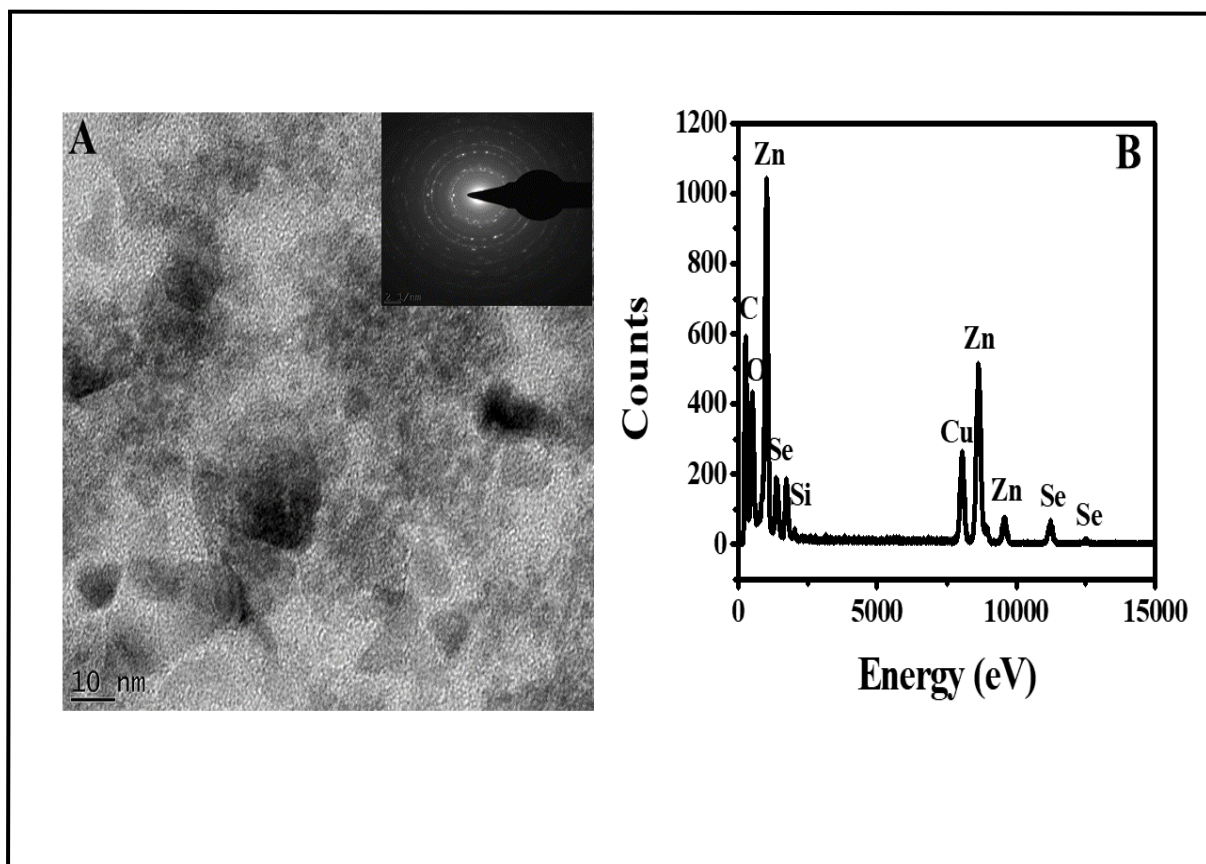


Figure 4. 22: (A) HRTEM image of ZnSe and (B) EDX results. Inset: SAED of ZnSe

The image (A) shows that the particles are well dispersed, small, and spherical in shape. The SAED shows clear ring patterns indicating pure crystalline QD. All the expected elements, Zn, SE, C, and O are observed confirming the successful formation of the QD. C and O are from the OA binding ligand while Cu is from the copper grid.

### 4.3. Optical properties of G2PPT-co-PEDOT-PSSA: ZnSe QD blends

#### 4.3.1. Ultraviolet Visible Spectroscopy (UV-Vis)

Figure 4.23 below illustrates the UV-Vis absorption spectra of the blended active layer G2PPT-co-PEDOT-PSSA: ZnSe QD with the polymer acting as a donor and the QD acting as an acceptor at different ratios in a solvent mixture of DMSO and toluene.

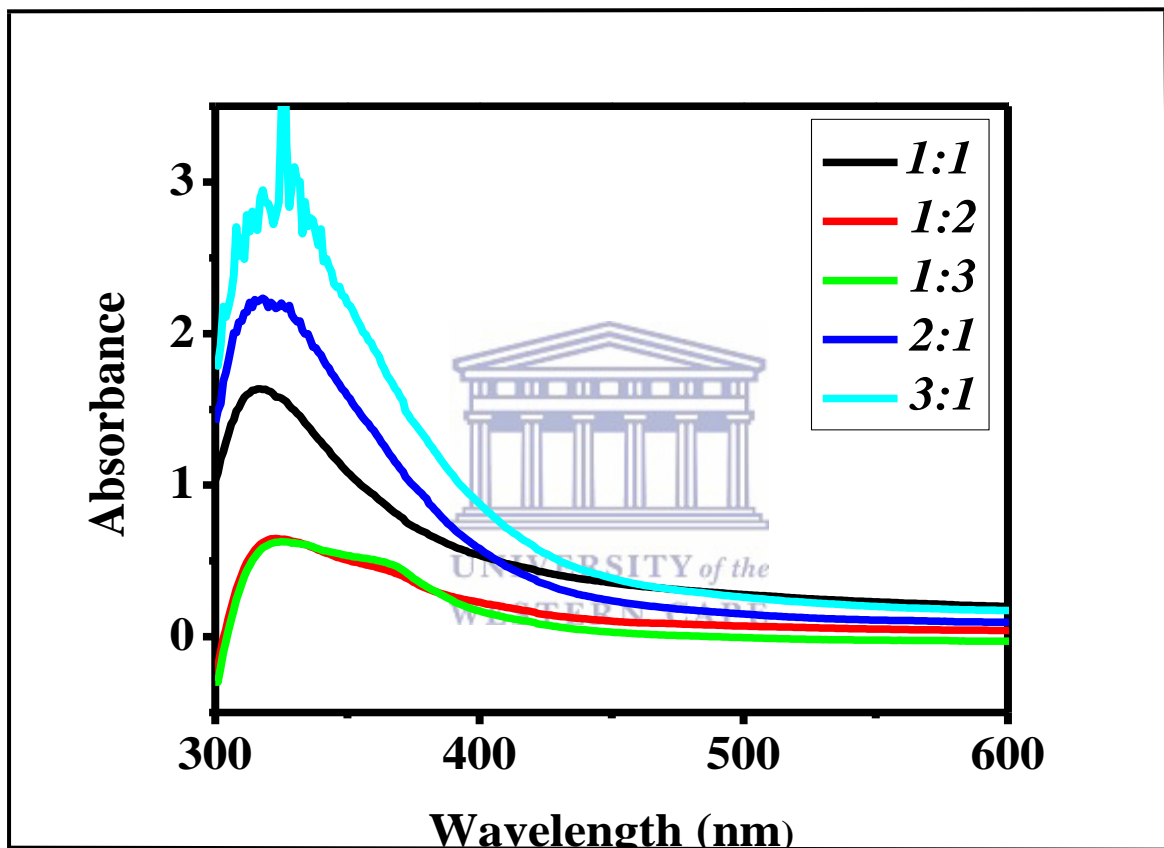


Figure 4. 23: UV-Vis absorption spectra of G2PPT-co-PEDOT-PSSA: ZnSe QD blends in different ratios in terms of volume.

From the results it is observed that increasing the content of G2PPT-co-PEDOT-PSSA also increases the absorbance as seen from the spectra of 2:1 and 3:1. This is indicative of the G2PPT-co-PEDOT-PSSA being responsible for the absorption of the light in order to facilitate electron excitement which is what was expected from a donor material. On the other hand, increasing the content of the QD (1:2 and 1:3) results in the appearance of two distinct

absorption peaks at 323 and 365 nm. In comparison to the absorption spectra of G2PPT-co-PEDOT-PSSA (figure 4.5(B)), the absorption peak shifts from 342 nm in G2PPT-co-PEDOT-PSSA to 365 nm in the blends, which shows the presence of ZnSe QD. The shift is of vital importance for solar cells application because it indicates reduction of the band gap, hence requiring less energy to excite electrons from the valence band to the conduction band as compared to the donor material alone.

### 4.3.2. Photoluminescence (PL) Spectroscopy

The influence of the presence of the QD in the photoluminescence spectra of G2PPT-co-PEDOT-PSSA is a very significant parameter that needs to be explored so as to determine the applicability of a compound as an acceptor in the photovoltaic system. With the information obtained from UV-Vis, only photoluminescence studies of the 1:3 blend was investigated because it showed the presence of the QD. The mixture was excited at different excitation wavelength ranging from 278-398 nm at a difference of 15 nm to check the particle size distribution. The PL spectra is presented in **figure 4.24** below.

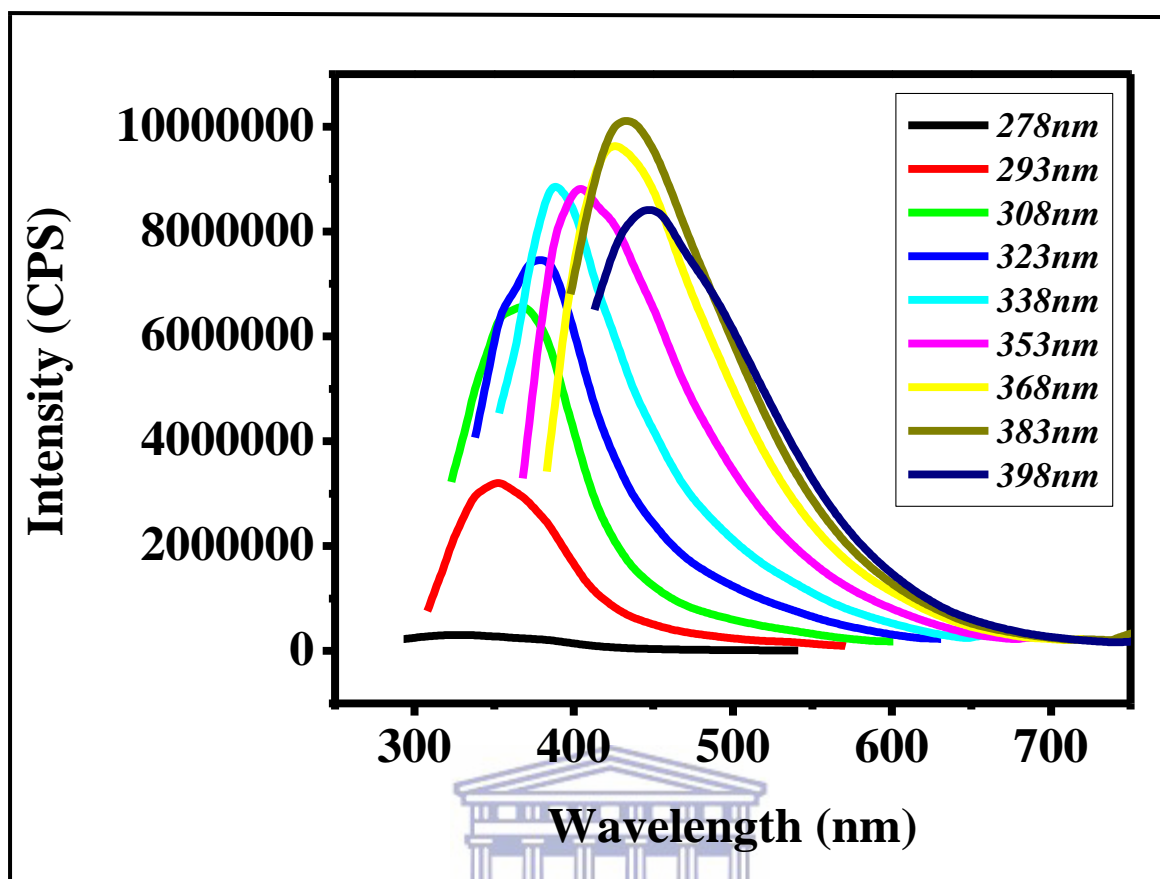


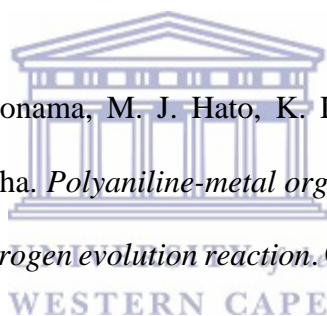
Figure 4. 24: Photoluminescence of G2PPT-co-PEDOT-PSSA: ZnSe QD (1:3) blends in a mixture of DMSO/toluene.

From the results, different emission peaks are observed which indicates polydispersity of the particles. The emission is attributed to the electron transfer from the donor to the acceptor which is evident by the decrease in PL intensity in comparison with the emission spectra of G2PPT-co-PEDOT-PSSA (figure 4.7(D)).

#### 4.4. References

- [1]- C. Jianga, G. Chen, X. Wang. *High-conversion synthesis of poly(3, 4-ethylenedioxythiophene) by chemical oxidative polymerization*. *Synthetic Metals* 162 (2012) 1968-1971.
- [2]- D. Bhattacharyya, R. M. Howden, D. C. Borrelli, K. K. Gleason. *Vapor Phase Oxidative Synthesis of Conjugated Polymers and Applications*. *Journal of Polymer Science Part B: Polymer Physics* 50 (2012) 1329-1351.
- [3]- W. Lövenich. *PEDOT—Properties and Applications*. *Polymer Science* 56 (2014) 135-143.
- [4]- T. Meen, K. Chen, Y. Chen, W. Chen, D. Chou, W. Lan, C. Huang. *The effect of dilute sulfuric acid on sheet resistance and transmittance in poly(3, 4-thylenedioxythiophene):poly(styrenesulfonate) films*. *International Journal of Photoenergy* (2013) 1-6.
- [5]- A. W. M. Diah, J. P. Quirino, W. Belcher, C. I. Holdsworth. *Investigation of poly(styrene sulfonic acid) in poly(3, 4-ethylenedioxythiophene)/poly(styrene sulfonic acid) dispersions by capillary electrophoresis*. *Electrophoresis* 35 (2014) 1976-1983.
- [6]- A. Baleg, N. Jahed, Anne. Yonkeu, N. Njomo, G. Mbambisa, K. M. Molapo, X. G. Fuku, G. Fomo, H. Makelane, A. Tsegaye, T. T. Waryo, P. Baker, S. Vilakazi, R. Tshikhudo, E. I. Iwuoha. *Impedimetry and microscopy of electrosynthetic poly(propylene imine)-copolypyrrole conducting dendrimeric star copolymers*. *Electrochimica Acta* 128 (2014) 448-457.
- [7]- R. A. Olowu, P. M. Ndangili, A. Baleg, C. O. Ikpo, N. Njomo, P. Baker, E. I. Iwuoha. *Spectroelectrochemical dynamics of dendritic poly(propylene imine)-poly(thiophene) star copolymer aptameric 17 $\beta$ -estradiol biosensor*. *International journal of Electrochemical Science* 6 (2011) 1686-1708.

- [8]- A. A. Baleg, N. M. Jahed, O. A. Arotiba, S. N. Mailu, N. R. Hendricks, P. G. Baker, E. I. Iwuoha. *Synthesis and characterization of poly(propylene imine) dendrimer-poly(pyrrole) conducting star copolymer*. Journal of Electroanalytical Chemistry 652 (2011) 18-25.
- [9]- Q. Zhao, R. Jamal, L. Zhang, M. Wang, T. Abdiryim. *The structure and properties of PEDOT synthesized by template-free solution method*. Nanoscale Research Letters 9 (2014) 557.
- [10]- O. Pyshkina, A. Kubarkov, V. Sergeyev. *Poly(3,4-ethylenedioxythiophene):Synthesis and Properties*. Material Science and Applied Chemistry 21 (2010) 51-54.
- [11]- M. Reyes-Reyes, I. Cruz-Cruz, R. n Lo´pez-Sandoval. *Enhancement of the Electrical Conductivity in PEDOT:PSS Films by the Addition of Dimethyl Sulfate*. J. Phys. Chem. C 114 (2010) 20220–20224.
- [12]- K. E. Ramohola, G. R. Monama, M. J. Hato, K. D. Modibane, K. M. Molapo, M. Masikini, S. B. Mdluli, E. I. Iwuoha. *Polyaniline-metal organic framework nanocomposite as an efficient electrocatalyst for hydrogen evolution reaction*. Composites part B 137 (2018) 129-139.
- [13]- M. El-Kemary, N. Nagy, I. El-Mehasseb. *Nickel oxide nanoparticles: Synthesis and spectral studies of interactions with glucose*. Materials Science in Semiconductor Processing 16 (2013) 1747–1752.
- [14]- H. S. Abdulla, A. I. Abbo. *Optical and Electrical Properties of Thin Films of Polyaniline and Polypyrrole*. International Journal of Electrochemical Science 7 (2012) 10666 – 10678.
- [15]- X. Wang, J. Song, L. Gao, J. Jin, H. Zheng, Z. Zhang. *Optical and electrochemical properties of nanosized NiO via thermal decomposition of nickel oxalate nanofibres*. Nanotechnology 16 (2005) 37–39.
- [16]- K. B. Ramohlola, M. Masikini, S. B. Mdluli, G. R. Monama, M. J. Hato, K. M. Molapo, E. I. Iwuoha, K. D. Modibane. *Electrocatalytic hydrogen production properties of poly(3-*



*Aminobenzoic acid*) doped with metal organic frameworks. *International Journal of Electrochemical Science* 12 (2017) 4392-4405.

[17]- N. Gupta, D. Kumar. *Investigations on poly (aniline-co-o-toluidine)/polystyrene sulphonic acid composite*. *Indian Journal of Engineering & Material Sciences* 16 (2009) 403-409.

[18]- D. M. Welsh, L. J. Kloeppner, L. Madrigal, M. R. Pinto, B. C. Thompson, K. S. Schanze, K. A. Abboud, D. Powel, J. R. Reynolds. *Regiosymmetric dibutyl-substituted poly (3, 4-propylenedioxythiophene) as highly electron-rich electroactive and luminescent polymers*. *Macromolecules* 35 (17) (2002) 6517-6525.

[19]- K. E. Asmunch, E. J. Samuelsent, L. A. A. Pettersson, O. Inganas, T. Johansson, R. Feidenhans. *Structure of thin films of poly(3, 4-ethylenedioxythiophene)*. *Synthetic Metals* 101 (1999) 561.

[20]- D. Kelkar, A. Chourasia. *Structural, thermal, and electrical properties of doped poly(3, 4-ethylenedioxythiophene)*. *Chemistry & Chemical Technology* 10 (2016) 395-400.

[21]- J. Pouget, M. Jozefowicz, A. Epstein, X. Tang, A. MacDiarmid. *X-ray structure of polyaniline*. *Macromolecules* 24 (1991) 779-789.

[22]- P. Chutia, A. Kumar. *Electrical conduction mechanism of poly(3, 4-ethylenedioxythiophene) nanofiber bundles at low temperature*. *Applied Physics A* 120 (2015) 1059-1068.

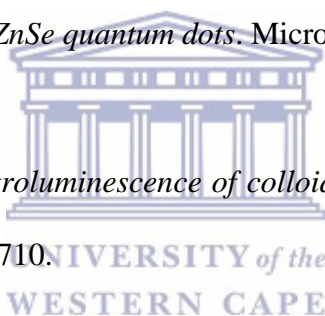
[23]- E. Guerrini, S. Trasatti. *Electrocatalysis in water electrolysis*. *Catalysis for sustainable Energy production* (2009) 235.

[24]- A. S. Adekunle. *Electrochemical and Electrocatalytic Properties of Carbon Nanotubes Integrated with Selected Metal and Metal Oxide Nanoparticles*. PhD Thesis, Department of Chemistry, University of Pretoria, (2010).



- [25]- B. Dong, J. Xu, L. Zheng, J. Hou. *Electrodeposition of conductive poly(3-methoxythiophene) in ionic liquid microemulsions*. Journal of Electroanalytical Chemistry 628 (2009) 60-66.
- [26]- M. J. Klink, E. I. Iwuoha, E. E. Ebenso. *The electro-catalytic and redox-mediator effects of nanostructured PDMA-PSA modified electrodes as phenol derivative sensors*. International Journal of Electrochemical Science 6 (2011) 2429-2442.
- [27]- R. O. Akinyeye, I. Michira, M. Sekota, A. Ahmed, D. Tito, P. G. L. Baker, C. M. A. Brett, M. Kalaji, E. Iwuoha. *Electrochemical synthesis and characterization of 1,2-Naphthaquinane-4-sulfonic acid doped polypyrrole*. Electroanalysis 19 (2007) 303-309.
- [28]- A. Baleg. *Synthesis and electrochemistry of novel conducting dendrimeric star copolymers on poly (propylene imine) dendrimer*. PhD Thesis, Department of Chemistry, University of the Western Cape, (2011).
- [29]- M. E. G. Lyons. *Mediated electron transfer at redox active mololayers. Part 2: Analysis of the chronoamperometric response to a potential step perturbation*. Sensors 2 (2002) 314-330.
- [30]- H. Dhyani, M. D. Ali, S. P. Pal, S. Srivastava, P. R. Solanki, B. D. Malhotra, P. Sen. *Mediator-free biosensor using capped CdS quantum dots for detection of total cholesterol*. Royal Society of Chemistry (2015) 1-6.
- [31]- C. Dai, P. Song, J. D. Wadhawan, A. C. Fisher, N. S. Lawrence. *Screen printed alizarin-based carbon electrodes: monitoring pH in unbuffered media*. Electroanalysis 27 (2015) 917-923.
- [32]- L. Chen, Y. Jiang, C. Wang, X. Liu, Y. Chen, J. Jie. *Green chemical approaches to ZnSe quantum dots: preparation, characterisation and formation mechanism*. Journal of Experimental Nanoscience 5 (2010) 106-117.

- [33]- S. Laurent, D. Forge, M. Port, A. Roch, C. Robic, L. V. Elst, R. N. Muller. *Magnetic iron oxide nanoparticles: Synthesis, stabilising, vectorization, physicochemical characterizations, and biological applications*. Chemical Reviews 108 (2008) 2064-2110.
- [34]- S. J. Rosenthal, J. McBride, S. J. Pennycook, L. C. Feldman. *Synthesis, surface studies, composition and structural characterization of CdSe, core/shell, and biological nanocrystals*. Sur Sci Rep 64 (2007) 111-157.
- [35]- K. Senthilkumar, T. Kalaivani, S. Kanagesan. *Synthesis and characterization studies of ZnSe quantum dots*. Journal of Materials Science Materials in Electronics 23 (2012) 2048-2052.
- [36]- J. J. Andrade, A. G. Brasil Jr, P. M. A. Farias, A. Fontes, B. S. Santos. *Synthesis and characterization of blue emitting ZnSe quantum dots*. Microelectronics Journal 40 (2009) 641-643.
- [37]- S. C. Dey, S. S. Nath. *Electroluminescence of colloidal ZnSe quantum dots*. Journal of Luminescence 131 (2011) 2707-2710.



# CHAPTER FIVE

## 5. Conclusion and Recommendations

---

### 5.1. Conclusion

In this study we explored the potential application of a newly developed active layer based on a hybrid formation by blending the star copolymer G2PPT-co-PEDOT-PSSA as a donor and ZnSe QD as acceptor. In summary, ZnSe QD and novel dendritic star copolymer G2PPT-co-PEDOT-PSSA with PEDOT and PSSA arms and PPI dendrimer core of generation 2, were all successfully synthesized by making use of chemical experimental protocols. Chemical synthesis of the star copolymer involved functionalization of the PPI dendrimer with 2-thiophene aldehyde via a Schiff base condensation reaction followed by copolymerization with EDOT monomer using iron chloride as an oxidising agent. Chemical synthesis of the ZnSe QD involved preparation of Zn and Se precursor solutions using oleic acid as a capping agent and 1-octadecene as non-coordinating solvent at very high temperatures.

For the star copolymer G2PPT-co-PEDOT-PSSA,  $^1\text{H}$  NMR gave a new chemical shift at 8.3 ppm for N=CH, which confirmed the incorporation of thiophene aldehyde into the PPI dendrimer structure, and also showed the disappearance of the signal at 6.6 ppm, which confirmed the  $\alpha - \alpha$  coupling on the thiophene ring suggesting the growth of PEDOT on the surface of G2PPT dendrimer. FTIR was found to be in agreement with  $^1\text{H}$  NMR as it showed the presence of N=C vibrations at  $1637\text{ cm}^{-1}$  in the dendrimer moiety, and the disappearance of C-H out of plane bending vibrations at  $889\text{ cm}^{-1}$  at the  $\alpha -$  position of PEDOT confirming

the growth of PEDOT on the surface of G2PPT. Both  $^1\text{H}$  NMR and FTIR did not show any additional functionality as a result of the introduction of PSSA due to the weak bondage that is known to exist between PEDOT and PSSA. XRD analysis revealed a broadly amorphous structure associated with PEDOT at  $2\theta \sim 26^\circ$ . However, two new diffraction peaks with low intensities at  $2\theta \sim 35^\circ$  and  $40^\circ$  were observed, indicative of the presence of the dendrimer with its own unique properties, thus confirming a newly formed star copolymer. TGA analysis revealed improved thermal stability upon copolymer formation compared to pristine PEDOT and G2PPT. In addition, TGA results demonstrated that the thermal stability is directly proportional to the stacking of the polymers. The improved thermal stability proves pivotal for use of this material in photovoltaics application. Morphological analysis by SEM showed that the star copolymer exhibits a coral-or tubular-like structures with many tentacles which are separated from each other compared to the flake-like structures exhibited by pristine PEDOT. The morphological changes were indicative of a successful copolymer formation. On the other hand, HRTEM revealed spherical, cloudy-like microporous structures while EDX showed all the expected elements of the structure being present. Electronic transitions or optical properties were studied by employing UV-Vis. The results showed increase in absorption bands with shifts towards longer wavelengths upon copolymer formation compared to parent polymers. The shift was attributed to increase in conjugation, thus resulting in increased electron density. The Tauc relation was then used to determine the energy band gap of the materials. The energy gap values enable us to deduce whether a material is suitable to be considered a semiconductor for photovoltaics. The band gap was determined and found to be 2.96, 2.92, and 2.85 eV for PEDOT, G2PPT-co-PEDOT, and G2PPT-co-PEDOT-PSSA respectively. This makes the star copolymer a promising material for photovoltaics application. Emission studies were done by using PL. The results revealed that the emission of the star copolymer is an average of its constituents (478 nm). In addition, the presence of PSSA caused a shift from 478 to 472 nm

(blue shift) in emission due to increase in size chains, which alters the torsion angle and leads to lower conjugation length. The electrochemical responses of the materials were studied using CV and SWV in support of CV. The electrochemistry was performed in TBAP/DMSO electrolytic system using GCE as a working electrode. From the study, all the polymers exhibited a 2-electron transfer system as expected. The voltammograms depicted a one redox couple which was indicative of a diffusion of electrons along the polymer chains. However, the current response increased with the introduction of PSSA and copolymer formation. This was attributed to the increase in conjugation, thus increasing the free movement of  $\pi$  – electrons along the polymer chains. With the help of CV, the HOMO and LUMO were determined which enabled the determination of the electrochemical band gap, which was found to be 0.201, 0.202, and 0.199 eV for PEDOT, G2PPT-co-PEDOT, and G2PPT-co-PEDOT-PSSA respectively. SWV was found to be in agreement with results Obtained from CV.

Absorption properties of ZnSe QD together with band gap determination were found to be in accordance with literature. An absorption peak wavelength was observed at 416 nm with a band gap of 2.95 eV. HRTEM revealed that the particles are well-dispersed, small, and spherical in shape. EDX showed the presence of all expected elements (Zn and Se) without any impurities. This means that the QD was successfully prepared.

The UV-Vis of the blends was done at different ratios in a solvent mixture of DMSO and toluene. From the results, the blend ratio of 1:3 (G2PPT-co-PEDOT-PSSA: ZnSe QD) showed good absorption properties with two distinct absorption bands shifting towards longer wavelength, 323 and 365 nm. The shift is of vital importance for photovoltaics because it indicates reduction of band gap, hence requiring less energy to excite electrons from the valence band to the conduction band. The influence of the presence of the ZnSe QD in the emission properties was investigated using PL. The results revealed that the presence of the QD caused a decrease in the PL intensity compared to PL intensity of the donor. This indicates

an electron transfer process from the donor to the acceptor, thus confirming that the ZnSe QD was indeed used as an acceptor. Hence the new novel properties mentioned above such as the optical band gap, electrochemical band gap, absorption, and luminescence of the star copolymer G2PPT-co-PEDOT-PSSA and the hybrid G2PPT-co-PEDOT-PSSA: ZnSe QD makes the hybrid a potential material/semiconductor for future consideration in the use of PV devices.

## 5.2. Recommendations

The following aspect of the development of an organic-inorganic, donor-acceptor hybrid active layer for photovoltaics needs further investigation.

- In depth scanning electron microscopy and X-ray photoelectron spectroscopy (XPS) needs to be studied to better understand the surface chemistry of the dendritic star copolymer. XPS is capable of giving us a more detailed chemical interaction or bonding between the atoms within the structure of the star copolymer. S, and P orbitals can be revealed by XPS and the information can be correlated to fluorescence studies as to get an insight of where exactly is the emission coming from. Knowing the interacting orbitals can help better understand the energy levels,  $S_0-S_n$ , of the Jablonski diagram and its emissions.
- Gas permeation chromatography (GPC) needs to be employed to investigate the molecular weight and polydispersity of the star copolymer because the degree of polymerization has an effect on the requirements of the properties of materials for PVs. Moreover, employing GPC can help us control the degree of polymerization for specific desirable properties for PVs. It also helps to confirm the formation of the star copolymer by comparing its molecular weight to the molecular weight of the parent polymers, hence showing the growth of PEDOT on the surface of G2PPT.

- In depth fluorescence studies needs further investigation to determine the life time, quantum yield, decay constant, and quenching effects. This would help in knowing the exact factors that are responsible for the loss of energy, thus helping us to devise concrete strategies to counteract the loss of energy.
- Thermogravimetric analysis (TGA) coupled to FTIR needs to be employed in order to know the exact functional group or species that is thermally degraded. This would help us in picking up or choosing the right material to functionalize with in order to improve the thermal stability.
- One-pot synthesis of the star copolymer-quantum dot hybrid needs to be done and compare its results to the results of the blends. This brings stability to the material.
- Photovoltaic properties such as the power conversion efficiency (PCE), fill factor (FF), open circuit voltage (OCV) etc needs thorough investigation.
- Electrochemical impedance spectroscopy (EIS) together with Hall effects measurements needs to be studied for resistivity and conductivity of the materials. This would help in concluding as to whether the material is a better semiconductor or not.